

THE FORMATION OF ALUNITE UNDER HYDROTHERMAL  
CONDITIONS: CHEMISTRY, UNIT-CELL PARAMETERS,  
AND VIBRATIONAL SPECTRA

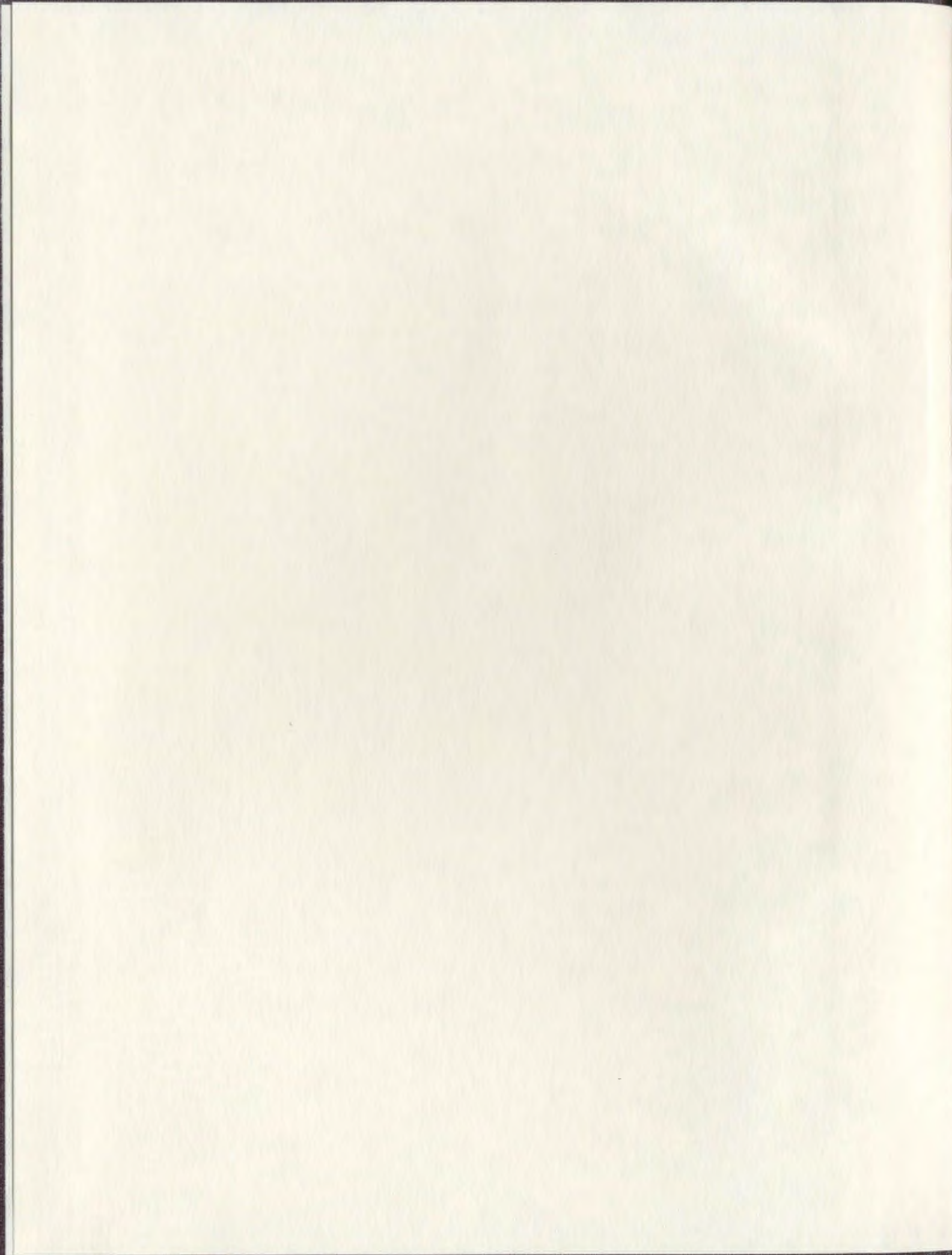
CENTRE FOR NEWFOUNDLAND STUDIES

---

**TOTAL OF 10 PAGES ONLY  
MAY BE XEROXED**

(Without Author's Permission)

WOLFRAM RUDOLPH



## **INFORMATION TO USERS**

**This manuscript has been reproduced from the microfilm master. UMI films the text directly from the original or copy submitted. Thus, some thesis and dissertation copies are in typewriter face, while others may be from any type of computer printer.**

**The quality of this reproduction is dependent upon the quality of the copy submitted. Broken or indistinct print, colored or poor quality illustrations and photographs, print bleedthrough, substandard margins, and improper alignment can adversely affect reproduction.**

**In the unlikely event that the author did not send UMI a complete manuscript and there are missing pages, these will be noted. Also, if unauthorized copyright material had to be removed, a note will indicate the deletion.**

**Oversize materials (e.g., maps, drawings, charts) are reproduced by sectioning the original, beginning at the upper left-hand corner and continuing from left to right in equal sections with small overlaps.**

**Photographs included in the original manuscript have been reproduced xerographically in this copy. Higher quality 6" x 9" black and white photographic prints are available for any photographs or illustrations appearing in this copy for an additional charge. Contact UMI directly to order.**

**ProQuest Information and Learning  
300 North Zeeb Road, Ann Arbor, MI 48106-1346 USA  
800-521-0600**

**UMI<sup>®</sup>**





**National Library  
of Canada**

**Acquisitions and  
Bibliographic Services**

**395 Wellington Street  
Ottawa ON K1A 0N4  
Canada**

**Bibliothèque nationale  
du Canada**

**Acquisitions et  
services bibliographiques**

**395, rue Wellington  
Ottawa ON K1A 0N4  
Canada**

*Your file Votre référence*

*Our file Notre référence*

**The author has granted a non-exclusive licence allowing the National Library of Canada to reproduce, loan, distribute or sell copies of this thesis in microform, paper or electronic formats.**

**The author retains ownership of the copyright in this thesis. Neither the thesis nor substantial extracts from it may be printed or otherwise reproduced without the author's permission.**

**L'auteur a accordé une licence non exclusive permettant à la Bibliothèque nationale du Canada de reproduire, prêter, distribuer ou vendre des copies de cette thèse sous la forme de microfiche/film, de reproduction sur papier ou sur format électronique.**

**L'auteur conserve la propriété du droit d'auteur qui protège cette thèse. Ni la thèse ni des extraits substantiels de celle-ci ne doivent être imprimés ou autrement reproduits sans son autorisation.**

0-612-66795-2

**Canada**



# Memorial

University of Newfoundland

This is to authorize the Dean of Graduate Studies to deposit two copies of my thesis/report entitled

The formation of alunite under hydrothermal conditions: chemistry, unit cell parameters and vibrational spectra.

in the University Library, on the following conditions. I understand that I may choose only ONE of the Options here listed, and may not afterwards apply for any additional restriction. I further understand that the University will not grant any restriction on the publication of thesis/report abstracts.

(After reading the explanatory notes at the foot of this form, delete TWO of (a), (b) and (c), whichever are inapplicable.)

The conditions of deposit are:

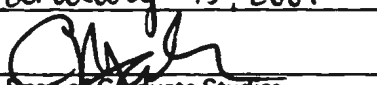
~~(a)~~ that two copies are to be made available to users at the discretion of their custodians,

OR

(b) that access to, and quotation from, this thesis/report is to be granted only with my written permission for a period of one year from the date on which the thesis/report, after the approval of the award of a degree, is entrusted to the care of the University, namely, \_\_\_\_\_ 19 \_\_\_\_, after which time the two copies are to be made available to users at the discretion of their custodians,

OR

(c) that access to, and quotation from, this thesis/report is to be granted only with my written permission for a period of \_\_\_\_\_ years from the date on which the thesis/report, after approval for the award of a degree, is entrusted to the care of the University; namely, \_\_\_\_\_, 19 \_\_\_\_, after which time two copies are to be made available to users at the discretion of their custodians.

Date January 13, 2001  
  
 \_\_\_\_\_  
 Dean of Graduate Studies

Signed Dr. L. Reddy  
 Witnessed by Hameen Moore

NOTES

- Restriction (b) will be granted on application, without reason given.  
 However, applications for restriction (c) must be accompanied with a detailed explanation, indicating why the restriction is thought to be necessary, and justifying the length of time requested. Restrictions required on the grounds that the thesis is being prepared for publication, or that patents are awaited, will not be permitted to exceed three years.  
 Restriction (c) can be permitted only by a Committee entrusted by the University with the task of examining such applications, and will be granted only in exceptional circumstances.
- Thesis writers are reminded that, if they have been engaged in contractual research, they may have already agreed to restrict access to their thesis until the terms of the contract have been fulfilled.

**The formation of alunite under hydrothermal conditions: chemistry, unit-cell parameters, and vibrational spectra.**

By

© Wolfram W. Rudolph

A thesis submitted to the  
School of Graduate Studies  
in partial fulfilment of the  
requirements for the degree of  
Master of Science

Department of Earth Sciences  
Memorial University of Newfoundland

August 2001

St. John's

Newfoundland

## Table of Contents

	Page
1. Abstract	1
2. Introduction	3
3. Objective of the Study and Organization	7
4. Aluminium(III) hydration in aqueous solution A Raman spectroscopic investigation and an ab-initio molecular orbital study of Aluminium(III) water clusters	9
4. 1. Abstract	9
4. 2. Introduction	11
4. 3. Experimental details and data analysis	13
4. 4. Results and discussion	15
4. 4. 1. Hydration of Al(III) - General remarks	15
4. 4. 2. The $[\text{Al}(\text{OH}_2)_6^{3-}]$ vibrational spectrum - $\text{AlCl}_3$ , $\text{Al}(\text{ClO}_4)_3$ , and $\text{Al}(\text{NO}_3)_3$ solutions	16
4. 4. 3. Vibrational spectra of $\text{Al}_2(\text{SO}_4)_3$ solution	21
4. 4. 4. Ab initio results	22
4. 5. Conclusions	31
4. 6. References	57
5. Study of aqueous $\text{Al}_2(\text{SO}_4)_3$ solution under hydrothermal conditions: sulfate ion pairing, hydrolysis and formation of hydronium alunite	61
5. 1. Abstract	61
5. 2. Introduction	62

5. 3.	Experimental	63
5. 4.	Results and discussion	68
5. 4. 1.	The aluminum hexaaqua(III) ion, $[\text{Al}(\text{OH}_2)_6]^{3+}$ , $\text{AlCl}_3$ , $\text{Al}(\text{NO}_3)_3$ , and $\text{Al}(\text{ClO}_4)_3$ solutions	68
5. 4. 2.	$(\text{NH}_4)_2\text{SO}_4$ - solution spectra; the vibrational spectrum of unligated sulfate	70
5. 4. 3.	$\text{NH}_4\text{HSO}_4$ aqueous solution, Hydrogen Sulfate Ion	72
5. 4. 4.	$\text{Al}_2(\text{SO}_4)_3$ aqueous solution spectra, sulfato complexes	73
5. 5.	Hydronium Alunite	78
5. 6.	Conclusions	80
5. 7.	References	97
6.	Studies on synthetic alunites: synthesis and X-ray characterization	101
6. 1.	Abstract	101
6. 2.	Introduction	102
6. 3.	Experimental Section	103
6. 3. 1.	Synthesis of alunite samples	103
6. 3. 2.	Analytical methods	105
6. 4.	Results	108
6. 4. 1.	Chemical characterization, thermal analysis and morphological studies of the alunite crystal powders	108
6. 4. 2.	Unit cell parameters	110
6. 5.	Discussion	111
6. 5. 1.	Structural Arrangements in Alunite	112

<b>6. 5. 2. Chemical Composition</b>	<b>112</b>
<b>6. 5. 3. Unit cell parameters of alunite</b>	<b>114</b>
<b>6. 6. Conclusions</b>	<b>117</b>
<b>6. 7. References</b>	<b>133</b>
<b>7. Raman and infrared absorption studies on synthetic alunites</b>	<b>137</b>
<b>7. 1. Abstract</b>	<b>137</b>
<b>7. 2. Introduction</b>	<b>137</b>
<b>7. 3. Experimental Section</b>	<b>139</b>
<b>7. 3. 1. Synthesis of alunite samples</b>	<b>139</b>
<b>7. 3. 2. Analytical and spectroscopic methods</b>	<b>139</b>
<b>7. 4. Results</b>	<b>142</b>
<b>7. 4. 1. Chemical characterization and morphological studies of the alunite crystal powders</b>	<b>142</b>
<b>7. 4. 2. Vibrational spectroscopic results on synthetic alunites</b>	<b>143</b>
<b>7. 5. Discussion</b>	<b>144</b>
<b>7. 5. 1. Structure of alunite</b>	<b>145</b>
<b>7. 5. 2. Assignment of the vibrational modes</b>	<b>145</b>
<b>7. 5. 2. 1. Factor group analysis</b>	<b>146</b>
<b>7. 5. 2. 2. Band Assignment</b>	<b>148</b>
<b>7. 6. Conclusions</b>	<b>152</b>
<b>7. 7. References</b>	<b>175</b>

<b>8.</b>	<b>Summary</b>	<b>178</b>
<b>9.</b>	<b>References</b>	<b>182</b>
<b>10.</b>	<b>Appendices</b>	<b>186</b>

## List of Tables

Table	Page
<p>4.1. The <math>\text{AlO}_6</math> skeleton modes (<math>\text{AlO}_6</math> unit possesses <math>\text{O}_h</math> symmetry), Raman and i.r. spectroscopic frequencies (<math>\text{cm}^{-1}</math>) in aqueous <math>\text{Al}(\text{ClO}_4)_3</math>, <math>\text{AlCl}_3</math> and <math>\text{Al}(\text{NO}_3)_3</math> solutions. (In <math>\text{Al}(\text{ClO}_4)_3</math> solutions the intensive <math>\text{ClO}_4^-</math> mode at <math>461 \text{ cm}^{-1}</math> overlaps <math>\nu_2(\text{e}_g)\text{AlO}_6</math> completely.) Additionally the modes of <math>\text{AlO}_6</math> in crystalline <math>\text{AlCl}_3 \cdot 6\text{H}_2\text{O}</math> (space group <math>\text{R-3c}</math> (<math>\text{D}^6_{3d}</math>) (<math>z = 2</math>)) are given for comparison</p>	33
<p>4.2. The Al-O symmetric stretching frequency as a function of n, the coordination number, of the aqua Al(III) cluster ion for four different basis sets/ levels of theory</p>	34
<p>4.3. Literature compilation of calculated Al-O distances as a function of the level of theory and basis set applied</p>	35
<p>4.4. Optimized geometry of hexaaqua Al(III)</p>	36
<p>4.5. Unscaled HF/6-31G*, HF/6-31+G* and MP2/6-31G* Frequencies (in <math>\text{cm}^{-1}</math>), intensities and force constants of the modes of the hexaaqua-Al(III) ion; <math>\Gamma_{\text{vib}} = 3a_g(\text{R,tp}) + a_u(\text{n.a.}) + 3e_g(\text{R,dp}) + e_u(\text{n.a.}) + 5f_g(\text{R,dp}) + 8f_u(\text{i.r.})</math></p>	37
<p>4.6. Our experimental frequencies (<math>\text{cm}^{-1}</math>) for the skeletal <math>\text{AlO}_6</math> modes (<math>\text{O}_h</math>) in aqueous <math>\text{AlCl}_3</math> solutions. The scaled ab initio frequencies for four different basis sets at the HF and MP2 levels of theory are presented</p>	39
<p>4.7. Calculated Electronic Binding Energies, <math>\Delta E_b^0</math>, at 0 K and the Computed Enthalpies for the Al(III) Hexaaqua Cluster, <math>\Delta H_b^{298}</math>, at 298.15 K (All Energies</p>	

in kJ/mol) at Four Different Basis Sets/Level of Theory .....	40
4.8. Structural parameters, energy (Hartree) and thermodynamic parameters ( $\Delta E_B$ , binding energy, at zero K and $\Delta H^\ominus$ , the enthalpy of the cluster formation at 298.15 K) calculated for the $[\text{Al}(\text{OH}_2)_{18}]^{3+}$ cluster denoted Al[6+12] .....	41
4.9. Unscaled HF/6-31G* Frequencies, intensities (i.r., Raman) and force constants of the octadeca- aqua aluminium (III) ( $\Gamma_{\text{vib}} = 13a(\text{R}) + 13e(\text{R}) + 40f(\text{i.r.,R})$ and $\Gamma_{\text{AlO}_6} = a(\text{R}) + e(\text{R}) + 4f(\text{i.r.,R})$ ) .....	42
5.1. The $\text{AlO}_6$ skeleton modes ( $\text{AlO}_6$ unit possesses $O_h$ symmetry), Raman and i.r. spectroscopic frequencies in aqueous $\text{Al}(\text{ClO}_4)_3$ and $\text{AlCl}_3$ and solutions. (In these solutions no inner-sphere complexes are formed, while in $\text{Al}_2(\text{SO}_4)_3$ solutions sulfato complex formation occurs) .....	82
5.2. Correlation table for the point groups $T_d$ , $C_{3v}$ and $C_{2v}$ . Sulfate in undisturbed form (dilute aqueous $(\text{NH}_4)_2\text{SO}_4$ solution), and two lower symmetry environments. The Raman and i.r. activities are given as well the numbers of Raman bands inclusive the number of polarized modes and the number of i.r. active modes coinciding with the Raman modes. The wavenumbers for the sulfate modes in undisturbed form ( $T_d$ ) are given in $\text{cm}^{-1}$ .....	83
5.3. The assignment of the $\text{HSO}_4^-$ modes, Raman band positions ( $\text{cm}^{-1}$ ), fwhh ( $\text{cm}^{-1}$ ), and degree of polarization of the hydrogen sulfate modes in 0.85 M $(\text{NH}_4)\text{HSO}_4$ solution at 22 and 184 °C .....	84
5.4. Parameters of the band components of the isotropic Raman spectrum of a	

0.98 mol·L <sup>-1</sup> aqueous Al <sub>2</sub> (SO <sub>4</sub> ) <sub>3</sub> solution at 184°C in the wavenumber region between 780 - 1350 cm <sup>-1</sup> .....	85
5.5. Raman and infrared data for (H <sub>3</sub> O)Al <sub>3</sub> (SO <sub>4</sub> ) <sub>2</sub> (OH) <sub>6</sub> (hydronium alunite) at 25°C .	86
6.1. Synthesis conditions for two alunites synthesised prior to the systematic study (# A001 and A002) the hydronium alunite/alunite solid solution series (# A007 to A014) and end member alunites (hydronium alunite (H-alunite), natroalunite, alunite, ammonioalunite and rubidium alunite (Rb-alunite) .....	119
6.2. Analytical results for hydronium alunite/alunite solid solution series. Included is the mole ratio K : Al in synthetic alunite and in solution prior to the precipitation of alunite .....	121
6.3. Thermogravimetric data on the endothermic reactions for end member alunites, H-alunite, alunite, Na-alunite, NH <sub>4</sub> -alunite and Rb-alunite .....	122
6.4. Our unit cell parameters and crystal data for hydronium alunite, hydronium gallunite, alunite, natroalunite, ammonioalunite and Rb-alunite .....	124
6.5. Mol ratio X <sub>K</sub> , unit cell parameters, <i>a</i> and <i>c</i> , ratio <i>c/a</i> , unit-cell volume and crystallographic density for synthetic alunites of the general formula (H <sub>3</sub> O,K)Al <sub>3</sub> (SO <sub>4</sub> ) <sub>2</sub> (OH) <sub>6</sub> .....	125
6.6. Unit cell parameters and unit cell volume taken from the literature for end member alunites: alunite, H-alunite, Na-alunite, NH <sub>4</sub> -alunite and the basic gallium salt of the alunite type (H <sub>3</sub> O)Ga <sub>3</sub> (SO <sub>4</sub> ) <sub>2</sub> (OH) <sub>6</sub> .....	126
7.1. Analytical results for alunite/hydronium alunite solid solution series .....	154

7.2. Raman and infrared data for $\text{KAl}_3(\text{SO}_4)_2(\text{OH})_6$ (alunite) and $\text{KAl}_3(\text{SO}_4)_2(\text{OD})_6$ (alunite-d) at 25°C .....	155
7.3 Raman and infrared data for $(\text{H}_3\text{O})\text{Al}_3(\text{SO}_4)_2(\text{OH})_6$ (H-alunite) at 25°C .....	157
7.4. Raman data for alunite solid solution series from the pure potassium end member to H-alunite, $\hat{\nu} = 298 \text{ K}$ .....	159
7.5. Infrared data (ATR) for alunite solid solution series from the pure potassium end member to H-alunite, $\hat{\nu} = 298 \text{ K}$ .....	161
7.6. Factor group analysis for alunite ( $D_{3d}^5$ ) .....	163
7.7. Characteristic internal vibrations (in $\text{cm}^{-1}$ ) of $\text{H}_3\text{O}^+$ .....	164

## List of Figures

Figures	Page
<p>4.1. Raman spectrum of a 2.00 mol/L <math>\text{Al}(\text{ClO}_4)_3</math> solution (I-parallel and I-perpendicular) in the wavenumber range from 100 - 1800 <math>\text{cm}^{-1}</math> (exciting wavelength 488.0 nm; slit width 1.4 <math>\text{cm}^{-1}</math>). The insert in the right corner gives the symmetric stretching mode of perchlorate in more detail</p>	47
<p>4.2. Concentration profile of the Raman spectra (I-parallel) of <math>\text{Al}(\text{NO}_3)_3</math> solutions in the wavenumber range from 280 to 1850 <math>\text{cm}^{-1}</math>. The concentrations are from top to bottom: 2.50, 2.00, 1.00, 0.50, and 0.21 mol/L. The conditions of the Raman measurement are: Exciting wavelength 488.0 nm; slit width 2.5 <math>\text{cm}^{-1}</math>. Note, that the modes of the <math>\text{AlO}_6</math> unit (<math>\nu_1(a_{1g})</math>, <math>\nu_2(e_g)</math>, and <math>\nu_3(f_{2g})</math>) are well separated from the <math>\text{NO}_3^-</math> vibrations. For explanations see text</p>	48
<p>4.3. Raman spectra of <math>\text{AlCl}_3</math> solutions at five different concentrations: 3.14, 2.00, 1.50, 1.00 and 0.50 <math>\text{molL}^{-1}</math> 25 °C in the wavenumber range from 250 - 650 <math>\text{cm}^{-1}</math></p>	49
<p>4.4 Raman spectra (<math>R_{\text{pol}}</math>, <math>R_{\text{dcpol}}</math> and <math>R_{\text{iso}}</math>) of a 2.85 mol/L <math>\text{AlCl}_3</math> solution in the wavenumber region between 70- 1300 <math>\text{cm}^{-1}</math> at 25°C. The insert gives the spectra of a 3.40 mol/L <math>\text{AlCl}_3</math> in the wavenumber region 240 - 650 <math>\text{cm}^{-1}</math></p>	50
<p>4.5. Infrared spectrum of a 3.14 <math>\text{molL}^{-1}</math> <math>\text{AlCl}_3</math> solution at 25 °C</p>	51
<p>4.6. Raman spectra of a 1.014 molal <math>\text{Al}_2(\text{SO}_4)_3</math> solution at a) 25, b) 58 and c) 106 °C</p>	52
<p>4.7. The structural model of <math>[\text{Al}^{3+}(\text{OH}_2)_6]</math> (<math>T_h</math> symmetry)</p>	55
<p>4.8. The structural model of <math>[\text{Al}^{3+}(\text{OH}_2)_{18}]</math> (T symmetry)</p>	56

- 5.1. Polarized Raman spectra in I - format of aqueous  $\text{AlCl}_3$  solutions at  $22^\circ\text{C}$  in the wavenumber range from 240 to  $680\text{ cm}^{-1}$  ( $\text{AlO}_6$  modes:  $\nu_1(a_{1g}) = 525\text{ cm}^{-1}$ ,  $\nu_2(e_g) = 438\text{ cm}^{-1}$  and  $\nu_5(f_{2g}) = 332\text{ cm}^{-1}$ ). From top to bottom: 3.14 M; 2.00 M ; 1.50 M; 1.00 M and 0.50 M. Note, that on top of the spectrum of the 3.14 M solution, the weak mode  $\nu_2(e_g)$  is drawn with twice the intensity ..... 88
- 5.2. Raman spectrum of a 3.00 M aqueous  $(\text{NH}_4)_2\text{SO}_4$  solution at  $22^\circ\text{C}$ . Panel A gives the wavenumber range from 40 to  $800\text{ cm}^{-1}$  (deformation modes of sulfate). Panel B gives the wavenumber range from 800 to  $1350\text{ cm}^{-1}$  (S-O stretching modes). For explanations see text. In panel A the spectra in R format  $R_{\text{pol}}$ ,  $R_{\text{dcpol}}$  and  $R_{\text{iso}}$  are presented. In panel B only  $R_{\text{iso}}$  and  $R_{\text{dcpol}}$  are given for clarity. The mode  $\nu_1(a_1)$   $\text{SO}_4^{2-}$  at  $981\text{ cm}^{-1}$  is presented 1/10 of its size ..... 89
- 5.3. The Raman spectra (R- format) of an aqueous  $\text{Al}_2(\text{SO}_4)_3$  solution, 0.98 M, at  $25^\circ\text{C}$ . In panel A the wavenumber range from 40 -  $800\text{ cm}^{-1}$  is given. Note in the isotropic spectrum the mode  $\nu_1(a_{1g})$   $\text{AlO}_6$  at  $525\text{ cm}^{-1}$ , and the shoulder at the lower wavenumbers at ca.  $480\text{ cm}^{-1}$ . Panel B gives the wavenumber range from 800 - 1400. Note the shoulder at ca.  $1011\text{ cm}^{-1}$  (stemming from sulfato complex) and the weak mode at  $1054\text{ cm}^{-1}$  (mode  $\nu_1(\text{HSO}_4^-)$ ) ..... 90
- 5.4. The Raman spectra (R- format) of an aqueous  $\text{Al}_2(\text{SO}_4)_3$  solution, 0.98 M, at  $58^\circ\text{C}$ . In panel A the wavenumber range from 40 -  $800\text{ cm}^{-1}$  is given. Note in the isotropic spectrum, that instead of a single mode  $\nu_1(a_{1g})$   $\text{AlO}_6$  at  $525\text{ cm}^{-1}$  a double band is observable (maxima at 525 and  $490\text{ cm}^{-1}$ ). The mode at  $668\text{ cm}^{-1}$  and 365

cm<sup>-1</sup> are indicative of the sulfato complex. Panel B gives the wavenumber range from 800 - 1400. Note at higher frequencies to the sulfate mode ( $\nu_1(e)$  -SO<sub>4</sub><sup>2-</sup> at 983) the pronounced shoulder at ca. 1010 cm<sup>-1</sup> (sulfato complex) and the weaker mode at 1054 cm<sup>-1</sup> (hydrogen sulfate,  $\nu_1(a_1)$  (HSO<sub>4</sub><sup>-</sup>)). The weak broad mode at 892 cm<sup>-1</sup> is also indicative of hydrogen sulfate, namely  $\nu_2(a_1)$  (HSO<sub>4</sub><sup>-</sup>) . . . . . 91

5.5. The Raman spectra (R- format) of an aqueous Al<sub>2</sub>(SO<sub>4</sub>)<sub>3</sub> solution, 0.98 M, at 106°C. In panel A the wavenumber range from 40 - 800 cm<sup>-1</sup> is given. Note in the isotropic spectrum, that the mode at 525 cm<sup>-1</sup> ( $\nu_1(a_{1g})$  AlO<sub>6</sub>) a mode at 490 cm<sup>-1</sup> is observable. The mode at 668 cm<sup>-1</sup> and 365 cm<sup>-1</sup> are indicative for the sulfato complex. In addition, a weak mode at 585 cm<sup>-1</sup> is observable, stemming from hydrogen sulfate, namely  $\nu_3(a_1)$  (HSO<sub>4</sub><sup>-</sup>). Panel B gives the wavenumber range from 800 - 1400. Note at higher frequencies to the sulfate mode ( $\nu_1(e)$  -SO<sub>4</sub><sup>2-</sup> at 981.5) the pronounced shoulder at ca. 1010 cm<sup>-1</sup> (sulfato complex) and the weaker mode at 1054 cm<sup>-1</sup> (hydrogen sulfate,  $\nu_1(a_1)$  (HSO<sub>4</sub><sup>-</sup>)). The weak broad mode at 886 cm<sup>-1</sup> is also indicative of hydrogen sulfate, namely  $\nu_2(a_1)$  (HSO<sub>4</sub><sup>-</sup>). The weak broad modes at 1155 cm<sup>-1</sup> and ca. 1250 cm<sup>-1</sup> are indicative for the sulfato complex . . . . . 92

5.6. Temperature profile (15 °C to 106 °C) of the isotropic Raman spectra in R-format of an 0.98 M (1.012 m) aqueous Al<sub>2</sub>(SO<sub>4</sub>)<sub>3</sub> solution. In panel A the wavenumber range from 40 - 800 cm<sup>-1</sup> is given. Note in the isotropic spectrum, that the mode at 525 cm<sup>-1</sup> ( $\nu_1(a_{1g})$  AlO<sub>6</sub>) is disappearing successively with

temperature increase and a new band at  $490\text{ cm}^{-1}$  is observable. The modes at  $365\text{ cm}^{-1}$ ,  $465\text{ cm}^{-1}$  and at  $668\text{ cm}^{-1}$ , also indicative for the ligated sulfate, and are also rising with temperature. In the spectrum at  $106\text{ }^{\circ}\text{C}$  the hydrogen sulfate mode at  $585\text{ cm}^{-1}$ ,  $\nu_3(a_1)$  ( $\text{HSO}_4^-$ ) is observable. Panel B gives the wavenumber range from  $800 - 1400$ . Note the mode of “free” sulfate,  $\nu_1(e)$   $-\text{SO}_4^{2-}$ , at  $984\text{ cm}^{-1}$  shifting slightly with temperature from  $984\text{ cm}^{-1}$  at  $15\text{ }^{\circ}\text{C}$  to  $981.5\text{ cm}^{-1}$  at  $106\text{ }^{\circ}\text{C}$ . The modes indicative for ligated sulfate at  $1010\text{ cm}^{-1}$ ,  $1030\text{ cm}^{-1}$  (shoulder),  $1155\text{ cm}^{-1}$  and  $1250\text{ cm}^{-1}$  increase in intensity continuously with temperature. The modes of  $\text{HSO}_4^-$ , at  $1054\text{ cm}^{-1}$  (with a shoulder at  $1044\text{ cm}^{-1}$ ) and at  $896\text{ cm}^{-1}$  (this mode is strongly temperature dependent) increase also with temperature ..... 93

5.7. Temperature profile of the isotropic Raman spectra in R-format of an  $0.98\text{ M}$  ( $1.012\text{ m}$ ) aqueous  $\text{Al}_2(\text{SO}_4)_3$  solution from room temperature ( $22\text{ }^{\circ}\text{C}$ ) to  $184\text{ }^{\circ}\text{C}$ , the temperature alunite is precipitating. The wavenumber range from  $800- 1350\text{ cm}^{-1}$  is given. The explanation under panel B , Figure 6, is applicable here as well. Note that the free sulfate disappeared almost completely at  $184\text{ }^{\circ}\text{C}$ , transformed into ligated sulfate and hydrogen sulfate ..... 94

5.8. Isotropic Raman spectrum in R- format of a  $0.98\text{ M}$  ( $1.012\text{ molal}$ )  $\text{Al}_2(\text{SO}_4)_3$  solution at  $184\text{ }^{\circ}\text{C}$  at  $760 - 1380\text{ cm}^{-1}$ . In addition, the synthetic band profile is given, as well as, the component bands and the baseline. Note the component at  $870\text{ cm}^{-1}$  and  $1044/1054\text{ cm}^{-1}$ , which are due to  $\text{HSO}_4^-$ . The unligated sulfate mode at  $978\text{ cm}^{-1}$  has almost disappeared. The other modes

at 1010, 1033, 1154 and 1245 $\text{cm}^{-1}$ are due to the ligated sulfate .....	95
5.9. Overview infrared and Raman spectrum of $(\text{H}_3\text{O})\text{Al}_3(\text{SO}_4)_2(\text{OH})_6$ at 25°C. In the upper panel the i.r spectrum is given whilst in the lower panel the Raman spectrum is given .....	96
6.1. SEM photograph of synthetic alunite. Scale bar is 6 $\mu\text{m}$ . This image was obtained with a Hitachi S570 scanning electron microscope using an accelerating voltage of 20 keV and a current of 100 nA .....	129
6.2. The axis ratio $c/a$ for the alunite - hydronium alunite solid solution series as a function of the mole fraction $X_K$ .....	130
6.3. Drawing of the interpenetration of T-O-T layers for alunite .....	131
6.4. The axis ratio $c/a$ for natroalunite, alunite, ammonioalunite and rubidium-alunite as a function of the effective ionic radius of $\text{Na}^+$ , $\text{K}^+$ , $\text{NH}_4^+$ , and $\text{Rb}^+$ .....	132
7.1 Raman and infrared spectrum of alunite at 25 °C. Upper panel: infrared spectrum; lower panel: Raman spectrum .....	165
7.2. Raman spectra of alunite and alunite-d at 25 °C in the wavenumber range from 100 to 1300 $\text{cm}^{-1}$ .....	166
7.3. Raman spectra of alunite and alunite-d in the OH and OD stretching range, respectively . .....	167
7.4. Raman and i.r. spectrum of hydronium alunite at 25 °C. Upper panel: infrared spectrum; lower panel: Raman spectrum .....	168
7.5. Raman concentration profile for solid solution series	

**( $[K_{1-x}(H_3O)_xAl_3(SO_4)_2(OH)_6]$ ; with  $x = 0$  to  $1$ ; samples A014 to A007) are presented in the wavenumber range from  $100$  to  $1300\text{ cm}^{-1}$  (panel A) and from  $3250$  to  $3750\text{ cm}^{-1}$  (panel B). For the composition of the solid solution samples compare Table 7.1 ..... 169**

**7.6. Infrared (ATR spectra) concentration profile for solid solution series ( $[K_{1-x}(H_3O)_xAl_3(SO_4)_2(OH)_6]$ ; with  $x = 0$  to  $1$ ; samples A014 to A007) are presented in the wavenumber range from  $600$  to  $1800\text{ cm}^{-1}$  (panel A) and from  $2000$  to  $3800\text{ cm}^{-1}$  (panel B). For the composition of the solid solution samples compare Table 7.1 ..... 171**

**7.7. Drawing of the c- axis projection to illustrate the  $AlO_2(OH)_4$  octahedra linked by corner- shared OH groups forming an octahedral sheet ..... 173**

**7.8. Correlation diagram for the symmetry properties of the normal modes of  $SO_4$  in alunite space group R-3m ( $D_{3d}^5$ ) ..... 174**

## Acknowledgements

The writer would like to thank his thesis advisor, Dr. R. Mason, for guidance and help to prepare this work. The writer would also like to thank Dr. Dieter Fischer, IPF Dresden, Saxony, for measuring the ATR spectra and the diffuse reflectance spectra and Dr. Gert Irmer, TU Freiberg, Mining Academy, Saxony for allowing the use of his Raman spectrometer and for help during the measurements.

I would like to thank Mr. Chris Finch, Department of Mines and Energy, Newfoundland for the use of his ICP-OES instrument and for help during the measurements.

I would like to thank Dr. Peer Schmidt, TU Dresden, Institut fuer Anorganische Chemie, for the thermal measurements.

Last not least I would like to thank Dr. C. C. Pye, St. Mary's University, Halifax for helping me to perform, partially, the ab initio calculations and for helpful discussions during the course of this work. Dr. Pye, one of the co-authors of the first paper of this thesis has also performed the high level calculations and the calculations of the second - sphere aluminium(III) - water complex. I would like to thank him for this work as well. Furthermore, I would like to acknowledge a scholarship from graduate studies of Memorial University NF, during the period 1997 till 1998.

## 1. Abstract

Raman spectra have been measured for aqueous  $\text{Al}_2(\text{SO}_4)_3$  solutions from 25°C to hydrothermal conditions at 184 °C under steam saturation. The Raman spectrum at 184 °C contained four polarized bands in the S-O stretching wavenumber range which suggest that a new sulfato complex, where sulfate acts as a bridging ligand, possibly bidentate or tridentate, is formed in solution in addition to a 1:1 aluminium(III) sulfato complex, where sulfate is monodentate, which is the only ion pair identified at room temperature. Under hydrothermal conditions it was possible to observe the hydrolysis of Al(III) aqua-ion by measuring the relative intensity of bands due to  $\text{SO}_4^{2-}$  and  $\text{HSO}_4^-$  according to the coupled equilibrium reaction  $[\text{Al}(\text{OH}_2)_6]^{3+} + \text{SO}_4^{2-} \rightleftharpoons [\text{Al}(\text{OH}_2)_5\text{OH}]^{2+} + \text{HSO}_4^-$ . The precipitate in equilibrium with the solution at 184°C could be characterized as hydronium alunite,  $(\text{H}_3\text{O})\text{Al}_3(\text{SO}_4)_2(\text{OH})_6$ .

Alunites of the substitution series potassium alunite  $[\text{KAl}_3(\text{SO}_4)_2(\text{OH})_6]$  - hydronium alunite  $[(\text{H}_3\text{O})\text{Al}_3(\text{SO}_4)_2(\text{OH})_6]$  have been synthesized from acidic solutions (pH values 1.5 to 3.0) between 100 to 205 °C and between 1 and 18 bars in both sealed quartz and teflon lined bombs. The composition of the starting solutions ranged from 0 to 300 % potassium with aluminium fixed at ca. 0.6 M and sulfate ranging from 0.16 - 0.18 M.

For reasons of comparison a few end members of the alunite group have been synthesized such as sodium alunite  $[\text{NaAl}_3(\text{SO}_4)_2(\text{OH})_6]$ , ammonium alunite  $[(\text{NH}_4)\text{Al}_3(\text{SO}_4)_2(\text{OH})_6]$ , and rubidium alunite  $[\text{RbAl}_3(\text{SO}_4)_2(\text{OH})_6]$ .

A combination of results from chemical analysis, x- ray powder diffractometry, infrared absorption spectroscopy and Raman spectroscopy indicates that, firstly, the hydronium ion exists in the interlayer site, the 12 - fold cation site of the alunite structure as a discrete functional group, and secondly, a complete solid solution series exist between  $K^+$  and  $H_3O^+$ .

A so called basic gallium sulfate (BGS) of the alunite type was also synthesized, the unit cell parameters were determined and compared with the unit cell parameters of hydronium alunite.

## 2. Introduction

Minerals of the alunite-jarosite family have the general formula  $AB_3(XO_4)_2(OH)_6$ , where A is a large monovalent, divalent or even trivalent cation, such as  $H_3O^+$ ,  $Na^+$ ,  $NH_4^+$ ,  $Tl^+$ ,  $Ca^{2+}$ ,  $Sr^{2+}$ ,  $Ba^{2+}$ ,  $Pb^{2+}$ ,  $Ce^{3+}$  in 12-fold coordination. The B sites are occupied by cations like  $Al^{3+}$ ,  $Fe^{3+}$ ,  $Ga^{3+}$ ,  $Cu^{2+}$ , and  $Zn^{2+}$  in octahedral coordination. The anion  $(XO_4)^{2-}$  is mostly  $SO_4^{2-}$ , but can be also  $PO_4^{3-}$ ,  $AsO_4^{3-}$ ,  $CO_3^{2-}$ ,  $CrO_4^{2-}$ , or  $SiO_4^{2-}$ . Al(III) and Fe(III) are the major occupants of the B sites, but with the wealth of possibilities of combinations in the A and  $(XO_4)$  sites, the minerals are usually considered in three groups based on the nature of the anions (Palache et al. 1951; Strunz, 1978, Ramdohr and Strunz, 1978): I) alunite-jarosite group, with two divalent  $(XO_4)$  anions and usually monovalent A cations; II) beudantite or woodhouseite group, with one divalent and one trivalent  $(XO_4)$  anion and usually divalent A cations; III) plumbogummite, crandallite, or goyazite group, with two trivalent  $(XO_4)$  anions and either divalent or trivalent A cations.

The subdivisions above reflect the strong relationship between A and  $(XO_4)$  occupancy. Substitution of one trivalent for one divalent anion as in beudantite group is accompanied by a concurrent change in the A site cation from monovalent to divalent. Complete replacement by a trivalent anion is accompanied by substitution of a trivalent cation on the A site as in the case of florencite,  $CeAl_3(PO_4)_2(OH)_6$ . If the A site cation remains divalent, protonation of one of the trivalent anions also results in a stable compound, as in the case of gorceixite,  $BaAl_3H(PO_4)_2(OH)_6$  (Radoslovich, 1982).

The substitution of a divalent ion in the A site can also be realized by occupying

only half of the A site positions in an orderly fashion, like  $\text{Ca}^{2+}$  in minamiite,  $\text{Ca}_{0.5}\text{Al}_3(\text{SO}_4)_2(\text{OH})_6$  (Ossaka et al., 1987), or  $\text{Pb}^{2+}$  in plumbojarosite,  $\text{Fe}_{0.5}\text{Fe}_3(\text{SO}_4)_2(\text{OH})_6$  (Szymanski, 1985).

In this research work, we deal exclusively with members of alunite group (B = Al(III)) with the exception of a basic gallium sulfate, which we call, informally, “hydronium gallunite” (B = Ga(III)). Alunite sensu stricto  $[\text{KAl}_3(\text{SO}_4)_2(\text{OH})_6]$  is one of the most abundant minerals of the alunite-jarosite group (Scott, 1987) and is formed over a wide temperature range (ca. 20 to 400 °C) as a secondary mineral produced from Al-rich minerals (e.g. feldspars) in oxidizing, sulfur-rich environments. Alunite is not only of significance as a source of aluminium and potassium but also of importance in hydrothermal ore deposits (Meyer and Hemley, 1967) and other geological settings. Alunite occurs in hydrothermal ore deposits (Meyer and Hemley, 1967; Hemley et al., 1969; Brimhall, 1980), hot springs (Schoen et al., 1974; Aoki, 1983), sedimentary rocks (Goldbery, 1980), and low - to intermediate - grade aluminous metamorphic rocks (Schoch et al., 1985). Therefore, the detailed investigation of the formation, synthesis and characterization of alunites is of great significance to economic geology, sedimentology and environmental science.

The general formula of the minerals belonging to the alunite - jarosite supergroup of minerals can be written as  $\text{AB}_3(\text{SO}_4)_2(\text{OH})_6$ , where A is a large monovalent or divalent cation, such as  $\text{H}_3\text{O}^+$ ,  $\text{Na}^+$ ,  $\text{K}^+$ ,  $\text{NH}_4^+$ ,  $\text{Ag}^+$ ,  $\text{Tl}^+$ ,  $\frac{1}{2}\text{Ca}^{2+}$ ,  $\frac{1}{2}\text{Pb}^{2+}$  in 12-fold coordination with six oxygen and six hydroxyl ions. Rubidium can also substitute in the A site, but this

substitution has been done in vitro (Rudolph and Mason, 2001). No rubidium alunite has been described as a naturally occurring mineral so far. The B sites, octahedrally coordinated with two oxygen and four hydroxyl ions, are occupied by  $\text{Al}^{3+}$  (alunite group) or  $\text{Fe}^{3+}$  (jarosite group). Also Ga(III) can be substituted in the B site as has been shown as a synthetic mineral by Johansson (1963). The sulfur site is surrounded by four oxygen ions. The crystal structure of alunite was first described by Hendricks (1937), who determined that the mineral belongs to the hexagonal space group R3m. Later, Wang et al. (1965) confirmed the structural model by Hendricks, but found that refinement of the structure indicated the space group R-3m. Menchetti and Sabelli (1976) refined the alunite (and jarosite) structure further.

Substitution of  $\text{Na}^+$  for  $\text{K}^+$  is common in alunites from each of these environments, and a complete range of  $\text{Na}^+$  contents up to greater than 95 % (Chitale and Guven, 1987) has been reported. A great number of other cations may also substitute for  $\text{K}^+$ , namely  $\text{H}_3\text{O}^+$  (Ripmeester et al., 1986),  $\text{NH}_4^+$  (Altaner et al., 1988),  $\text{Ca}^{2+}$  or  $\text{Sr}^{2+}$ , which are generally accompanied by substitution of an equimolar amount of  $\text{PO}_4^{3-}$  for  $\text{SO}_4^{2-}$  to maintain neutrality (Botinelly, 1976; Scott, 1987) but may also be compensated for by vacancies on the alkali site (Ossaka et al. 1982). However, these substitutions are in most cases rare compared to the amount of  $\text{Na}^+$  present.

Although  $\text{H}_3\text{O}^+$  substitution has been reported, (Ripmeester et al., 1986) no systematic study was performed on the alunite members of the solid solution series  $\text{K}^+$  -  $\text{H}_3\text{O}^+$ . Furthermore, the substitution of hydronium seems to be accompanied by other

forms of non-OH water in alunite (cf. Stoffregen and Alpers, 1992) which obscured the clear detection of hydronium in the alunite structure. One of the major unsolved problems with respect to the crystal chemistry of alunite is the nature of the hydrous species that occurs in the 12 - coordinated interlayer site. Although Shishkin (1951) showed that  $\text{H}_3\text{O}^+$  can be replaced by  $\text{NH}_4^+$  through ion exchange in ammonium jarosite, direct structural evidence of  $\text{H}_3\text{O}^+$  in jarosite and alunite has not been confirmed. Infrared spectroscopic studies of these compounds were carried out by Kubisz (1972) and by Wilkins, Mateen and West (1974). According to the first author "the existence of pyramidal  $\text{H}_3\text{O}^+$  ion in jarosite and alunite structures may be regarded as definitely proven." While the latter authors were not able "either to confirm or disprove the existence of oxonium<sup>1</sup> in synthetic members of the alunite-jarosite group by infrared spectroscopy". The evidence for  $\text{H}_3\text{O}^+$  in the alunite structure seems to be more indirect and inferred.

---

<sup>1</sup>  
The terminus oxonium ion for hydronium ion is the more exact one, but the older name hydronium ion is still widely used and is also used throughout the text.

### 3. Objective of the Study and Organization

This study has three objectives. The first objective was to characterize the hexaaquaaluminium(III) species, one of the species necessary (besides sulfate) to form alunite, by Raman and infrared spectroscopy. *Ab initio* molecular orbital calculations were applied to model the hexaaquaaluminium(III) ion, which is the main species in simple aqueous aluminium(III) salt solutions. The geometry of  $[\text{Al}(\text{OH}_2)_6]^{3+}$  ion has been optimised and resulted in symmetry  $T_h$ . The calculated vibrational spectrum of the  $[\text{Al}(\text{OH}_2)_6]^{3+}$  ion has been compared with the experimental vibrational spectral data and good agreement could be observed. The results of this study have been published in a first paper by Rudolph, Mason and Pye, 2000.

The second objective was to investigate aqueous aluminium sulfate solutions as a function of temperature by Raman and infrared spectroscopy until hydronium alunite was precipitated. We have studied aqueous  $\text{Al}_2(\text{SO}_4)_3$  using Raman spectroscopy from room temperature to hydrothermal conditions at 184 °C under steam saturation. The Raman spectrum at 184 °C contained four polarized bands in the S-O stretching wavenumber range which suggest that a new sulfato complex, where sulfate acts as a bridging ligand, possibly bidentate or tridentate, is formed in solution in addition to a 1:1 aluminium(III) sulfato complex, where sulfate is monodentate, which is the only ion pair identified at room temperature. Under hydrothermal conditions it was possible to observe the hydrolysis of aluminium(III) aqua-ion by measuring the relative intensity of bands due to  $\text{SO}_4^{2-}$  and  $\text{HSO}_4^-$  according to the coupled equilibrium reaction  $[\text{Al}(\text{OH}_2)_6]^{3+} + \text{SO}_4^{2-} \rightleftharpoons$

$[\text{Al}(\text{OH})_2\text{OH}]^{2-} + \text{HSO}_4^-$ . The precipitate in equilibrium with the solution at 184°C was characterized as hydronium alunite,  $(\text{H}_3\text{O})\text{Al}_3(\text{SO}_4)_2(\text{OH})_6$ , by chemical analysis, X-ray diffraction, Raman and infrared spectroscopy. The results of the solution study and the characterization of the hydrothermally formed hydronium alunite were published by Rudolph and Mason, 2001.

The third objective was to determine the effect of temperature and pressure and chemical composition on the hydrothermal synthesis of alunite - hydronium alunite solid solutions and a few end member alunites, such as alunite, natroalunite, ammonium alunite and rubidium alunite. Furthermore a basic gallium sulfate (BGS) of the alunite type was synthesised. The alunites were characterized by chemical analysis, SEM, and X-ray powder diffraction. Also thermal studies have been applied on the alunite end members. This work was directed towards an understanding of the physico - chemical conditions of the formation of natural alunite deposits and the associated gold-, silver-, lead-, and zinc-bearing minerals. The material of this work has been prepared for publication by Rudolph and Mason, 2001. Finally, Raman and infrared spectroscopy has been carried out on the synthetic alunite - hydronium alunite solid solutions. This research work will be published in the near future (Rudolph and Mason, 2001). Vibrational analysis has been applied in order to investigate the different types of chemical species in these alunites, particularly hydrogen-oxygen species, the sulfate anions and the  $\text{AlO}_2(\text{OH})_4$  unit. Deuterated samples  $[\text{KAl}_3(\text{SO}_4)_2(\text{OD})_6]$ , and  $[(\text{D}_3\text{O})\text{Al}_3(\text{SO}_4)_2(\text{OD})_6]$  were prepared to facilitate the identification of O-H/O-D vibrations and to make assignments more reliable.

#### 4. Aluminium(III) hydration in aqueous solution

##### A Raman spectroscopic investigation and an *ab-initio* molecular orbital study of Aluminium(III) water clusters

Wolfram W. Rudolph, Roger Mason, and Cory C. Pye

#### 4.1. Abstract

Raman spectra of aqueous Al(III)- chloride, nitrate, and perchlorate solutions were measured over broad concentration (0.21 mol/L - 3.14 mol/L) and temperature (25 -125 °C) ranges. The weak, polarized band at 525 cm<sup>-1</sup> and two depolarized modes at 438 cm<sup>-1</sup> and 332 cm<sup>-1</sup> have been assigned to  $\nu_1(a_{1g})$ ,  $\nu_2(e_g)$  and  $\nu_3(f_{2g})$  of the hexaaquaaluminium(III) ion, respectively. The infrared active mode at 598 cm<sup>-1</sup> has been assigned to  $\nu_3(f_{1u})$ . The vibrational analysis of the species [Al(OH<sub>2</sub>)<sub>6</sub>]<sup>3+</sup> was done on the basis of O<sub>h</sub> symmetry (OH<sub>2</sub> as point mass). The polarized mode  $\nu_1(a_{1g})$  AlO<sub>6</sub> has been followed over the full temperature range and band parameters (band maximum, full width of half height and band intensity) have been examined. The position of the  $\nu_1(a_{1g})$  AlO<sub>6</sub> mode shifts only about 3 cm<sup>-1</sup> to lower frequencies and broadens about 20 cm<sup>-1</sup> for a 100°C temperature increase. The Raman spectroscopic data suggest that the hexaaquaaluminium(III) ion is thermodynamically stable in chloride, nitrate and perchlorate solutions over the temperature and concentration range measured. No inner-sphere complexes in these solutions could be detected spectroscopically.

Aluminium sulfate solutions show a different picture and thermodynamically stable aluminium sulfato complexes could be detected. The sulfato complexes are entropically driven, so that their formation is favoured at higher temperatures.

*Ab initio* geometry optimizations and frequency calculations of  $[\text{Al}(\text{OH}_2)_6]^{3-}$  were carried out at the Hartree-Fock and second order Møller-Plesset levels of theory, using various basis sets up to 6-31+G\*. The global minimum structure of the hexaqua Al(III) species corresponds with symmetry  $T_h$ . The unscaled vibrational frequencies of the  $[\text{Al}(\text{OH}_2)_6]^{3-}$  are reported. The unscaled vibrational frequencies of the  $\text{AlO}_6$  unit are lower than the experimental frequencies (ca. 15 %), but scaling the frequencies reproduces the measured frequencies. The theoretical binding enthalpy for  $[\text{Al}(\text{OH}_2)_6]^{3-}$  was calculated and accounts for ca. 50 % of the experimental single ion hydration enthalpy for Al(III).

*Ab initio* geometry optimizations and frequency calculations are also reported for  $[\text{Al}(\text{OH}_2)_{18}]^{3-}$  ( $\text{Al}[6+12]$ ) cluster with 6 water molecules in the first sphere and 12 water molecules in the second sphere. The global minimum corresponds with T symmetry. Calculated frequencies of the aluminium  $[6+12]$  cluster correspond with the observed frequencies in solution. The  $\nu_1$   $\text{AlO}_6$  (unscaled, HF/6-31G\*) mode occurs at  $542 \text{ cm}^{-1}$  in fair agreement with the experimental value. The theoretical binding enthalpy for  $[\text{Al}(\text{OH}_2)_{18}]^{3-}$  was calculated and is slightly underestimated compared to the experimental single ion hydration enthalpy for Al(III). The water molecules of the first sphere form strong H-bonds with water molecules in the second hydration shell because of the strong polarizing effect of the Al(III) ion.

**KEY WORDS:** Raman spectra, *ab-initio* calculations of Al(III)- water clusters, Al(III)-hexaaqua ion, AlCl<sub>3</sub>, Al(ClO<sub>4</sub>)<sub>3</sub>, Al(NO<sub>3</sub>)<sub>3</sub>, and Al<sub>2</sub>(SO<sub>4</sub>)<sub>3</sub> - solutions.

#### 4. 2. Introduction

The structure of aqueous metal ions has been of interest to chemists studying the properties of aqueous solutions. Aluminium(III) as the third most abundant element, plays an important chemical role, in particular, in industry, geochemistry, environmental chemistry and medical chemistry (as a potential health hazard) (cf. Ref. 1). In the past sixty years or so, Raman spectroscopy has been used to elucidate the spectroscopic characteristics of hydrated cations, ion pairs and hydrolysis, while theoretical calculations have proven to be a valuable tool in understanding the complex behaviour of electrolyte solutions only in the past decade or two. Theoretical calculations have been used to model vibrational frequencies, and are used to verify the empirical spectroscopic assignments of aqua metal ions.

Though Raman spectroscopy has been used to elucidate the spectra of cations in aqueous solution, many features have been left unobserved. The strong quasielastic Rayleigh wing, which extends more than 500 cm<sup>-1</sup>, prohibits the clear detection of the weak low frequency modes of the metal aqua ions [2]. Raman difference spectroscopy has been developed to circumvent this difficulty. Subtraction of a synthetic background has also been employed to obtain baseline corrected Raman spectra. Both methods have their limitations, because dissolved ions (anions) alter the low frequency Raman spectrum of water [3]. Therefore, the Raman difference spectra obtained by subtracting the spectrum

of pure water from the spectrum of an aqueous solution must be viewed with caution (cf. Ref. 4-6).

On the other hand, it is not necessary to employ the Raman difference spectroscopic technique or to subtract a synthetic Rayleigh wing from the aqueous electrolyte spectra in order to obtain baseline corrected spectra. For most accurate relative intensity measurements, it has been shown [7] that it is essential to normalize the low frequency Raman data for the Bose-Einstein temperature factor,  $B$ , and a frequency factor,  $\nu$ . The construction of reduced or  $R$  - spectra, allowing an easier observation of the low wavenumber region (region of the Al-O modes) was discussed in ref. [6 and 7].

In this study, Raman spectra of aluminium chloride, perchlorate, nitrate, and sulfate solutions were obtained as a function of concentration and temperature in order to characterize the species formed and to measure the equilibria taking place in these solutions. It is known, that perchlorate is an extremely weak base which does not penetrate the first hydration sphere, therefore allowing the characterization of the hexaaquaaluminium(III) species. Nitrate, chloride and sulfate on the other hand quite frequently form ion pairs/complexes with metal ions.

Additionally, we modelled the vibrational spectra of hexaaqua Al(III) ion using *ab initio* molecular orbital calculations. *Ab initio* calculations were performed on the Al(III) hexaaqua species in order to support the interpretation of the spectroscopic data. For this purpose, Hartree-Fock (HF) and second order Møller- Plesset (MP) perturbation theory calculations with several different basis sets were employed. The geometry of the

hexaaquaaluminium(III) ion was optimized as explained in detail in the Experimental section. The explicit incorporation of the second hydration sphere was also undertaken by modelling the octadecaaqua cluster,  $[\text{Al}(\text{OH}_2)_{18}]^{3+}$ .

#### 4. 3. Experimental details and data analysis

The  $\text{Al}(\text{ClO}_4)_3$  stock solution was prepared by dissolving  $\text{Al}(\text{OH})_3$  with a stoichiometric amount of  $\text{HClO}_4$ . The salt was twice recrystallised.  $\text{AlCl}_3 \cdot 6\text{H}_2\text{O}$  was purified by bubbling  $\text{HCl}$  gas through a  $\text{AlCl}_3$  solution.  $\text{Al}(\text{NO}_3)_3 \cdot 9\text{H}_2\text{O}$  was recrystallised twice from an aqueous solution with ca. 0.2 m  $\text{HNO}_3$ . An  $\text{Al}_2(\text{SO}_4)_3$  stock solution was prepared by dissolving commercial-grade salt and precipitating the salt by adding p.a. (pro analysi) ethanol to the solution. The salts were dried over  $\text{CaCl}_2$  and stock solutions were prepared. The Al content of the solutions was determined complexometrically with xylenol orange as indicator. Solution densities were determined with a pycnometer (5 ml) at 25 °C. For further details concerning the preparation of the stock solutions of the aluminium salts and the chemical analysis see ref. (6c, 8, 9).

Raman spectra were obtained with a Coderg PHO Raman spectrometer using the 488.0 nm argon ion laser line with a power level of 0.9 W at the sample. The slit width of the double monochromator was set normally at  $1.8 \text{ cm}^{-1}$ . The scattered light was detected with a photo multiplier tube (PM tube) cooled to -20 °C, integrated with a photon counter and processed with a box-car averager interfaced to a personal computer. Two data points were collected per wavenumber. To increase the signal-to-noise ratio 6 data sets were collected for each scattering geometry ( $I_{\parallel}$  and  $I_{\perp}$ ). A quarter wave plate was used before

the slit served to compensate for grating preference.  $I_{\parallel}$  and  $I_{\perp}$  spectra were obtained with fixed polarisation of the laser beam by rotating the polaroid film by 90 °; which was placed between the sample and the entrance slit to give the scattering geometries:

$$I_{\parallel} = I(Y[ZZ]X) = 45\alpha'^2 + 4\gamma'^2 \quad (1).$$

$$I_{\perp} = I(Y[ZV]X) = 3\gamma'^2 \quad (2).$$

The isotropic spectrum,  $I_{iso}$  or  $I_{\alpha}$  was then constructed:  $I_{iso} = I_{\parallel} - 4/3 \cdot I_{\perp}$  (3).

Further spectroscopic details about the high temperature measurements using a home built oven and quartz tubes as ample containers, the band fit procedure and the procedure about R normalized Raman spectra are given in previous publications [5,6,10].

Raman spectra were also measured with equipment at the TU Freiberg Mining Academy as described in ref. [5 and 6c]. The spectra were excited with a 488.0 nm line of an Ar<sup>+</sup> laser at power levels ranging from 0.8 to 1.2 W. After passing the Zeiss double monochromator GDM 1000, with gratings with 1300 grooves per mm, the scattered light was detected with a cooled PM tube ITT 130 in the photon counting mode. The  $I_{\parallel}$  and  $I_{\perp}$  spectra (cf. Equations 1 and 2) were obtained with fixed polarisation of the laser beam by rotating an analyser placed between the sample and the entrance slit. Differences in monochromator transmittance for both polarizations were eliminated with a scrambler. The spectral slit widths employed varied and were normally set at 1.4 to 2.5 cm<sup>-1</sup>.

For quantitative measurements the perchlorate band,  $\nu_1$ -ClO<sub>4</sub><sup>-</sup> at 935 cm<sup>-1</sup>, was used as an internal standard. From the  $R_{iso}$  spectra the relative isotropic scattering coefficient  $S(\nu_1 \text{ AlO}_6)$  was obtained. The use of S values instead of J values has the

advantage that these relative scattering coefficients can be put on an absolute scale if an absolute standard reference is considered [cf. Ref. 6].

*Ab initio* calculations with the STO-3G [11], 3-21G [12], and 6-31G\*[13] basis sets were employed using the Gaussian 92 computer program [14]. All structures, unless otherwise indicated, were confirmed to be local minima by analytic frequency evaluation. To examine the effects of basis set extension, diffuse functions were added to the oxygen atoms, and for species with less than 6 waters, to aluminum, to give the 6-31+G\* basis [15]. The validity of neglecting the aluminium diffuse function on the hexaaqua complex was then checked by carrying out single point energy and force field calculations at the true HF/6-31+G\* level with the structure optimized without the aluminium diffuse function. The total energy was lowered by 2.90 and 4.30 kJ/mol at the HF/6-31+G\* and MP2/6-31+G\* levels, respectively. The displacement tolerances were within three times the default limits, so we did not see the need to re-optimize at these levels. Finally, second order Møller-Plesset perturbation theory (with frozen core electrons) was used to approximate correlation effects (as MP2/6-31G\* and MP2/6-31+G\*) for geometry, energy and analytic frequencies. For the octadeca - aquaaluminum(III) ion, the level of theory was restricted to the Hartree-Fock level.

#### 4. 4. Results and Discussion

##### 4. 4. 1. Hydration of Al(III) - General Remarks

Al(III) ions, because of their high charge to ionic radius ratio are strongly hydrated in aqueous solutions. Brønsted and Volqvartz [16] assumed the formation of  $[\text{Al}(\text{OH}_2)_6]^{3+}$

ions in these solutions. Much later the existence of the hexaaquaaluminium(III) ions was experimentally verified through  $^{17}\text{O}$  NMR spectroscopy [17] and it was also verified that the aqua ion is thermodynamically stable and kinetically very inert. The water exchange rate for water in  $[\text{Al}(\text{OH}_2)_6]^{3+}$  gave the following parameters:  $k_{\text{ex}}(25^\circ\text{C}) = (1.29 \pm 0.04) \text{ s}^{-1}$ ,  $\Delta H^\ddagger = (84.7 \pm 0.32) \text{ kJ}\cdot\text{mol}^{-1}$ ,  $\Delta S^\ddagger = (41.6 \pm 0.8) \text{ J}\cdot\text{K}^{-1}\cdot\text{mol}^{-1}$  and  $\Delta V^\ddagger = (5.7 \pm 0.2) \text{ cm}^3\cdot\text{mol}^{-1}$  [18]. Despite the 3+ charge it is believed that the  $\text{Al}^{3+}$  coordination sphere is too tightly packed to facilitate associative attack by an incoming water and so the parameters have been interpreted as indicative of a mechanism of water ligand dissociation. Kowall et al. [19] could show computationally a limiting dissociative mechanism (D) for the water exchange reaction on  $[\text{Al}(\text{OH}_2)_6]^{3+}$ . This means, the transition state structure is of the type  $\{[(\text{OH}_2)_5\text{Al}\cdots\text{OH}_2]^{3+}\}^\ddagger$ .

The structure of aluminium chloride hexahydrate,  $\text{AlCl}_3\cdot 6\text{H}_2\text{O}$ , has also been studied with X-ray and neutron diffraction [20] and a hexagonal unit cell has been confirmed. The space group was determined to be  $R3C (D_{3d}^6)$ . The structure is shown to consist of chains of the type:  $-\text{Al}(\text{OH}_2)_6]^{3+}-3\text{Cl}^- - \text{Al}(\text{OH}_2)_6]^{3+}-3\text{Cl}^-$ , proceeding parallel to the hexagonal c axis. The six water molecules surrounding a central aluminium ion form an essentially regular close-packed octahedron. The two hydrogen atoms associated with a given oxygen atom lie very nearly on the lines connecting the oxygen atom with the two nearest-neighbour chloride ions, one of which is a member of the same chain as the oxygen atom, while the other is a member of a neighbouring chain. The Al-O bond length was determined to be  $1.88 \pm 0.02 \text{ \AA}$  and the O-H distance is  $1.04 \pm 0.04 \text{ \AA}$ , while the other

O-H distance is  $0.99 \pm 0.06 \text{ \AA}$ .

#### 4. 4. 2. The $[\text{Al}(\text{OH}_2)_6]^{3+}$ vibrational spectrum - $\text{AlCl}_3$ , $\text{Al}(\text{ClO}_4)_3$ , and $\text{Al}(\text{NO}_3)_3$ solutions

The Raman spectra in the low frequency region of aluminium chloride solutions reveal only the hexaaqua modes (besides very weak librations and translations of the water molecules). For the perchlorate, nitrate and sulfate spectra, additional modes due to the internal vibrations of the anions are detected. In this chapter only the solution spectra of  $\text{Al}(\text{ClO}_4)_3$ ,  $\text{Al}(\text{NO}_3)_3$  and  $\text{AlCl}_3$  are discussed, because, as will be demonstrated below, no contact ion pairing between Al(III) and the corresponding anions can be observed and therefore the undisturbed hexaaquaaluminium(III) ion can be characterized.

The  $\text{ClO}_4^-$  ion possesses  $T_d$  - symmetry and has nine modes of internal vibrations spanning the representation  $\Gamma_{\text{vib}}(T_d) = a_1 + e + 2f_2$ . All modes of vibration are Raman active, but in i.r. only the  $f_2$  modes are active. The spectrum of an  $\text{Al}(\text{ClO}_4)_3$  solution shows the predicted four Raman-active bands for the tetrahedral  $\text{ClO}_4^-$ . The  $\nu_1(a_1)$   $\text{ClO}_4^-$  band centred at  $935 \text{ cm}^{-1}$  is totally polarised ( $\rho = 0.006$ ) whereas  $\nu_3(f_2)$   $\text{ClO}_4^-$  centred at  $1114 \text{ cm}^{-1}$  is depolarised as are the deformation modes  $\nu_4(f_2)$   $\text{ClO}_4^-$  at  $631 \text{ cm}^{-1}$  and  $\nu_2(e)$   $\text{ClO}_4^-$  at  $464 \text{ cm}^{-1}$ . The perchlorate mode  $\nu_2(e)$  at  $464 \text{ cm}^{-1}$  overlaps one of the weak  $\text{AlO}_6$  modes. Figure 4.1 presents the Raman spectrum of a 2 mol/L  $\text{Al}(\text{ClO}_4)_3$  solution at room temperature.

In aqueous  $\text{Al}(\text{NO}_3)_3$  solution, the nitrate anion possesses  $D_{3h}$  symmetry, and has six modes of internal vibrations spanning the representation  $\Gamma_{\text{vib}}(D_{3h}) = 1a_1' + 1a_2'' + 2e'$ .

The mode  $\nu_1(a_1')$  is Raman active but forbidden in infrared, while the  $e'$  modes are Raman and infrared active. The mode with the character  $a_2''$  is only infrared active. The aqueous solution, nitrate shows the following Raman modes:  $\nu_1(a_1')$  at  $1051\text{ cm}^{-1}$  (polarized),  $\nu_3(e')$  at  $1380$  (this mode shows two band components at  $1348$  and  $1410\text{ cm}^{-1}$  in dilute aqueous solutions; for asymmetric hydration of the nitrate anion as a possible explanation cf. for instance ref. 2) and  $\nu_4(e')$  at  $720\text{ cm}^{-1}$ , respectively. The infrared active mode,  $\nu_2(a_2'')$  can be observed at  $828\text{ cm}^{-1}$  and the overtone  $2\nu_2$  at  $1658\text{ cm}^{-1}$  is Raman active ( $a_1'$ ) and polarized. Figure 4.2 presents the Raman spectra of  $\text{Al}(\text{NO}_3)_3$  in the concentration range from  $0.21\text{ mol/L}$  to  $2.50\text{ mol/L}$  at room temperature. The spectra do not indicate any spectroscopic signs of the penetration of the nitrate anion into the first hydration sphere of  $\text{Al}(\text{III})$ . In concentrated solutions, the splitting of the  $\nu_3(e')$  mode rises to  $90\text{ cm}^{-1}$ , and the existence of outer-sphere complexes can be invoked (cf. results and discussions in ref. 6c).

The vibrational modes of the  $\text{AlO}_6$  unit possess  $O_h$  symmetry under the assumption that the water molecules can be approximated as point masses. This assumption is certainly sufficient in aqueous solutions. The 15 normal modes of the  $\text{AlO}_6$  unit span the representation  $\Gamma_{\nu,b}(O_h) = a_{1g}(R) + e_g(R) + 2f_{1u}(\text{i.r.}) + f_{2g}(R) + f_{2u}(\text{n.a.})$ . The modes  $\nu_1(a_{1g})$  (polarized),  $\nu_2(e_g)$  and  $\nu_5(f_{2g})$  (both depolarized) are Raman active and the modes  $\nu_3(f_{1u})$  and  $\nu_4(f_{1u})$  are i.r. active while the mode  $\nu_6(f_{2u})$  is not observable in solution spectra. Raman spectra of  $\text{AlCl}_3$  solutions were measured at five different concentrations, as shown in Figure 4.3 in the wavenumber range from  $250$  to  $650\text{ cm}^{-1}$ . Figure 4.4 presents the Raman spectrum of a  $2.78\text{ mol/L}$   $\text{AlCl}_3$  solution in R format (polarized, depolarized

and isotropic). The polarized mode at  $525\text{ cm}^{-1}$  is due to the  $\text{Al}^{3+}$ -oxygen symmetric stretching mode of the  $[\text{Al}(\text{OH}_2)_6]^{3+}$  cation,  $\nu_1(a_{1g}) \text{ AlO}_6$ . In the depolarized Raman spectrum the following modes can be assigned to  $\nu_2(e_g)$  and  $\nu_3(f_{2g})$  at  $438\text{ cm}^{-1}$  and  $332\text{ cm}^{-1}$ , respectively. The i.r spectrum of a  $3.14\text{ mol/L AlCl}_3$  solution is presented in Figure 4.5. The i.r. active mode  $\nu_3(f_{1u})$  was observed at  $598\text{ cm}^{-1}$ , while the second i.r active mode could not be observed. Our assignment of the  $\text{AlO}_6$  modes together with the values of  $[\text{Al}(\text{OH}_2)_6]^{3+}$  in solution [21], and in crystalline  $\text{AlCl}_3 \cdot 6\text{H}_2\text{O}$  [21,22] are given in Table 4.1. The Al(III) ion shows the three predicted Raman active  $\text{AlO}_6$  modes and the Raman frequencies do not coincide with the i.r. active mode reinforcing the centrosymmetric symmetry of the complex. The shift by deuteration of the  $\text{Al-OH}_2$  modes were studied in the  $\text{AlCl}_3 - \text{D}_2\text{O}$  system and are also given in Table 4.1. The shift in  $\nu_1$  on deuteration is given by  $\nu_1'$ :  $\nu_1[\text{m}(\text{H}_2\text{O})]/\text{m}[(\text{D}_2\text{O})]^{1/2} = 525 * \sqrt{18.02/20.03} = 498\text{ cm}^{-1}$ . The observed deuteration shift of  $\nu_1'$  is close to the calculated value and supports the assignment. In crystalline  $\text{AlCl}_3 \cdot 6\text{H}_2\text{O}$   $\nu_1$  is obtained at  $524\text{ cm}^{-1}$  ( $\nu_1' = 504\text{ cm}^{-1}$ ).

Besides the isotropic mode,  $\nu_1 \text{ AlO}_6$  at  $525 \pm 2\text{ cm}^{-1}$  (full width at half-height (fwhh) =  $44 \pm 2\text{ cm}^{-1}$ ) a weak, broad band centred at  $195 \pm 10\text{ cm}^{-1}$  can be observed in aqueous  $\text{AlCl}_3$  solution (cf. Figure 4.4). The band around  $195\text{ cm}^{-1}$  can also be seen in pure water and is moderately intense but slightly polarized. This band has been assigned to a restricted translational mode of the H-bonded water molecules. This band is strongly anion and concentration dependent (cf. ref. 4a and 24 and references cited therein). In concentrated  $\text{AlCl}_3$  solutions other H-bonds are important, namely  $\text{OH} \cdots \text{Cl}^-$  and the

intensity of the band due to  $\text{OH}\cdots\text{Cl}^-$  is weak in the isotropic Raman spectrum. The strengths of the  $\text{OH}\cdots\text{Cl}^-$  and  $\text{O}\cdots\text{OH}^-$  hydrogen bonds are similar, and therefore the frequency of this mode is not shifted [4a]. The parameters of the symmetric stretching mode of  $[\text{Al}(\text{OH}_2)_6]^{3+}$  for a 2.00 mol/L  $\text{AlCl}_3$  as a function of temperature shows the following: at 25 °C  $\nu = 525 \text{ cm}^{-1}$  ( fwhh = 44  $\text{cm}^{-1}$  ), at 75 °C  $\nu = 524 \text{ cm}^{-1}$  ( fwhh = 54  $\text{cm}^{-1}$  ) and at 125 °C  $\nu = 522 \text{ cm}^{-1}$  ( fwhh = 64  $\text{cm}^{-1}$  ). The frequency of the  $\nu_1(a_{1g}) \text{AlO}_6$  mode in aqueous solution does not show a significant shift with temperature. The half-width broadens with temperature, which is due to so called inhomogeneous broadening (cf. ref. 23 and references therein). Furthermore, the symmetry of the  $\nu_1$  mode persists. All those spectroscopic data suggest that the chloride does not penetrate the inner- sphere of the water molecules.

$\text{Al(III)}$  is a hard cation and this is reflected by its scattering intensity. The relative molar scattering intensity,  $S_h$  of the symmetric stretching mode  $\nu_1 \text{MO}_6$  of the aluminium triad  $\text{Al(III)} = 0.033$ ,  $\text{Ga(III)} = 0.14$  and  $\text{In(III)} = 0.22$  reflects the increase in the softness of these group III metal ions with an increase in the atomic number. The group IIIb metal ion,  $\text{Sc(III)}$ , gives an  $S_h$  value for the symmetric stretching mode ( $\nu_1 \text{MO}_6$ ) of 0.035 only slightly higher than  $\text{Al(III)}$  and also quite hard in the terminology of inorganic chemistry.

As a summary, this Raman spectroscopic analysis show clearly show, that over the applied temperature and concentration range and the varying anions (perchlorate, nitrate and chloride) the hexaaquaaluminium(III) complex is stable and no water- anion exchange in the first hydration sphere takes place. It is noteworthy that in  $\text{Al}_2(\text{SO}_4)_3$  solutions, water

anion exchange does takes place (cf. ref. 24). The vibrational spectra of  $\text{Al}_2(\text{SO}_4)_3$  solutions will be discussed below.

#### 4. 4. 3. Vibrational spectra of $\text{Al}_2(\text{SO}_4)_3$ solutions

When a polyatomic anion such as sulfate replaces water in the first coordination sphere of the cation, marked changes are expected to occur in the spectrum of the ligand, so that it is possible to differentiate between the bands of the ligated and the unligated sulfate. Additionally, a shift or splitting of the metal aqua modes and the appearance of a metal-ligand vibration at low frequencies ( $100 - 600 \text{ cm}^{-1}$ ) should be detectable [25].

In Figure 4.6 a, b and c we present the spectra of a 1.014 molal  $\text{Al}_2(\text{SO}_4)_3$  solution at 25, 58, and 106°C in the frequency range between  $40 \text{ cm}^{-1}$  and  $1400 \text{ cm}^{-1}$ . The Raman spectra of  $\text{Al}_2(\text{SO}_4)_3$  solutions reveal, that the sulfate penetrates the first hydration sphere of Al(III). All the expected features, which indicate sulfate ion pairing, can be observed in the aluminum sulfate spectra. Splitting of the Al(III) aqua mode, the appearance of a  $\text{Al}^{3+} - \text{OSO}_3^{2-}$  ligand mode and the split of the sulfate modes into "free" sulfate and ligated sulfate. (The "free" sulfate, which can be observed in the spectra of  $(\text{NH}_4)_2\text{SO}_4$  solution, was discussed by Rudolph et al. in ref. 24. The spectrum of aqueous  $(\text{NH}_4)_2\text{SO}_4$  solutions shows the "free", undistorted  $\text{SO}_4^{2-}$  ion has  $T_d$  - symmetry, and the nine modes of internal vibrations having the representation  $\Gamma_{\text{vib}}(T_d) = a_1 + e + 2f_2$  are: the  $\nu_1(a_1) - \text{SO}_4^{2-}$  band centred at  $981.4 \text{ cm}^{-1}$  is totally polarized ( $\rho = 0.006$ ), whereas  $\nu_3(f_2) - \text{SO}_4^{2-}$ , centred at  $1110 \text{ cm}^{-1}$ , and the deformation modes  $\nu_4(f_2) - \text{SO}_4^{2-}$  at  $617 \text{ cm}^{-1}$  and  $\nu_2(e) - \text{SO}_4^{2-}$  at  $452 \text{ cm}^{-1}$ , are depolarised.

The mode at 1012 cm<sup>-1</sup>, which does not occur in (NH<sub>4</sub>)<sub>2</sub>SO<sub>4</sub> solution (cf. Figure 4.6), represents the sulfato complex. The sulfato complex formation can be written according to eq.(4):  $[\text{Al}^{3+}(\text{H}_2\text{O})_6 \cdot \text{SO}_4^{2-}] \rightleftharpoons [\text{Al}^{3+}(\text{H}_2\text{O})_5\text{OSO}_3^{2-}] + \text{H}_2\text{O}$  (4). Reaction (4) is clearly an endothermic process (increase in aquaaluminium(III)sulfato complex with enhancing temperature). Further details of our qualitative and quantitative Raman study of the Al<sub>2</sub>(SO<sub>4</sub>)<sub>3</sub> - H<sub>2</sub>O system as a function of temperature and concentration are given in [24].

#### 4. 4. 4. *Ab initio* results

First, we considered hydrated aluminium ions of the general type  $[\text{Al}(\text{OH}_2)_n]^{3+}$ , where all waters are in the first/inner-sphere, denoted as Al[n+0], with n from 1 to 6. The point group of the mono- through hexaaqua complexes are C<sub>2v</sub>, D<sub>2d</sub>, D<sub>3h</sub>, S<sub>4</sub>, C<sub>3v</sub>, and T<sub>h</sub> symmetry, respectively. Structural parameters and thermodynamic data of the clusters under consideration can be obtained from the corresponding author. Schematic presentations of the Al-O bond length, the OH bond length, the HOH angle and the incremental binding enthalpy at 298 K are given in Figures 1S - 4S of the Supplementary Information service, respectively. There have been several previous investigations dealing with the hydration of trivalent aluminium water clusters using *ab initio* calculations. However, none of these discuss the calculation of vibrational frequencies. There is only one tabulation of frequencies of which we are aware (cf. Ref. 26). We feel that a more thorough exposition is warranted. This is one of a few studies dealing with the results using HF and MP2 calculations in combination with a series of different basis sets (STO-

3G to 6-31+G\*). For clarity only the results using the 6-31G\* and 6-31+G\* basis sets are presented.

In Figure 1S the Al-O bond lengths are plotted as a function of the number of water molecules,  $n$ , in the first sphere. The bond lengths increase with increasing  $n$ , a consequence of the steric interactions within the first shell and the concomitant decrease in aluminum-water interaction. Figure 2S and 3S present the O-H bond length and H-O-H angle as a function of coordination number. The decrease in O-H bond length can be explained by the increase in Al-O distance, because the farther away the aluminum is from the oxygen, the less it can polarize and weaken the O-H bond.

The frequency of the symmetric stretching mode,  $\nu_1\text{AlO}_n$ , as a function of  $n$  are presented in Table 4.2. For increasing  $n$ , the frequency of the symmetric stretching mode,  $\nu_1\text{AlO}_n$  is decreasing monotonically. It is noteworthy that the frequency  $\nu_1\text{AlO}_6$  is underestimated, as illustrated by both our data and those of Wasserman et al. [26].

The incremental gas phase hydration enthalpies for the reaction:  $\text{Al}^{3+} + n \text{H}_2\text{O} \rightarrow [\text{Al}(\text{OH}_2)_n]^{3+}$  as a function of  $n$  are plotted in Figure 4S. As shown in this Figure, as the coordination number increases, the hydration enthalpy becomes less exothermic and, thus the binding energy per water molecule becomes smaller. This behaviour can be attributed to an increasing water-water repulsion when the first coordination sphere is subsequently filled. The gas phase binding enthalpy for the hexaaqua cluster varies from -1337 to -1511 kJ/mol, depending on the level of theory.

Besides the structure and energetics of the aluminium water clusters, the main aim

was to calculate the vibrational spectrum of the aquaaluminium(III) ion. As we demonstrated in recent papers [10,27] for a realistic description of the metal -oxygen modes a second hydration sphere has to be taken into account. Therefore, we calculated a much larger aluminium water cluster, the octadecaaqua Al(III) denoted as Al[6+12]. In part A we will give the results for the  $[\text{Al}(\text{OH}_2)_6]^{3-}$ , which models the complete inner-sphere. In part B we will describe the aluminium hexaaqua ion with a complete second hydration sphere.

#### A. Hexaaquaaluminium(III) ion, $[\text{Al}(\text{OH}_2)_6]^{3-}$

A summary of the Al-O bond length compiled from literature data are given in Table 4.3. These literature data, combined with our results discussed later, demonstrate the sensitivity of the computed Al-O bond length to the calculation quality. Clearly, a single-zeta basis set is inadequate, giving bond lengths that are much too short. Split-valence or double zeta basis sets are better, giving values closer to the experimental value of 1.90 Å [28]. Our results contrast with our results for zinc (cf. Results in ref. 27 a) in that adding polarization functions decreases the Al-O bond length whereas including correlation increases it.

Literature values of the Al-O distance range from 1.79 (CNDO) to 1.956 Å (Mp2-*fc/cc-pVDZ*). Marcos and co-workers [29] report a value of 1.907 Å at the 3-21G\* level, and a value of 1.925 Å when the second sphere is modelled with a self-consistent reaction field. Our ab initio results give an opposite trend to Marcos results, giving 1.901 Å for the hexaaquaaluminium(III) cluster and 1.883 Å if 12 water molecules are explicitly included

in the second hydration sphere (results at the 3-21G level). This trend persists at all levels investigated. These findings indicate only a small (0.02 Å) hydration effect on the Al-O bond length. These findings imply that the gas phase geometries for the  $[\text{Al}(\text{OH}_2)_6]^{3-}$  cluster are almost independent of solvent effects. Therefore, the comparison of the calculated *in vacuo* Al-O distance with the experimental observed value in aqueous solution is legitimate.

Our *ab initio* calculations demonstrate that the hexaaquaaluminium(III) complex is a stable species, and our Al-O and O-H bond length and the H-O-H bond angle, and the total energy in a.u. for the hexaaquaaluminium(II) ion ( $T_h$  symmetry) are given in Table 4.4. Our values correspond well with the high level calculations published [26,30-32]. The equilibrium aluminium-oxygen distance ( $r_e$ ) of 1.935 Å at HF/6-31G\* level is in fair agreement with the X ray diffraction result of 1.90 Å [28]. (It has to be noted that diffraction measurements give  $r_s$ , the averaged position of atoms at temperature of experiment, and not  $r_e$ .) Figure 4.7 presents the model for  $[\text{Al}(\text{OH}_2)_6]^{3-}$ .

The  $[\text{Al}(\text{OH}_2)_6]^{3-}$  species, taking the hydrogens into account, possesses  $T_h$  symmetry. In Table 4.5 the unscaled HF/6-31G\*, HF/6-31+G\* and MP2/6-31G\* frequencies together with the assignment of the modes are reported. The 51 normal modes have the representation  $\Gamma_{\text{vib}} = 3a_g + a_u + 3e_g + e_u + 5f_g + 8f_u$ . The calculated frequencies at the three highest levels of theory represent the vibrational spectrum of  $[\text{Al}(\text{OH}_2)_6]^{3-}$  in solution in principle. However, the calculated frequency (at HF/6-31G\* level) is almost 62  $\text{cm}^{-1}$  (ca. 14 %) smaller than the observed symmetric stretching mode,  $\nu_1 \text{AlO}_6$  at 525  $\text{cm}^{-1}$

Inspection of Tables 4.4 and 4.5 indicate that adding diffuse functions to the basis set or including correlation energy by means of MP2 calculations does not change this disagreement. As pointed out in previous publications, the discrepancy is due to the lack of the second hydration sphere. This could be rectified by scaling the frequencies or, preferably, by including the second sphere water molecules explicitly.

The calculated frequencies may be scaled in such a way to reproduce the measured  $\nu_1$   $\text{AlO}_6$  frequency. The scaled frequencies are given in Table 4.6. Although this technique allows good prediction of the  $\nu_3$  mode to within  $15 \text{ cm}^{-1}$ , the  $\nu_2$  mode and  $\nu_5$  mode are underestimated (to within 34, respectively  $103 \text{ cm}^{-1}$ ). It will be shown, that the resolution of this discrepancy involves the explicit incorporation of the second hydration sphere.

The electronic binding energy of the hexaaqua ion,  $[\text{Al}(\text{OH}_2)_6]^{3-}$ , was calculated according to  $\Delta E_b = -E_{\text{hexahydrate}} + 6 \cdot E_{\text{water}} + E_{\text{cation}}$ . (5).

The binding energies of the hexaaqua complex,  $[\text{Al}(\text{OH}_2)_6]^{3-}$ ,  $\Delta E_b$  (at 0 K) were calculated and are given in Table 4.7. After zero-point, vibrational, translational and rotational energy corrections were made, the theoretical binding energy,  $\Delta E_b^{298}$ , at 298.15 K could be obtained, and adding  $\Delta PV = R \cdot T \cdot \Delta n$  ( $\Delta n$ , the number of water molecules) gives  $\Delta H$ . The values for the binding enthalpy contributions due to the formation of the hexaaqua ion at different basis sets/levels of theory,  $\Delta H_b^{298}$ , are also included in Table 4.7. The single-ion hydration enthalpy,  $\Delta H_{\text{hyd}}^0$ , for Al(III) was measured to be  $-4659.7 \text{ kJ/mol}$  [33]. The calculated binding enthalpies,  $\Delta H_b^{298}$ , account only for ca. 50 % of the measured single ion hydration enthalpy at 298.15 K showing the importance of the second hydration sphere.

## B. Octadecaaqua Al(III) cluster ( Al[6+12])

The disagreement between theory and experiment for the  $\nu_1$  symmetric stretching mode was hypothesized to be due to the lack of the second hydration sphere. Ample evidence for this interpretation has been previously provided for the case of the tetraaqua Li(I) [4], the hexaaqua Cd(II) [23 b] the hexaaqua Mg(II) [23 a] and the hexaaqua Zn(II) [27 a] and hexaaqua Sc(III)[27 b] ions where, at the HF/6-31G\* level, the frequencies were raised by 18, 36, 28, 51, and 50  $\text{cm}^{-1}$ , respectively. In these examples, 12 explicit water molecules were included in the second hydration sphere (except Li(I), for which 4 waters were incorporated). The approach that we had so successfully developed earlier was applied to the aluminium hexaaqua ion. The octadecaaqua aluminium(III) cluster was optimized and a local minimum, corresponding with symmetry  $T_h$ , was found (structure C) and is presented in Figure 4.8. During the course of our optimization of the analogous Mg species, two other structures (denoted as A and B) with symmetry  $T_h$  were found (cf. Pye and Rudolph, in ref. 23 a). In structure A, the second- sphere water molecules are embedded in the symmetry planes, whereas in structure B, they are bisected by the symmetry planes. However, neither of these structures represented an energy minimum. Our results call therefore the structure of the same octadecaaqua metal ion(s) published by Siegbahn and coworkers [34] into question. The structure published by Siegbahn et al. [34] corresponds with our non- equilibrium structure B. The geometrical and thermochemical results of structure C are given in Table 4.8. The Al-O bonding undergoes a slight shortening of 0.025 Å when 12 water molecules are added to constitute the water

molecules in the second hydration sphere. The Al-O distance at HF/6-31G\* level for Al[6+0] is 1.935 Å, compared with Al[6+12] for which Al-O<sub>first- sphere</sub> is 1.910 Å and Al-O<sub>second- sphere</sub> is 4.114 Å. The H- bond distances are 1.786 Å (HF/6-31G\*) and 1.805 Å (HF/6-31+G\*). The decrease in Al-O bond length in the first hydration- sphere of the cluster Al[6+12] arises because the water molecules in the second sphere polarize the waters of the first shell, so that the interaction of Al<sup>3+</sup> and the first - shell water is enhanced.

To demonstrate the polarization of the water, we compare free water, water dimer, water in [Al(OH<sub>2</sub>)<sub>6</sub><sup>3+</sup>] and first-sphere water in [Al(OH<sub>2</sub>)<sub>18</sub><sup>3+</sup>]. The relevant OH distances for these species are 0.947, 0.952, 0.964 and 0.971, respectively. This ranks the water molecule by degree of polarization. Similarly, the Mulliken charges on the water hydrogens are 0.43, 0.48, 0.57, and 0.60, and on oxygen, -0.87, -0.93, -0.92, and -1.02, respectively. These data at the HF/6-31G\* level demonstrate clearly the polarization.

The electronic binding energy of the octadecaaqua ion, [Al(OH<sub>2</sub>)<sub>18</sub><sup>3+</sup>], was calculated according to  $\Delta E_b = -E_{\text{octadecahydrate}} + 18 \cdot E_{\text{water}} + E_{\text{cation}}$ . (6)

The binding energies of the octadecaaqua complex, [Al(OH<sub>2</sub>)<sub>18</sub><sup>3+</sup>],  $\Delta E_b$  (at 0 K) were calculated and are given in Table 4.8. The magnitude of the calculated enthalpy of formation (-4184.7 kJ/mol) is due to the electronic contribution to the binding energy (-4336.43 kJ/mol), with smaller corrections from zero-point, vibrational, translational, rotational, and PV energy contributions. This may be compared with the single ion hydration enthalpy (-4659.7 kJ/mol), which also contains corrections for water

vaporization and the Born energy of the octadecaaqua cluster. About 90 % of the energy is recovered. The 500 kJ/mol difference is similar to that found for scandium(III) [27 b].

For strong ion-dipole interactions such as those for metal ion water clusters, the basis set superposition error (BSSE) should be incorporated. The small BSSE correction would not affect our results significantly. On the other hand, BSSE corrections are not as important when one is using a diffuse basis set, since the diffuse functions correct for BSSE by describing the distant regions properly (cf. Feller and co-workers in ref. 35).

The unscaled frequencies for the  $[\text{Al}(\text{OH}_2)_{18}]^{3-}$  at the HF/6-31G\* level are given in Table 4.9. The 159 normal modes span the representation  $\Gamma_{\text{vib}}(\text{T}) = 13\text{a}(\text{R}) + 13\text{e}(\text{R}) + 40\text{f}(\text{IR}, \text{R})$ . The assignments as well of the normal modes are also given in Table 4.9. In some cases the  $\text{Al-O}_6$  modes ( $\Gamma_{\text{vib}}(\text{T}) \text{AlO}_6 = \text{a}(\text{R}) + \text{e}(\text{R}) + 4\text{f}(\text{IR}, \text{R})$ ) couple strongly with either librational modes of the second-sphere water molecules or restricted translational modes. Compared to our gas phase cluster model, in real solutions the symmetry allowed coupling would not be as severe. In any case the modes  $\nu_1$ ,  $\nu_2$ , and  $\nu_3$ , the stretching modes of  $\text{AlO}_6$  and the deformation modes at  $316 \text{ cm}^{-1}$ ,  $261 \text{ cm}^{-1}$  and  $204 \text{ cm}^{-1}$  (f modes) may be unambiguously assigned. The symmetric stretch of the  $\text{AlO}_6$  unit is actually coupled to a librational mode of the waters of the second sphere. They would normally both appear at  $519 \text{ cm}^{-1}$  at the HF/6-31G\* calculations, but they split into 497 and  $542 \text{ cm}^{-1}$  (cf. Results in Table 4.9). The close agreement of the calculated  $\nu_1 \text{ AlO}_6$  frequency with the experimental value shows again the importance of taking into account the second hydration sphere in the model calculations. The inclusion of the second hydration sphere, denoted

$[\text{Al}(\text{H}_2\text{O})_6^{3+}](\text{H}_2\text{O})_{12}]$ , [6+12], raises the frequency of the  $\nu_1 \text{AlO}_6$  mode by  $66 \text{ cm}^{-1}$  (14 percent), relative to the [6+0] species.

The internal modes of the water molecules,  $\nu_2(\text{OH})$ ,  $\nu_1(\text{HOH})$  and  $\nu_3(\text{OH})$  occur as groups, as inner-sphere and outer-sphere waters. Al(III) in aqueous solution is one of the rare cases, where one can experimentally distinguish between the modes of the strongly bound inner-sphere water molecules from modes of the water bulk phase (cf. Rudolph and Schönherr [21 b]). The stretching modes of the water molecules of the inner-sphere, show up at lower wavenumbers, e.g. the symmetric stretch OH at ca.  $3060 \text{ cm}^{-1}$ , whereas the deformation mode appears at higher wavenumbers, compared to bulk water. This spectroscopic behaviour is correctly reproduced by our model. We emphasize that, in order to compare them to experimental values, these experimental values have to be corrected for unharmonicity and the calculated frequencies have to be scaled in order to account for known deficiencies in theoretical techniques, however, the trends should be approximately the same. The wavenumbers in  $\text{cm}^{-1}$  of water (gas phase), outer-sphere water in the octadecaaqua cluster, inner-sphere hexaaqua, and inner-sphere water in the octadecaaqua cluster compare as follows: For the bending mode,  $\nu_2(\text{OHO})$ , we calculated 1826, 1820, 1850 and 1910 respectively. For the symmetric OH stretch,  $\nu_1(\text{OH})$  we calculated 4070, 4000, 3980, and 3700 respectively and for the asymmetric OH stretch we got 4189, 4106, 3950, and 3720 respectively. These trends clearly reflect both, coordination to the Al(III) cation and subsequent polarization, and that the hydrogen bonding to the outer-sphere water molecules having a large influence on the water modes as noted above.

#### 4. 5. Conclusions

The weak, polarized Raman band assigned to  $\nu_1(a_{1g})$   $AlO_6$  mode of the hexaaqua  $Al(III)$  ( $T_h$ ;  $O_h$  symmetry for  $AlO_6$  unit) has been studied over the temperature range from 25 to 125 °C. The isotropic scattering geometry in R format was employed in order to measure the true vibrational contribution of the band and account for the Boltzmann temperature factor  $B$  and the frequency factor,  $\nu$ . The band profile as a function of temperature has been examined analytically to extract the parameters: position of band maximum, fwhh, integral intensity of the band and relative molar scattering coefficient,  $S_h$ , over the temperature range measured. The dependence on concentration has also been measured. The position of the  $\nu_1(a_{1g})$   $AlO_6$  mode shifts only about 2  $cm^{-1}$  to lower frequencies and broadens about 19  $cm^{-1}$  for a 100 °C temperature increase. The Raman spectroscopic data suggest that the  $[Al(OH_2)_6]^{3+}$  ion is thermodynamically stable in chloride, perchlorate and nitrate solution over the temperature and concentration range measured.

Besides the polarized mode at 525  $cm^{-1}$ , two weak depolarized modes at 438  $cm^{-1}$  and 332  $cm^{-1}$  have been assigned to  $\nu_2(e_g)$  and  $\nu_5(f_{2g})$  of the aluminium hexaaqua ion. The infrared active mode at 598  $cm^{-1}$  has been assigned to  $\nu_3(f_{1u})$ .

*Ab initio* geometry optimizations of  $[Al(OH_2)_6]^{3+}$  were carried out at the Hartree-Fock and second order Møller- Plesset levels of theory, using various basis sets up to 6-31+G\*. The global minimum structure of the hexaaquaaluminium(III) species corresponds with symmetry  $T_h$ . The unscaled vibrational frequencies of the  $[Al(OH_2)_6]^{3+}$  were reported,

and the unscaled vibrational frequencies of the  $\text{AlO}_6$  unit are lower than the experimental frequencies (ca. 15 %), but scaling the frequencies reproduces the measured frequencies. The theoretical binding enthalpy for  $[\text{Al}(\text{OH}_2)_6]^{3-}$  was calculated and accounts for ca. 64% of the experimental single ion hydration enthalpy for Al(III). *Ab initio* geometry optimizations and frequency calculations are also reported for a  $[\text{Al}(\text{OH}_2)_{18}]^{3-}$  (Al[6+12]) cluster with 6 water molecules in the first sphere and 12 water molecules in the second sphere. The global minimum corresponds with T symmetry. The calculated frequencies of the aluminium [6+12] cluster correspond well with the observed frequencies in solution. The  $\nu_1$   $\text{AlO}_6$  (unscaled) mode occurs at  $519\text{ cm}^{-1}$  in fair agreement to the experimental value. The internal water modes in the aquaaluminium(III) clusters are compared with water (gas phase) and discussed in terms of the polarizing effect of Al(III) and the subsequent formation of strong H-bonds of the water molecules of the first-sphere with the ones in the second sphere. The theoretical binding enthalpy for  $[\text{Al}(\text{OH}_2)_{18}]^{3-}$  was calculated and is very close to the experimental single ion hydration enthalpy for Al(III).

#### Acknowledgment.

The authors thank the Computing and Communications Department, Memorial University of Newfoundland, for computer time with a special thanks to DEC for providing an Alpha server 4100. W. W. R. thanks Dr. Gert Irmer, TU Freiberg Mining Academy Freiberg/Saxony for the use of his Raman spectrometer and for helpful discussions.

Table 4.1: The  $\text{AlO}_6$  skeleton modes ( $\text{AlO}_6$  unit possesses  $O_h$  symmetry), Raman and i.r. spectroscopic frequencies ( $\text{cm}^{-1}$ ) in aqueous  $\text{Al}(\text{ClO}_4)_3$ ,  $\text{AlCl}_3$  and  $\text{Al}(\text{NO}_3)_3$  solutions. (In  $\text{Al}(\text{ClO}_4)_3$  solutions the intensive  $\text{ClO}_4^-$  mode at  $461 \text{ cm}^{-1}$  overlaps  $\nu_2(e_g)\text{AlO}_6$  completely.) Additionally the modes of  $\text{AlO}_6$  in crystalline  $\text{AlCl}_3 \cdot 6\text{H}_2\text{O}$  (space group  $R3c (D_{3d}^6)$  ( $z = 2$ )) are given for comparison.

assignments and activities of $\text{AlO}_6$	exper. * frequencies in $\text{H}_2\text{O}$	exper. * frequencies in $\text{D}_2\text{O}$	assignments and activities in crystalline $\text{AlCl}_3 \cdot 6\text{H}_2\text{O}$	exper. ** frequencies
$\nu_1(a_{1g})$ Ra	$525 \pm 1$ (0.005)	$505 \pm 1$ (0.005)	$\nu_1(A_{1g})$ Ra	524
$\nu_2(e_g)$ Ra	$438 \pm 2$ (0.75)	$420 \pm 2$ (0.75)	$\nu_2(E_g)$ Ra	432
$\nu_3(f_{1u})$ i.r.	$598 \pm 2$	$564 \pm 2$	$\nu_3(A_{2u})$ i.r.	536(TO), 546(LO)
$\nu_4(f_{1u})$ i.r.	not observed	not observed	$\nu_4(A_{2u})$ i.r.	313(TO), 314(LO)
$\nu_5(f_{2u})$ Ra	$332 \pm 2$ (0.75)	$302 \pm 2$ (0.75)	$\nu_5(A_{1u})$ Ra ( $E_u$ )	295 310
$\nu_6(f_{2u})$ -	not active	not active	$\nu_6(A_{2u})$ i.r. ( $E_u$ ) i.r.	239(TO), 254(LO) 226(TO), 261(LO) 213(TO), 216(LO)

\* Note: in brackets the depolarization ratio.

\* Data partially taken from W. W. Rudolph and S. Schönherr, Z. Phys. Chem. (Leipzig), **270** (1989) 1121-1134.

\*\* Raman data from W. W. Rudolph and S. Schönherr, Z. Phys. Chem. (Leipzig), **270** (1989) 1121-1134. and D. M. Adams, D. J. Hills, J. Chem. Soc. Dalton Trans. (1978) 782-788.

Infrared data from G. Wäschenbach, H. D. Lutz, Spectrochim. Acta, **42A** (1986) 983-984.

Table 4.2: The Al-O symmetric stretching frequency as a function of n, the coordination number, of the aqua Al(III) cluster ion for four different basis sets/ levels of theory.

n	HF/6-31G*	HF/6-31+G*	MP2/6-31G*	MP2/6-31+G*
1	789.0	795.9	756.1	755.8
2	598.3	604.6	577.3	578.7
3	565.3	566.2	548.0	544.8
4	534.1	533.8	518.7	515.2
5	495.3	495.1	484.6	479.7
6	463.1	461.8	454.6	449.3

Table 4.3: Literature compilation of calculated Al-O distances as a function of the level of theory and basis set applied.

Al-O bond length/Å	Ref.	Computational details
1.79	1	CNDO
1.91	2	6-21G
1.945 1.912	3	6-31G DZP
1.907 1.925	4	3-21G 3-21G + SCRF
1.905	5	3-21G*
1.956 1.927 1.911	6	MP2-fc/cc-pVDZ MP2-fc/cc-pVTZ MP2/cc-pwCVTZ
1.935	7	HF/6-31G*
1.940 1.948 1.944	8	HF/SBK+6-31G* MP2/SBK+6-31G* BP91/TZP
1.912 1.892 1.933	9	HF/3-21G** HF/3-21G** + 13H <sub>2</sub> O MP2/6-311+G**

- [1] V. M. Tretyak, V. I. Baranovskii, O. V. Sizova, G. V. Koshevnikova, *J. Struct. Chem.*, 19, 519-523 (1978) (Trans. of Zh. Strukt. Khim., 19, 594-599 (1978))
- [2] M. D. Newton, H. L. Friedman, *J. Chem. Phys.*, 83, 5210-5218 (1985)
- [3] M. M. Probst, *Chem. Phys. Letters*, 137, 229-233 (1987)
- [4] E. Sanchez Marcos, R. R. Pappalardo, D. Rinaldi, *J. Phys. Chem.*, 95, 8928-8932 (1991)
- [5] F. Ramondo, L. Bencivenni, V. Rossi, R. Caminiti, *J. Mol. Struct (Theochem)*, 277, 185-211 (1992)
- [6] E. Wasserman, J. R. Rustad, S. S. Xantheas, *J. Chem. Phys.*, 106, 9769-9780 (1997)
- [7] J. M. Ruiz, M. H. McAdon, J. M. Garces, *J. Phys. Chem. B*, 101, 1733-1744 (1997)
- [8] T. Kowall, P. Caravan, H. Bourgeois, L. Helm, F. P. Rotzinger, A. E. Merbach, *J. Am. Chem. Soc.*, 120, 6569-6577 (1998)
- [9] J. D. Kubicki, D. Sykes, S. E. Apitz, *J. Phys. Chem. A*, 103, 903-915 (1999)

Table 4.4: Optimized geometry of hexaaqua Al(III).

	Al-O (Å)	O-H (Å)	H-O-H (deg)	-E (Hartrees)
HF/STO-3G	1.830	0.980	106.2	688.489873
HF/3-21G	1.901	0.978	109.0	693.544333
HF/6-31G*	1.934	0.963	107.4	697.180895
MP2/6-31G*	1.942	0.985	107.0	698.342160
HF/6-31+G*	1.935	0.963	107.5	697.191601
MP2/6-31+G*	1.946	0.986	107.0	698.368824

Table 4.5: Unscaled HF/6-31G\*, HF/6-31+G\* and MP2/6-31G\* Frequencies (in cm<sup>-1</sup>), intensities and force constants of the modes of the hexaaqua-Al(III) ion;  $\Gamma_{\text{vib}} = 3a_g(\text{R,tp}) + a_u(\text{n.a.}) + 3e_g(\text{R,dp}) + e_u(\text{n.a.}) + 5f_g(\text{R,dp}) + 8f_u(\text{i.r.})$ .

HF/6-31-G* a)			HF/6-31+G* a)			MP2/6-31G* a)			mode	activity
freq.	I	f.c.	freq.	I	f.c.	freq.	I	f.c.		
161.0	3.74	0.068	162.5	0.775	0.068	149.5	6.66	0.061	$\delta$ O-Al-O( $f_u$ )	i.r.
225.4	0.109	0.140	229.8	0.0747	0.142	199.8		0.113	$\delta$ O-Al-O( $f_g$ )	R.a.
263.0	5.20	0.184	261.7	6.36	0.184	242.2	10.3	0.156	$\delta$ O-Al-O( $f_u$ )	i.r.
262.7	-	0.041	284.7	-	0.048	264.6	-	0.042	$\tau$ HOH( $e_u$ )	n.a.
355.3	1.64	0.076	372.8	0.713	0.0837	353.0		0.075	$\tau$ HOH( $f_g$ )	R.a.
362.1	0386	0.440	356.1	0.381	0.424	366.2		0.447	$\nu_{\text{as}}$ Al-O( $e_g$ )	R.a.
463.1	1.63	0.745	461.8	2.42	0.742	454.6		0.724	$\nu_s$ Al-O( $a_g$ )	R.a.
520.4	-	0.161	534.6	-	0.17	518.0	-	0.160	$\tau$ HOH( $a_u$ )	n.a.
527.9	35.6	0.549	522.2	17.7	0.60	506.3	278	0.240	$\nu_{\text{as}}$ Al-O( $f_u$ )	i.r.
572.6	2.83	0.218	579.0	2.49	0.223	518.4		0.176	$\omega$ HOH( $f_g$ )	R.a.
606.5	563	0.282	603.1	546	0.272	565.4	301	0.393	$\omega$ HOH( $f_u$ )	i.r.
762.3	0.0054	0.400	757.8	0.0367	0.396	716.6		0.355	$\rho$ HOH( $f_g$ )	R.a.
804.0	589	0.516	801.0	558	0.506	763.1	520	0.486	$\rho$ HOH( $f_u$ )	i.r.
1844.2	408	2.187	1841.5	406	2.182	1735.0	366	1.938	$\delta$ HOH( $f_u$ )	i.r.

Table 4.5: Unscaled HF/6-31G\*, HF/6-31+G\* and MP2/6-31G\* Frequencies (in cm<sup>-1</sup>), intensities and force constants of the modes of the hexaaqua-Al(III) ion;  $\Gamma_{\text{vib}} = 3a_g(\text{R,tp}) + a_u(\text{n.a.}) + 3e_g(\text{R,dp}) + e_u(\text{n.a.}) + 5f_g(\text{R,dp}) + 8f_u(\text{i.r.})$ .

1843.4	5.01	2.190	1839.7	3.49	2.183	1733.8		1.940	$\delta\text{HOH}(e_g)$	R.a.
1854.2	0.0856	2.195	1851.9	0.244	2.189	1745.7		1.944	$\delta\text{HOH}(a_g)$	R.a.
3880.0	28.9	9.266	3872.7	26.2	9.230	3618.6		8.055	$\nu_s\text{OH}(e_g)$	R.a.
3886.3	641	9.302	3878.2	600	9.262	3623.4	550	8.083	$\nu_s\text{OH}(f_u)$	i.r.
3912.9	207	9.450	3903.0	246	9.401	3645.8		8.198	$\nu_s\text{OH}(a_g)$	R.a.
3951.5	47.1	9.998	3948.2	39	9.980	3696.8		8.741	$\nu_{as}\text{OH}(f_g)$	R.a.
3953.3	839	10.01	3950	786	9.992	3698.0	738.7	8.749	$\nu_{as}\text{OH}(f_u)$	i.r.

\* R = Raman active with tp = totally polarized and dp = depolarized; i.r. = infrared active and n.a. = mode not allowed.

a) For each individual basis set/level of theory the i.r. activities (km/mol) and the Raman intensities ( $\text{\AA}^4/\text{a.u.}$ ) are given (because of the mutual exclusion rule only modes with subscript g are Raman active and modes with subscript u i.r. active), in the third column, the force constants (mdyn/ $\text{\AA}$ ) are given. At MP2 level only the i.r. intensity are given (km/mol) together with the force constants (mdyn/ $\text{\AA}$ ); no Raman activities were obtained at this level.

Table 4.6: Our experimental frequencies ( $\text{cm}^{-1}$ ) for the skeletal  $\text{AlO}_6$  modes ( $O_h$ ) in aqueous  $\text{AlCl}_3$  solutions. The scaled ab initio frequencies for four different basis sets at the HF and MP2 levels of theory are presented.

Modes	exper. Frequencies	HF/6-31G*	HF/6-31+G*	MP2/6-31G*	MP2/6-31+G*
$\nu_1(a_{1g})$ Ra	$525 \pm 1$ (0.003)	525	525	525	525
$\nu_2(e_g)$ Ra	$438 \pm 2$ (0.75)	410	404	422	416
$\nu_3(f_{1u})$ i.r	$598 \pm 2$	598	592	584	583
$\nu_4(f_{1u})$ i.r.	not observed	298	297	279	282
$\nu_5(f_{2g})$ Ra	$332 \pm 2$ (0.75)	255	261	230	229
$\nu_6(f_{2u})$ -	not active	182	184	172	177

Table 4.7: Calculated Electronic Binding Energies,  $\Delta E_b^0$ , at 0 K and the Computed Enthalpies for the Al(III) Hexaaqua Cluster,  $\Delta H_b^{298}$ , at 298.15 K (All Energies in kJ/mol) at Four Different Basis Sets/Level of Theory.

Basis set/level of theory	$\Delta E_b^0$	$\Delta H_b^{298}$
HF/6-31G*	-2986.62	-2909.93
HF/6-31+G*	-2904.51	-2827.53
MP2/6-31G*	-3103.87	-3029.61
MP2/6-31G*	-2970.21	-2895.16

Table 4.8: Structural parameters, energy (Hartree) and thermodynamic parameters ( $\Delta E_B$ , binding energy, at zero K and  $\Delta H_{298}^\ominus$ , the enthalpy of the cluster formation at 298.15 K) calculated for the  $[\text{Al}(\text{OH}_2)_{18}]^{3-}$  cluster denoted Al[6+12].

bond length (in Å)	HF/3-21G	HF/6-31G*	HF/6-31+G*
Al-O (first water sphere)	1.8830	1.9097	1.9090
Al-O (second water sphere)	3.9411	4.1145	4.1390
O-H (first water sphere)	0.9931	0.9708	0.9690
	0.9683	0.9526	0.9530
O-H(A) (second water sphere)	0.9807	0.9547	0.9546
	1.6398	1.7861	1.8051
O-H(B) (second water sphere)			
HO1...H bond length			
angle $\Theta$ (deg)			
HOH angle (first water sphere)	112.46	110.06	109.87
HOH angle (second water sphere)	112.15	106.94	106.91
energy (hartree)	-1601.352994	-1609.823966	-1609.884351
$\Delta E_B$ (0 K) (kJ/mol)	-5573.56	-4336.43	-4164.31
$\Delta H_{298}^\ominus$ (kJ/mol)	-5367.21	-4184.70	-4014.82

**Table 4.9: Unscaled HF/6-31G\* Frequencies, intensities (i.r., Raman) and force constants of the octadeca- aqua aluminium (III) ( $\Gamma_{\text{vib}} = 13a (\text{R}) + 13e (\text{R}) + 40f (\text{i.r.,R})$  and  $\Gamma_{\text{AlO}_6} = a (\text{R}) + e (\text{R}) + 4f (\text{i.r.,R})$ ).**

Freq.	i.r.	Raman	f. c.	char.	assignment
40	0.0146	0.0945	0.0046	f	(H <sub>2</sub> O) <sub>3</sub> twist
43.7	0	0.178	0.0059	e	(H <sub>2</sub> O) <sub>3</sub> twist
55	0	0.194	0.0085	a	(H <sub>2</sub> O) <sub>3</sub> trans.
59.2	1.77	0.049	0.0117	f	(H <sub>2</sub> O) <sub>3</sub> trans
88.6	0.954	0.0228	0.0271	f	(H <sub>2</sub> O) <sub>3</sub> rock
105.3	0.779	0.308	0.0268	f	translational mode + AlO <sub>6</sub> def.
108.3	0	0.0436	0.0286	e	translational mode + AlO <sub>6</sub> def.
115.4	23.87	0.025	0.034	f	(H <sub>2</sub> O) <sub>3</sub> H-bond, asym. str.
147.1	0.693	0.0094	0.0725	f	(H <sub>2</sub> O) <sub>3</sub> H-bond, asym. str.
156	0	0.195	0.0631	a	(H <sub>2</sub> O) <sub>3</sub> H-bond, asym. str.
157.7	5.01	0.016	0.0732	f	(H <sub>2</sub> O) <sub>3</sub> H-bond, sym.str.
177.2	1.083	0.061	0.103	f	(H <sub>2</sub> O) <sub>3</sub> H-bond, sym. str.
181.9	0	0.192	0.1066	e	(H <sub>2</sub> O) <sub>3</sub> H-bond sym. +AlO <sub>6</sub> def (H <sub>2</sub> O) <sub>3</sub> rock
188.6	0.477	0.036	0.118	a	(H <sub>2</sub> O) <sub>3</sub> H-bond, sym. str.
204.2	4.29	0.061	0.159	f	AlO <sub>6</sub> def.

Table 4.9: Unscaled HF/6-31G\* Frequencies, intensities (i.r., Raman) and force constants of the octadeca- aqua aluminium (III) ( $\Gamma_{\text{vib}} = 13a (\text{R}) + 13e (\text{R}) + 40f (\text{i.r.,R})$  and  $\Gamma_{\text{AlO}_6} = a (\text{R}) + e (\text{R}) + 4f (\text{i.r.,R})$ ).

261.2	9.023	0.001	0.204	f	AlO <sub>6</sub> def.
316.3	10.16	0.614	0.239	f	AlO <sub>6</sub> def.
322.8	43.2	3.272	0.080	f	(H <sub>2</sub> O) <sub>3</sub> rock
337.3	0	0.263	0.0765	e	H <sub>2</sub> O (2) lib.
339.7	122.13	0.061	0.09	f	H <sub>2</sub> O (2) lib.
351.7	52.04	0.232	0.160	f	H <sub>2</sub> O (2) lib.
432.7	0	0.774	0.332	e	AlO <sub>6</sub> str.
448.8	0	0.0023	0.129	a	H <sub>2</sub> O (2) lib.
449	103.4	1.225	0.137	f	H <sub>2</sub> O (2) lib.
468.4	0.005	0.292	0.144	f	H <sub>2</sub> O (2) lib.
473.4	100.63	3.866	0.145	f	H <sub>2</sub> O (2) lib.
477.4	0	2.741	0.165	e	H <sub>2</sub> O (2) lib.
496.8	0	1.14	0.246	a	H <sub>2</sub> O (2) lib. + AlO <sub>6</sub> stretch
497.9	185	0.265	0.179	f	H <sub>2</sub> O (2) lib.
520.1	12.986	0.472	0.176	f	H <sub>2</sub> O (2) lib.
542.1	0	0.0291	0.365	a	AlO <sub>6</sub> stretch + H <sub>2</sub> O (2) lib.

Table 4.9: Unscaled HF/6-31G\* Frequencies, intensities (i.r., Raman) and force constants of the octadeca- aqua aluminium (III) ( $\Gamma_{\text{vib}} = 13a(\text{R}) + 13e(\text{R}) + 40f(\text{i.r.,R})$  and  $\Gamma_{\text{AlO}_6} = a(\text{R}) + e(\text{R}) + 4f(\text{i.r.,R})$ ).

543.5	556.6	0.888	0.192	f	H <sub>2</sub> O (2) lib.
554.6	0	0.518	0.205	e	H <sub>2</sub> O (2) lib.
613.4	0.59	0.0622	1.343	f	AlO <sub>6</sub> asym. stretch.
711.1	2.073	0.315	0.310	f	H <sub>2</sub> O (1) wag
714.9	0	0.168	0.312	e	H <sub>2</sub> O (1) twist
745.6	0	0.0063	0.344	a	H <sub>2</sub> O (1) twist
756.5	8	0.012	0.358	f	H <sub>2</sub> O (1) twist
780.3	613	0.526	0.387	f	H <sub>2</sub> O (1) wag
805.7	0	0.092	0.408	a	H <sub>2</sub> O (1) rock
855.4	782.16	0.620	0.476	f	H <sub>2</sub> O (1) lib.
979.8	41.24	0.389	0.605	f	H <sub>2</sub> O (2) lib
1066.4	368	0.341	0.736	f	H <sub>2</sub> O (1) rock + H <sub>2</sub> O (1) lib
1817.4	192.7	4.416	2.1037	f	HOH bending outer- sphere
1818.4	0.52	4.212	2.105	f	HOH bending outer- sphere
1818.8	0	10.360	2.106	e	HOH bending outer- sphere
1821.9	254.4	1.15	2.116	f	HOH bending outer- sphere

Table 4.9: Unscaled HF/6-31G\* Frequencies, intensities (i.r., Raman) and force constants of the octadeca- aqua aluminium (III) ( $\Gamma_{\text{vib}} = 13a(\text{R}) + 13e(\text{R}) + 40f(\text{i.r.,R})$  and  $\Gamma_{\text{AlO}_6} = a(\text{R}) + e(\text{R}) + 4f(\text{i.r.,R})$ ).

1824.4	0	0.155	2.122	a	HOH bending outer- sphere
1902.3	0	0.644	2.301	e	HOH bending inner- sphere
1909.2	318	0.004	2.312	f	HOH bending inner- sphere
1928.3	0	0.564	2.340	a	HOH bending inner- sphere
3665.7	0	39.7	8.262	e	OH str. -sym. inner- sphere
3684.2	1108.7	17.97	8.365	f	OH str. -sym. inner- sphere
3710.8	164.14	21.5	8.863	f	OH str. -asym. inner- sphere
3734.1	2984	88.73	8.981	f	OH str. -asym. inner- sphere
3755.8	0	398.3	8.707	a	OH str. -sym. inner- sphere
3987.5	94.66	10.85	9.826	f	OH str. -sym. outer- sphere
3988.2	0	526.2	9.830	a	OH str. -sym. outer- sphere
4010.9	66.98	0.340	9.923	f	OH str. -sym. outer- sphere
4011.3	0	83.20	9.920	e	OH str. -sym. outer- sphere
4011.3	197.45	3.656	9.922	f	OH str. -sym. outer- sphere
4105.7	50.06	52.98	10.757	f	OH str. -asym. outer- sphere
4106.5	51.58	1.019	10.747	f	OH str. -asym. outer- sphere

**Table 4.9: Unscaled HF/6-31G\* Frequencies, intensities (i.r., Raman) and force constants of the octadeca- aqua aluminium (III) ( $\Gamma_{\text{vib}} = 13a(\text{R}) + 13e(\text{R}) + 40f(\text{i.r.,R})$  and  $\Gamma_{\text{AlO}_6} = a(\text{R}) + e(\text{R}) + 4f(\text{i.r.,R})$ ).**

4107.3	0	77.12	10.750	a	OH str. -sym. outer- sphere
4107.3	933.66	4.76	10.768	f	OH str. asym. outer- sphere
4107.6	0	110.5	10.770	e	OH str. asym. outer- sphere

Harmonic frequencies in  $\text{cm}^{-1}$ ; i.r. = infrared intensities in  $\text{km/mol}$ ; Raman scattering activities in  $\text{\AA}^4/\text{au}$ ; force constants in  $\text{mdyne/\AA}$ .

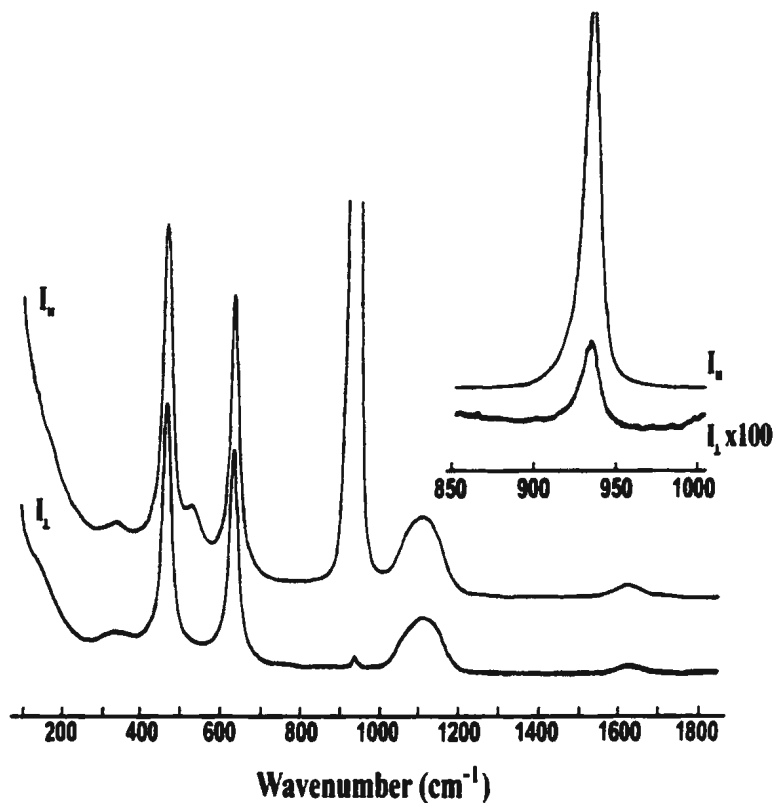
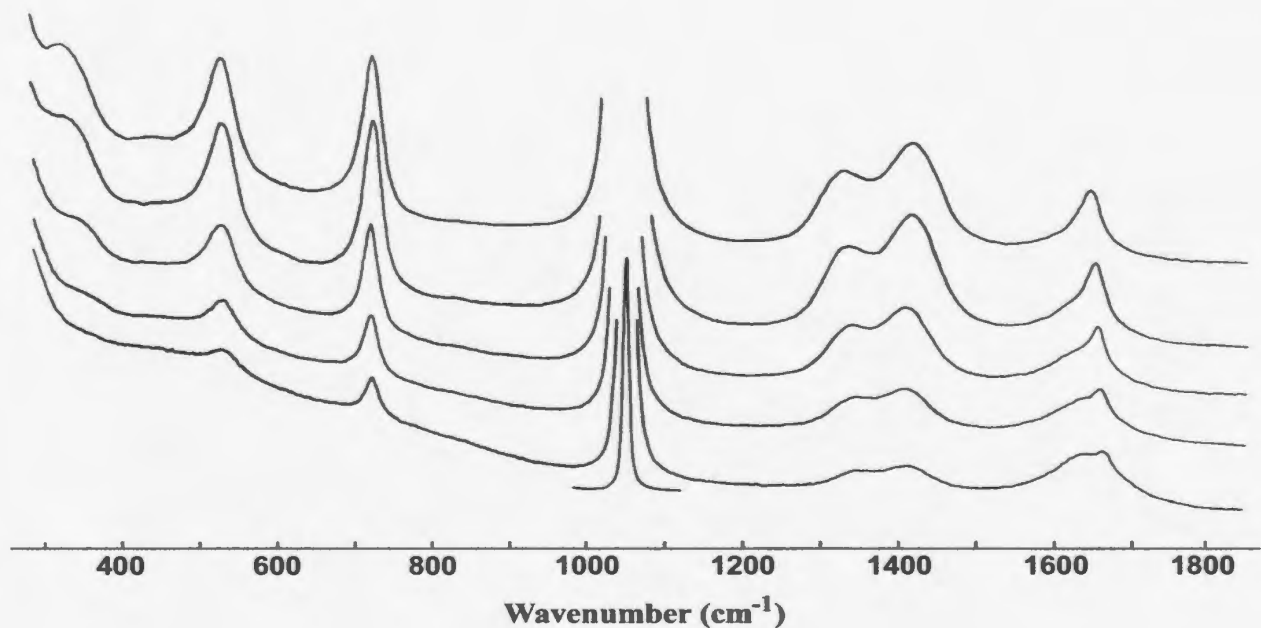
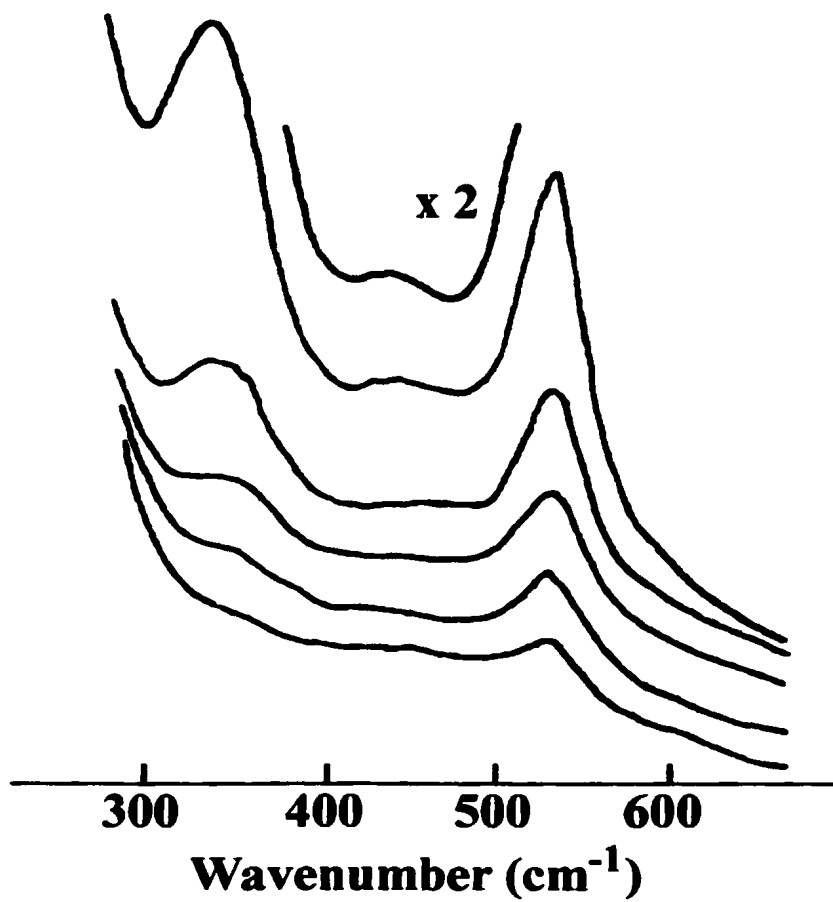


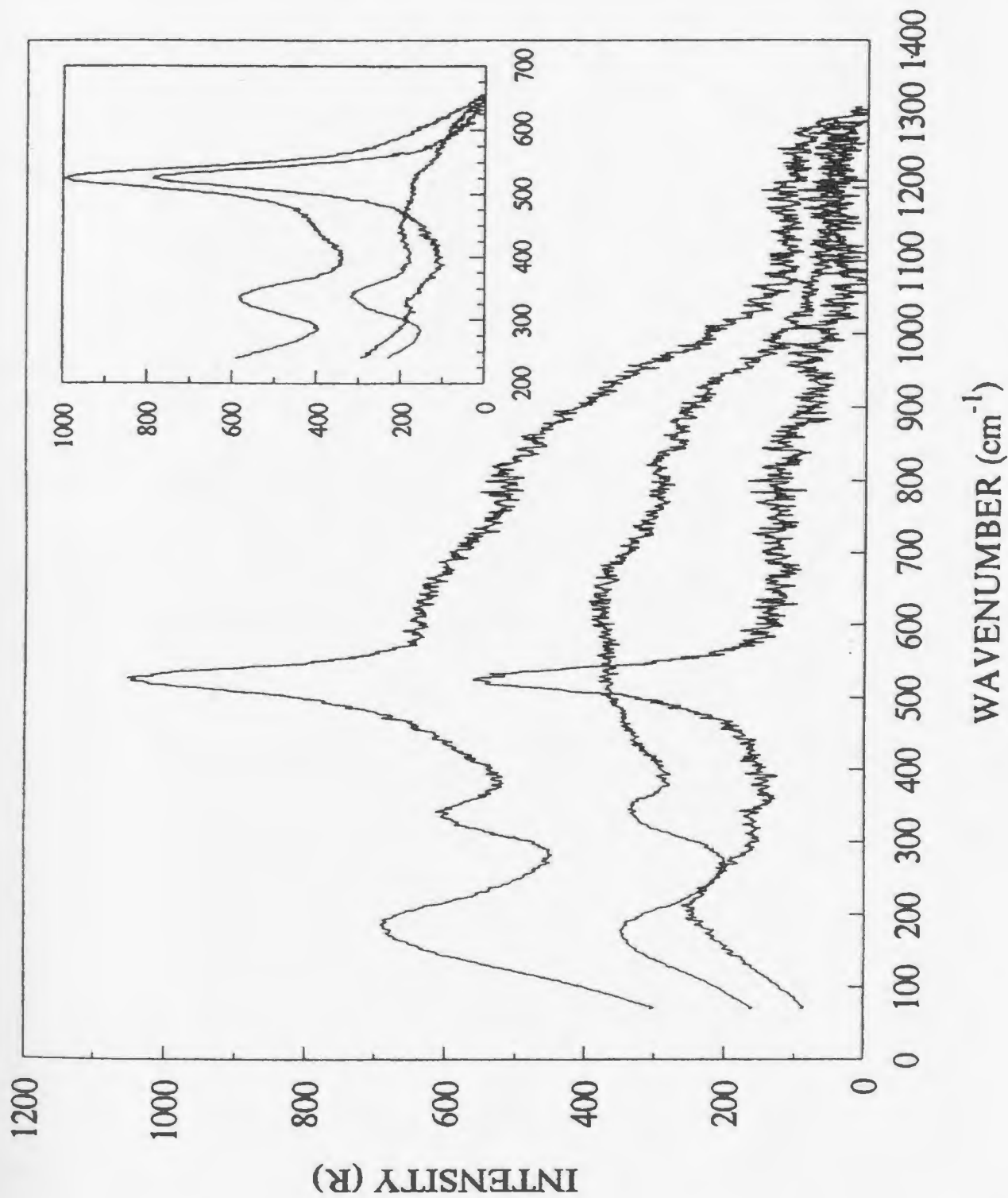
Figure 1: Raman spectrum of a 2.00 mol/L Al(ClO<sub>4</sub>)<sub>3</sub> solution (I-parallel and I-perpendicular) in the wavenumber range from 100 - 1800 cm<sup>-1</sup> (exciting wavelength 488.0 nm; slit width 1.4 cm<sup>-1</sup>). The insert in the right corner gives the symmetric stretching mode of perchlorate in more detail.



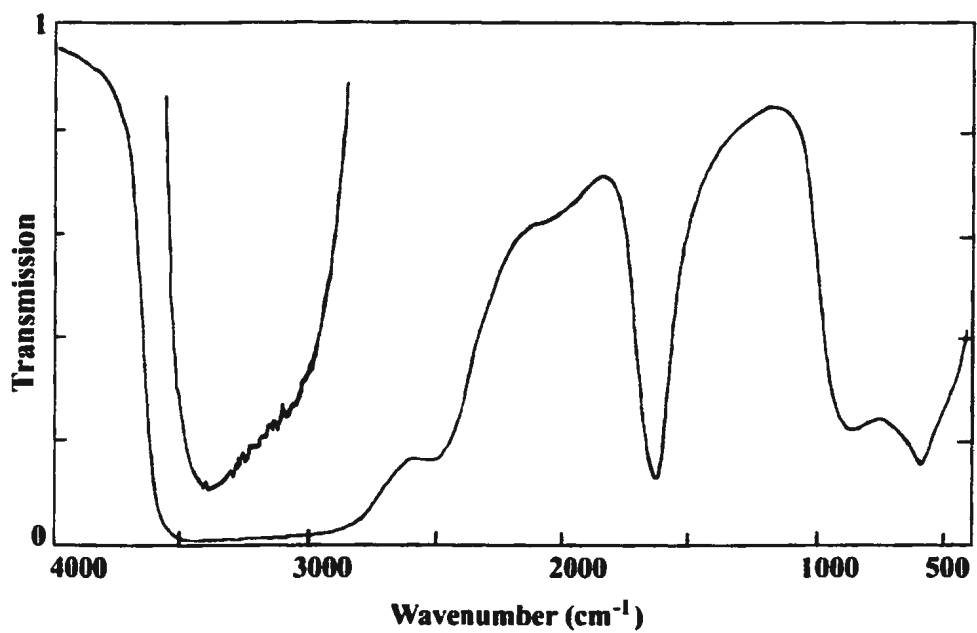
4.2. Concentration profile of the Raman spectra (I-parallel) of Al(NO<sub>3</sub>)<sub>3</sub> solutions in the wavenumber range from 280 to 1850 cm<sup>-1</sup>. The concentrations are from top to bottom: 2.50, 2.00, 1.00, 0.50, and 0.21 mol/L. The conditions of the Raman measurement are: Exciting wavelength 488.0 nm; slit width 2.5 cm<sup>-1</sup>. Note, that the modes of the AlO<sub>6</sub> unit ( $\nu_1(a_{1g})$ ,  $\nu_2(e_g)$ , and  $\nu_5(f_{2g})$ ) are well separated from the NO<sub>3</sub><sup>-</sup> vibrations. For explanations see text.



4.3. Raman spectra of  $\text{AlCl}_3$  solutions at five different concentrations: 3.14, 2.00, 1.50, 1.00 and 0.50  $\text{molL}^{-1}$  25 °C in the wavenumber range from 250 - 650  $\text{cm}^{-1}$ .



4.4 Raman spectra ( $R_{pol}$ ,  $R_{depol}$  and  $R_{iso}$ ) of a 2.85 mol/L  $AlCl_3$  solution in the wavenumber region between 70- 1300  $cm^{-1}$  at 25°C. The insert gives the spectra of a 3.40 mol/L  $AlCl_3$  in the wavenumber region 240 - 650  $cm^{-1}$ .



4.5. Infrared spectrum of a 3.14 molL<sup>-1</sup> AlCl<sub>3</sub> solution at 25 °C.

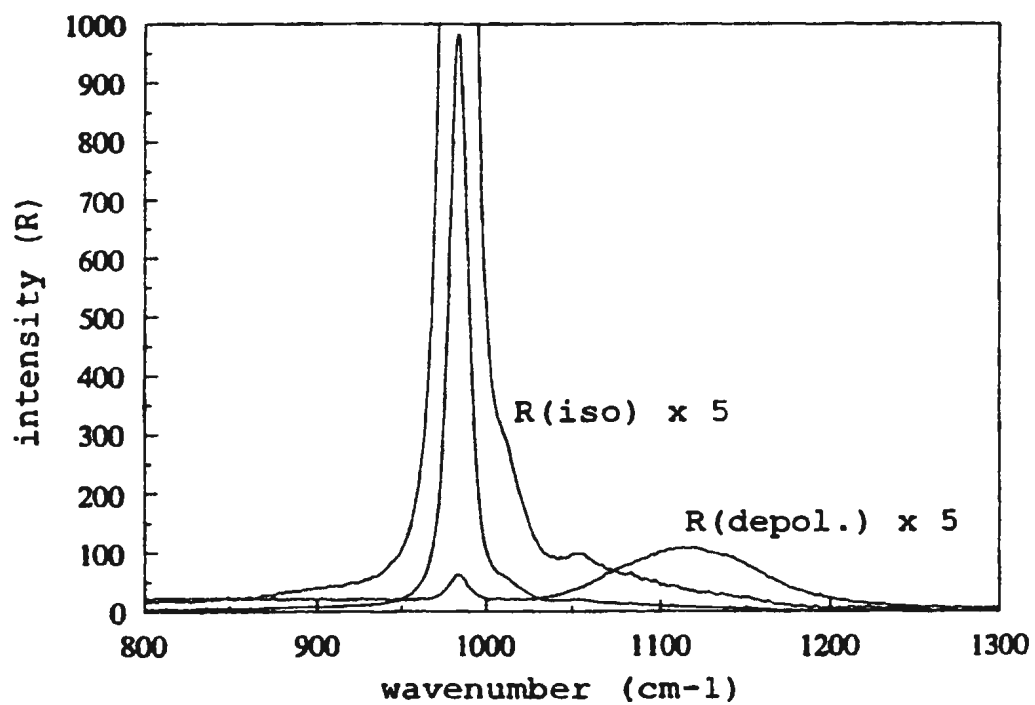
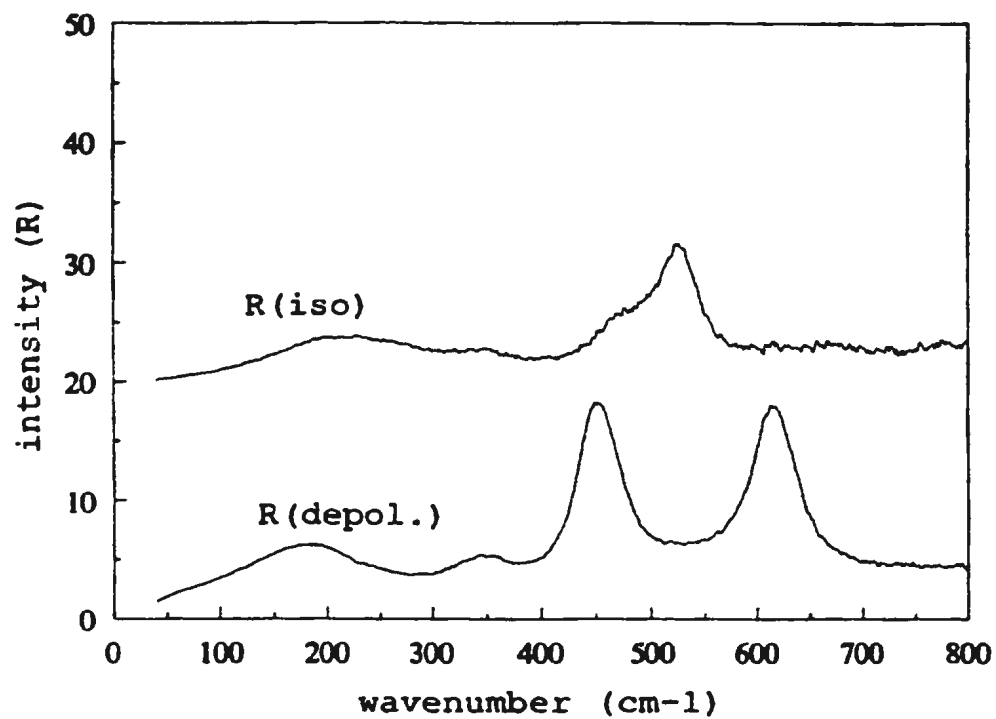


Figure 4.6 A: Raman spectra of a 1.014 molal  $\text{Al}_2(\text{SO}_4)_3$  solution at 25 °C.

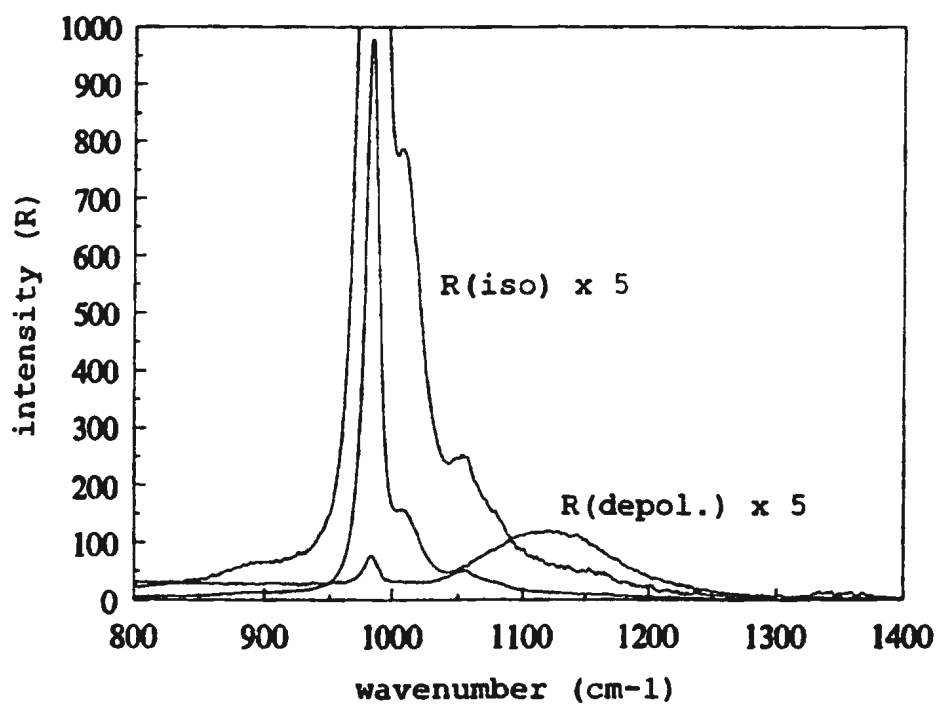
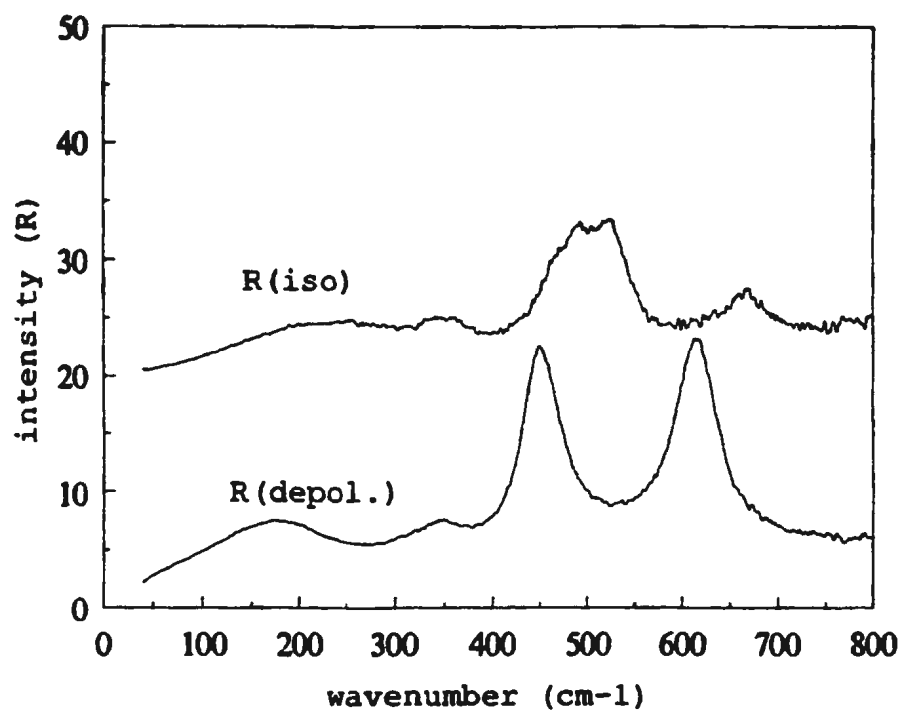


Figure 4.6 B: Raman spectra of a 1.014 molal  $\text{Al}_2(\text{SO}_4)_3$  solution at 58 °C.

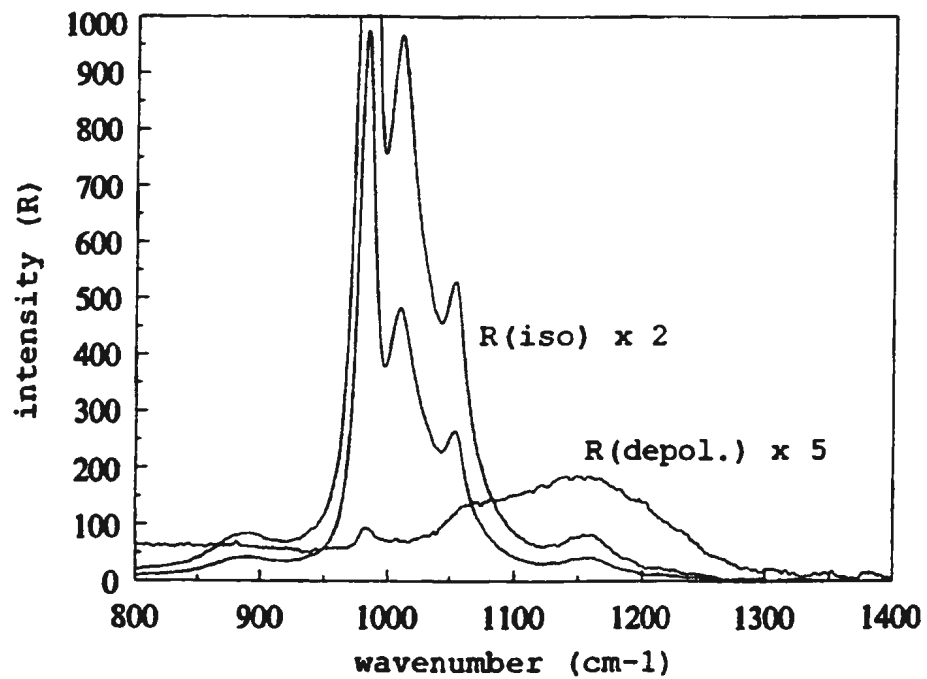
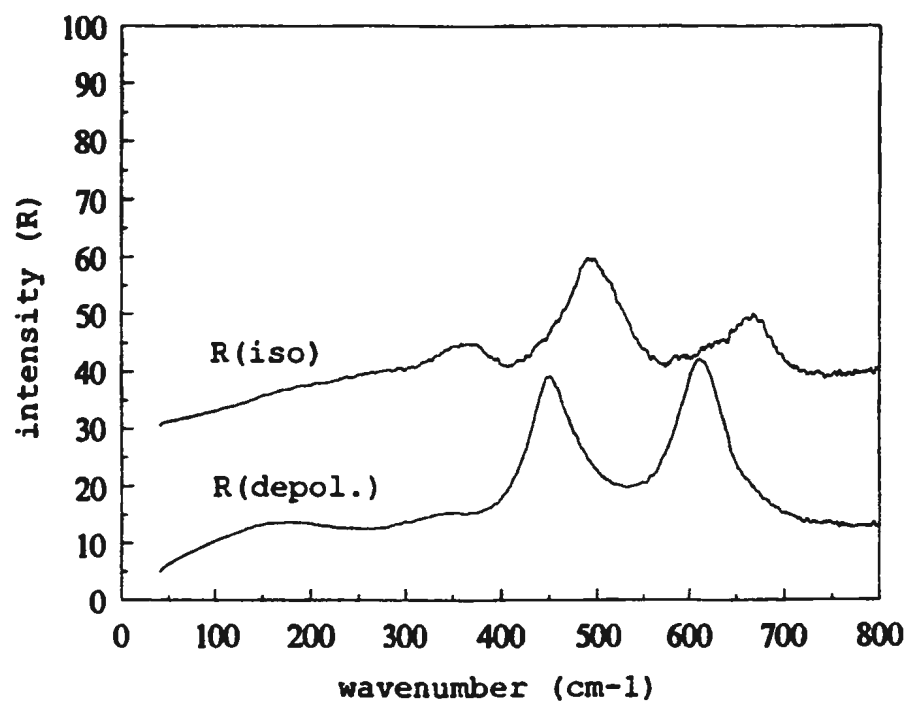
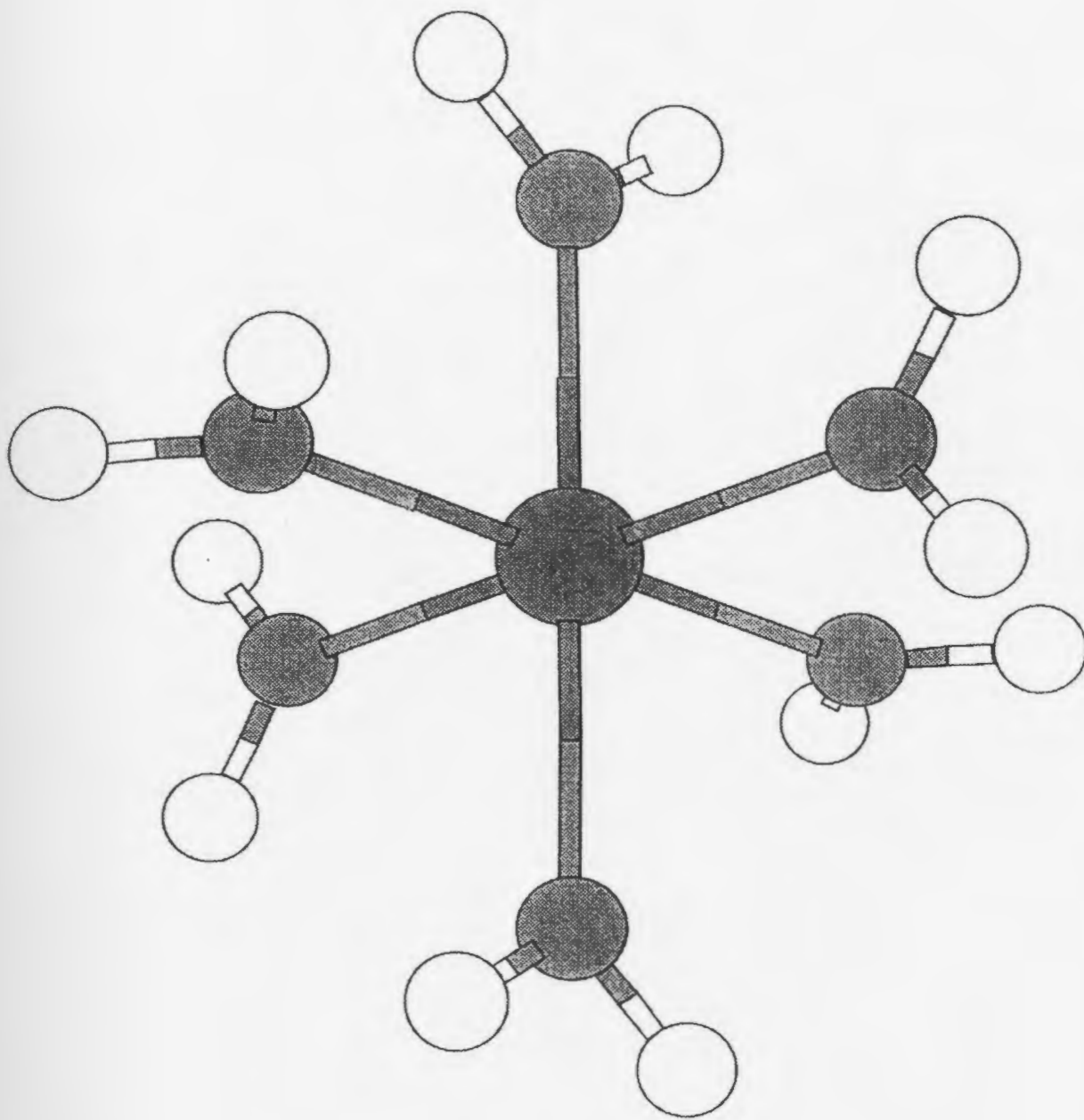
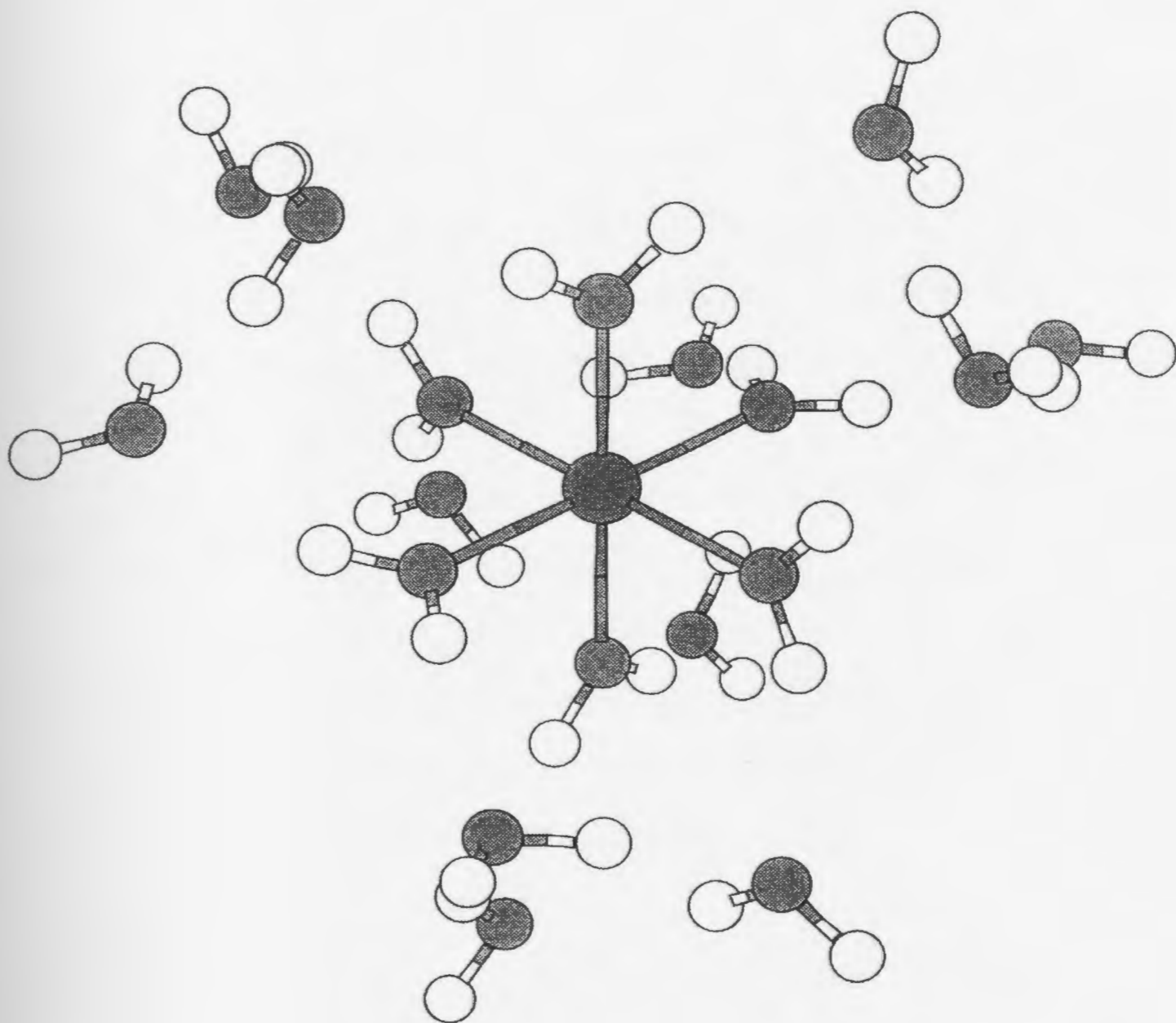


Figure 4.6 C: Raman spectra of a 1.014 molal  $\text{Al}_2(\text{SO}_4)_3$  solution at  $106^\circ\text{C}$ .



4.7. The structural model of  $[Al^{3+}(OH_2)_6]$  ( $T_h$  symmetry).



4.8. The structural model of  $[Al^{3+}(OH_2)_{18}]$  (T symmetry).

#### 4. 6. References

- 1) A. J. Downs, Editor, *Chemistry of Aluminium, Gallium, Indium and Thallium*, Blackie Academic & Professional, London etc. 1993.
- 2) a) D. E. Irish and M. H. Brooker, *Advances in Infrared and Raman Spectroscopy*, ed. by R. J. H. Clark and R. E. Hester Vol.2, p. 212 Heyden, London , 1976. b) M. H. Brooker, in *The Chemical Physics of Solvation*, Part B. Spectroscopy of Solvation, R. . Dogonadze, E. Kalman, A. A. Kornyshev and J. Ulstrup, eds.. Elsevier, Netherlands, 1986, p.119.
- 3) G. E. Walrafen, *J. Chem. Phys.* 1962, 36, 1035 and 1966, 44, 1546.
- 4) a) W. W. Rudolph, M. H. Brooker and C. C. Pye, *J. Phys. Chem.*, 1995, 99, 3793. b) C.C. Pye, W. W. Rudolph and R.A. Poirier, *J. Phys. Chem.*, 1996, 100, 601.
- 5) W. W. Rudolph and G. Irmer, *J. Solution Chem.*, 1994, 23, 663-684.
- 6) a) W. W. Rudolph, *Z. Phys. Chem.*, 1996, 194, 73-95. B) W. W. Rudolph, C. C. Pye, *Z. Phys. Chem.(München)*, 1999, 209, 243-258.C) W. W. Rudolph, Diploma Thesis, Bergakademie Freiberg, 1979.
- 7) M. H. Brooker, O. Faurskov Nielsen, E. Praestgaard, *J. Raman Spectrosc.*, 1988, 19, 71-77.
- 8) A. I. Vogel, *A Text-Book of Quantitative Inorganic Analysis*, Third Edition, Longman, London 1961.
- 9) W. E. Harris, B. Kratochvil, *An Introduction to Chemical Analysis*, Philadelphia: Saunders College Publishing, 1981, 75 pp. and 203 pp.

- 10) a) W. W. Rudolph, M. H. Brooker and P. R. Tremaine, *Z. Phys. Chem.*, **1999**, *209*, 181-207. b) W. W. Rudolph, M.H. Brooker and P. R. Tremaine, *J. Solution Chem.*, **1997**, *26*, 757-765. c) W. W. Rudolph, M.H. Brooker, P. R. Tremaine, *J. Sol. Chem.*, **1997**, *26*, 757-777. d) W. W. Rudolph, M.H. Brooker, P. R. Tremaine, *J. Sol. Chem.*, **1999**, *28*, 621. e) W. W. Rudolph, *Ber. Bunsenges. Phys. Chem.* **1998**, *102*, 183-196.
- 11) H, Li-F: W. J. Hehre, R. F. Stewart and J. A. Pople, *J. Chem. Phys.*, **1969**, *51*, 2657. He, Ne, Na-Ar: W. J. Hehre, R. Ditchfield, R. F. Stewart, J. A. Pople, *J. Chem. Phys.*, **1970**, *52*, 2769-2773.
- 12) H - Ne: J. S. Binkley, J. A. Pople and W. J. Hehre, *J. Am. Chem. Soc.*, **1980**, *102*, 939. Na - Ar: M. S. Gordon, J. S. Binkley, J. A. Pople, W. J. Pietro, W. J. Hehre, *J. Am. Chem. Soc.*, **1982**, *104*, 2797-2803.
- 13) C- F 6-31G: W. J. Hehre, R. Ditchfield, J. A. Pople, *J. Chem. Phys.*, **1972** *56*, 2257-2261. H, C- F polarization: P. C. Hariharan and J. A. Pople, *Theor. Chim. Acta (Berl.)*, **1973**, *28*, 213-222.; Na - Ar: M. M. Francl, W. J. Pietro, W. J. Hehre, J. S. Binkley, M. S. Gordon, D. J. Defrees, J. A. Pople, *J. Chem. Phys.*, **1982**, *77*, 3 654-3665.
- 14) M. J. Frisch, G. W. Trucks, H. B. Schlegel, P. M. W. Gill, B. G. Johnson, M. W. Wong, J. B. Foresman, M. A. Robb, M. Head-Gordon, E. S. Replogle, R. Gomperts, J. L. Andres, K. Raghavachari, J. S. Binkley, C. Gonzalez, R. L. Martin, D. J. Fox, D. J. Defrees, J. Baker, J. J. P. Stewart, J. A. Pople, Gaussian 92/DFT,

Revision F.4, Gaussian, Inc., Pittsburgh, PA., 1993.

- 15) H, Li - F diffuse: T. Clark, J. Chandrasekhar, G. W. Spitznagel, and P. v. R. Schleyer, *J. Comput. Chem.*, **1983**, *4*, 294-301.; Na-Cl diffuse: M. J. Frisch, J. A. Pople, J. S. Binkley, *J. Chem. Phys.*, **1984**, *80*, 3265-3269.
- 16) J. N. Brönsted, K. Volqvartz, *Z. Phys. Chem.*, **134**, (1928) 97.
- 17) a) R. E. Connick, D. N. Fiat, *J. Chem. Phys.* **39** (1963) 1349. B) D. N. Fiat, R. E. Connick, *J. Am. Chem. Soc.* **90** (1964) 608.
- 18) D. Hugi-Cleary, L. Helm, A. E. Merbach, *Helv. Chim. Acta.* **68**, (1985), 545.
- 19) T. Kowall, P. Caravan, H. Bourgeois, L. Helm, F. P. Rotzinger, A. E. Merbach, *J. Am. Chem. Soc.*, **1998**, *120*, 6569-6577.
- 20) D. R. Buchanan, P. M. Harris, *Acta Cryst.* **B24** (1968) 954-960.
- 21) a) W. Rudolph, S. Schönherr, *Z. Phys. Chem.(Leipzig)*, **1989**, *270*, 1121-1134. B) W. Rudolph, S. Schönherr, *Z. Phys. Chem.(München)*, **1991**, *173*, 167-177.
- 22) a) D. M. Adams, D. J. Hills, *J. Chem. Society, DaltonTrans.* **1978**, 782- 788. B) G. Wäschenbach, H. D. Lutz, *Spectrochim. Acta*, **1986**, *42A*, 983-984.
- 23) a) C. C. Pye, W. W. Rudolph, *J. Phys. Chem. A*, **1998**, *102*, 9933- b) W. W. Rudolph, C. C. Pye, *J. Phys. Chem. B*, **1998**, *102*, 3564-3573.
- 24) W. Rudolph, S. Schönherr, *Z. Phys. Chem.(München)*, **1991**, *172*, 31-48.
- 25) a) W. W. Rudolph, *J. Chem. Soc. Faraday Trans.*, **1998**, *94(4)*, 489-499. B) W. W. Rudolph, C. C. Pye, *J. Solution Chem.*, **1999**, *28*, 1045-1070.
- 26) E. Wasserman, J. R. Rustad, S. S. Xantheas, *J. Chem. Phys.*, **1997**, *106*,

9769-9780.

- 27) a) W. W. Rudolph, C. C. Pye, *PCCP*, **1999**, *1*, 4583-4593.  
b) W. W. Rudolph, C. C. Pye, *J. Phys. Chem. A*, **2000**, *104*, 1627-1639.
- 28) W. Bol, T. Welzen, *Chem. Phys. Lett.* **1977**, *49*, 189.
- 29) E. S. Marcos, R. R. Pappalardo, D. Rinaldi, *J. Phys. Chem.*, **1991**, *95*, 8928-8932.
- 30) J. M. Ruiz, M. H. McAdon, J. M. Garces, *J. Phys. Chem. B*, **1997**, *101*, 1733-1744.
- 31) T. Kowall, P. Caravan, H. Bourgeois, L. Helm, F. P. Rotzinger, A. E. Merbach, *J. Am. Chem. Soc.*, **1998**, *120*, 6569-6577.
- 32) J. D. Kubicki, D. Sykes, S. E. Aplitz, *J. Phys. Chem. A*, **1999**, *103*, 903-915.
- 33) D.T. Richens, *The Chemistry of Aqua Ions*, John Wiley, Chichester, **1997**,  
Appendix.
- 34) Pavlov, M; Siegbahn, P. E. M.; Sandström, M., *J. Phys. Chem. A*, **1998**, *102*, 219.
- 35) a) E. D. Glendening, D. Feller, *J. Phys. Chem.*, **1995**, *99*, 3060. b) D. Feller, E. D. Glendening, R. A. Kendall, K. A. Peterson., *J. Chem. Phys.*, **1994**, *100*, 4981.

## 5. Study of aqueous $\text{Al}_2(\text{SO}_4)_3$ solution under hydrothermal conditions: sulfate ion pairing, hydrolysis and formation of hydronium alunite

Wolfram W. Rudolph and Roger Mason

### 5. 1. Abstract

Raman spectra have been measured for aqueous  $\text{Al}_2(\text{SO}_4)_3$  solutions from 25°C to hydrothermal conditions at 184 °C under steam saturation. The Raman spectrum at 184 °C contained four polarized bands in the S-O stretching wavenumber range which suggest that a new sulfato complex, where sulfate acts as a bridging ligand, possibly bidentate or tridentate, is formed in solution in addition to a 1:1 aluminium(III) sulfato complex, where sulfate is monodentate, which is the only ion pair identified at room temperature. Under hydrothermal conditions it was possible to observe the hydrolysis of aluminium(III) aqua-ion by measuring the relative intensity of bands due to  $\text{SO}_4^{2-}$  and  $\text{HSO}_4^-$  according to the coupled equilibrium reaction  $[\text{Al}(\text{OH}_2)_6]^{3+} + \text{SO}_4^{2-} \rightleftharpoons [\text{Al}(\text{OH}_2)_5\text{OH}]^{2+} + \text{HSO}_4^-$ . The precipitate in equilibrium with the solution at 184°C could be characterized as hydronium alunite,  $(\text{H}_3\text{O})\text{Al}_3(\text{SO}_4)_2(\text{OH})_6$ , by chemical analysis, X-ray diffraction, Raman and infrared spectroscopy.

**Key words:** aluminum sulfate solution, Al(III)-hydrolysis, Al(III) sulfato complex formation, hydronium alunite, Raman and infrared spectroscopy, X-ray diffraction, unit cell parameters.

## 5. 2. Introduction

Aqueous aluminum sulfate solutions are important in a number of natural systems. These include natural thermal waters in regions of active or relatively recent volcanism (Zotov, 1969), where gold may be precipitated, and the alteration of aluminum bearing minerals in lower temperature, oxidizing, sulfur rich environments (Scott, 1987). In both high- and low-temperature environments a member of the alunite group of minerals may precipitate, leading in the former case to an association with gold mineralization, and in the latter to the alunitization of soils (Lückewille and Prenzel, 1993). Clearly, the nature and stability of aqueous complexes involving aluminum and sulfur will be important controls on the chemistry of such solutions, and understanding of their properties is a necessary part of understanding their interaction with rocks and soil, and of the reactions leading to the formation of alunite.

We have previously studied Raman spectra of aqueous, stoichiometric  $\text{Al}_2(\text{SO}_4)_3$  solutions at room temperature and established the existence of an inner-sphere aluminium(III) sulfato complex, which is confirmed by  $^{27}\text{-Al}$  NMR spectroscopy (Akitt et al., 1985; Rudolph and Schönherr, 1991). The present study was undertaken to obtain Raman data at higher temperatures, where the hydrolysis of the aquaaluminium(III) ion becomes important. The Raman spectra of these solutions were measured up to 184 °C, where precipitation of a member of the alunite group halted further measurements.

We compare our results with Raman spectra of  $\text{AlCl}_3$ -,  $\text{Al}(\text{NO}_3)_3$ - and  $\text{Al}(\text{ClO}_4)_3$ - ammonium-sulfate solutions (Rudolph and Schönherr, 1989 and Rudolph et al., 2000).

Comparison of the "free" sulfate in ammonium sulfate solutions with the ligated sulfate in the aquaaluminium(III) sulfato complex(es) allows us to draw conclusions about the nature and symmetry of the ligated sulfate. From previous studies (Rudolph, 1996) of the equilibrium sulfate/hydrogen sulfate, the modes for hydrogen sulfate, which is formed in these acidic  $\text{Al}_2(\text{SO}_4)_3$  solutions, could be assigned. These hydrothermal studies, which allow us to characterize the species present, are of importance for modelling transport processes in hydrothermal fluids and for hydrometallurgical processes.

The precipitate, formed in hydrothermal  $\text{Al}_2(\text{SO}_4)_3$  solution at 184 °C, has been characterized as hydronium alunite. We present Raman and infra-red spectra of hydronium alunite obtained at high temperature and at room temperature and discuss the reactions leading to its formation.

### 5. 3. Experimental

An  $\text{Al}_2(\text{SO}_4)_3$  stock solution was prepared by dissolving commercial-grade salt and was precipitated twice by pouring in p.a. (pro analysi) ethanol.  $\text{Al}_2(\text{SO}_4)_3 \cdot 18 \text{H}_2\text{O}$  was dried over  $\text{CaCl}_2$ . The Al(III) content of the solution was determined by colorimetric titration with standard EDTA and xylenol orange as an indicator (Vogel, 1961). The sulfate content was checked by titration with standardized  $\text{Ba}(\text{ClO}_4)_2$  solution using Thorin, 2-(2-dihydroxy-3,6-disulfo-1-naphthylazo) benzene arsonic acid, as an adsorption indicator (Harris and Kratochvil, 1981). Before titration, the solution was passed through a column with a cation exchanger (Dowex 50W-X8). The eluate was then titrated with the standardized  $\text{Ba}(\text{ClO}_4)_2$  solution and this elution technique prevented co-precipitation of

Al(III) with the BaSO<sub>4</sub> (Harris and Kratochvil, 1981). The Al<sub>2</sub>(SO<sub>4</sub>)<sub>3</sub> stock solution was 0.98 M (1.012 m). It is known that aluminium(III) solutions are very acidic. The pH value of the stock solution was determined with a glass electrode and was found to be 1.44. The solution densities were determined with a standardized 5 ml pycnometer at 20°C.

The preparation and analytical characterization of aqueous, stoichiometric AlCl<sub>3</sub>, Al(NO<sub>3</sub>)<sub>3</sub>, and Al(ClO<sub>4</sub>)<sub>3</sub> stock solutions has been described in detail in previous papers (Rudolph and Schönherr, 1989 and Rudolph et al., 2000). The preparation of aqueous (NH<sub>4</sub>)<sub>2</sub>SO<sub>4</sub> solutions has also been described elsewhere (Rudolph, 1996).

All solutions were filtered through a 0.22 micron Millipore filter into a 150 mm ID quartz tube before Raman spectroscopic measurement. The Raman spectroscopic technique for measuring aqueous solution spectra, including data treatment, was discussed in detail in previous papers (Rudolph and Pye, 1999).

The solution spectra were measured with a Coderg Raman spectrometer using an Argon ion laser at 488.0 nm as a light source with a power level at the sample about 0.9 W. The slit widths of the double monochromator were set at 1.8 cm<sup>-1</sup>. The scattered light was detected with a PMT cooled to -20 °C, integrated with a photon counter and processed with a box-car averager interfaced to a personal computer. Two data points were collected per wavenumber. In order to increase the signal-to-noise ratio, six data sets were collected for each scattering geometry (I<sub>||</sub> and I<sub>⊥</sub>). A quarter wave plate before the slit served to compensate for grating preference. I<sub>||</sub> and I<sub>⊥</sub> spectra were obtained with fixed polarisation of the laser beam by changing the polaroid film at 90 ° between the sample and the

entrance slit to give the scattering geometries:

$$I_{\parallel} = I(Y[ZZ]X) = 45\alpha^2 + 4\beta^2 \quad (1).$$

$$I_{\perp} = I(Y[ZV]X) = 3\beta^2 \quad (2).$$

The isotropic spectrum,  $I_{\alpha}$  (or  $I_{iso}$ ) was constructed as follows:

$$I_{\alpha} = I_{\parallel} - 4/3 \cdot I_{\perp} \quad (3).$$

The spectra in R format, or reduced spectra were constructed according to eq.(4):

$R_Q(\bar{\nu}) = I(\bar{\nu}) \cdot (\bar{\nu}_0 - \bar{\nu}_i)^{-4} \cdot \bar{\nu}_i \cdot B$  where  $I(\bar{\nu})$  is the measured Raman intensity,  $\bar{\nu}_0$  is the absolute wavenumber of the laser excitation line,  $\bar{\nu}_i$  is the wavenumber difference of the scattered radiation (i.e. Raman shift), and  $B = [1 - \exp(-h \cdot \bar{\nu}_i \cdot c/kT)]$  is the Boltzmann thermal population factor. The reduced isotropic spectra, or  $R_{\alpha}$  spectra, can be calculated according to equation (5):

$$R_{\alpha} = R_{\parallel} - 4/3 \cdot R_{\perp} \quad (5)$$

and the depolarized spectra  $R_{dcpol}$ , according to equation (6):  $R_{dcpol} = R_{\perp}$  (6).

Equation (4) is valid under the condition that the normal coordinates,  $Q_i$ , are taken to be harmonic and the polarizability expansion is terminated after the first-order term (i.e. the double harmonic approximation). The R- spectrum is equal to the scattering activity  $S_j$  and integration over the jth band in the R- spectrum will give the integrated molar scattering intensity  $S_j$  for the jth band.  $S_j$  is directly proportional to the square of the derivative of the

polarizability tensor,  $\alpha$  with respect to the normal coordinate  $(\partial\alpha/\partial Q_i)^2$ . A good assessment of the construction procedure for the reduction of Raman spectra is given in (Brooker et al., 1988). It shall be noted that the above described procedure is not a 'correction', but is a transformation or normalization of the Raman spectra that permits the comparison of spectra observed under differing sample conditions. Further spectroscopic details about the high temperature measurement, the band fit procedure and details about R normalized Raman spectra is described in a previous publication (Rudolph, 1996).

For quantitative measurements, the perchlorate band,  $\nu_1$ -ClO<sub>4</sub><sup>-</sup> at 935 cm<sup>-1</sup> was used as an internal standard. From the R<sub>iso</sub> spectra, the relative isotropic scattering coefficient S( $\nu_1$ SO<sub>4</sub><sup>2-</sup>) and S( $\nu_1$ HSO<sub>4</sub><sup>-</sup>) were obtained. Further details about S- values cf. Rudolph (1996 and 1998).

The digitalized spectra were fitted to a sum of Lorentzian-Gaussian product functions. Details of the fitting procedure were given by Rudolph, 1996.

The solid product was measured with a scanning Renishaw Model 1000 Raman spectrometer equipped with CCD detection and an imaging microscope. These samples were excited with the 514.5 nm laser line at 25 mW power level, employing a Spectra Physics Model 263 air cooled Argon ion laser.

The infrared (i.r.) spectra of the solids were measured with a Mattson Polaris FT-IR spectrometer. In order to measure the wavenumber range below 400 cm<sup>-1</sup> a hydronium alunite sample was measured with a Perkin-Elmer infrared spectrometer model PE 283

(double beam spectrometer), which allows the measurement of the wavenumber range from 4000 to 200  $\text{cm}^{-1}$ . The usual KBr sample preparation, the disk technique was used. Aqueous solutions were measured with KSR5 disk in capillary thickness.

$^{27}\text{Al}$ -NMR solution spectra were obtained with a General Electric NMR spectrometer GN-300, operating at 78.17 MHz. A  $1.00 \text{ mol}\cdot\text{L}^{-1}$   $\text{AlCl}_3$  solution was used as an external standard.

The precipitate was studied *in situ* by Raman spectroscopy and, after quenching and isolation of the precipitate, Raman, X-ray diffraction (XRD) and infrared spectroscopic measurements were also carried out. The white precipitate was prepared for powder X-ray diffraction by spreading it as a slurry (in acetone) on a glass slide. The powder spectrum was collected on a Rigaku RU-200 XRD machine in the  $2\theta$  range 10 - 70 ° using  $\text{CuK}\alpha$  radiation. The data were searched against the JCPDS Powder Diffraction database. For precise unit cell parameter determinations, the alunite was mixed with Si as an internal standard and the powder spectrum was collected in the  $2\theta$  range 10 - 90 ° using  $\text{CuK}\alpha$  radiation.

The aluminum, and sulfur content was determined with inductively coupled plasma optical emission spectroscopy (ICP-OES). The instrument used for all analyses of Al, and S was an ARL 3520 sequential ICP-OES. For more details about the analytical procedure see (Finch, 1993). Two independent measurements (from the sample preparation to the ICP OES measurement) were undertaken.

## 5. 4. Results and discussion

### 5. 4. 1. The aluminum hexaaqua(III) ion, $[\text{Al}(\text{OH}_2)_6]^{3+}$ , $\text{AlCl}_3$ , $\text{Al}(\text{NO}_3)_3$ , and $\text{Al}(\text{ClO}_4)_3$ solutions

A concentration profile of five different Raman spectra of aqueous  $\text{AlCl}_3$  at 25°C are given in Figure 5.1. Three Raman active modes can be observed at 332, 438 and 525  $\text{cm}^{-1}$  (see results in Table 5.1). These Raman active modes can also be observed in aqueous  $\text{Al}(\text{NO}_3)_3$ , and  $\text{Al}(\text{ClO}_4)_3$  solutions besides the modes of the anions (nitrate and perchlorate). The Raman spectra of stoichiometric aqueous solutions of  $\text{AlCl}_3$ ,  $\text{Al}(\text{NO}_3)_3$ , and  $\text{Al}(\text{ClO}_4)_3$  have been published recently in detail (cf. Rudolph et al., 2000) and therefore only a short description of the Raman spectroscopic results shall be given in order to compare to Raman spectroscopic result in aqueous  $\text{Al}_2(\text{SO}_4)_3$ .

Three Raman active modes which were not due to the anion vibrations modes could be observed and were assigned to the  $\text{AlO}_6$  modes of the  $[\text{Al}(\text{OH}_2)_6]^{3+}$  cation (cf. Rudolph et al., 2000). The  $\text{AlO}_6$  skeleton possesses  $O_h$  symmetry (water as point masses) and the 15 normal modes of the  $\text{AlO}_6$  unit span the representation  $\Gamma_{\text{vib}}(O_h) = a_{1g} + e_g + 2f_{1u} + f_{2g} + f_{2u}$ . The mode  $\nu_1(a_{1g})$  (polarized) and the modes  $\nu_2(e_g)$  and  $\nu_5(f_{2g})$  (both depolarized) are Raman active, the modes  $\nu_3(f_{1u})$  and  $\nu_4(f_{1u})$  are i.r. active, whilst the mode  $\nu_6(f_{2u})$  is not observable in solution spectra. The polarized mode at 525  $\text{cm}^{-1}$  is observed, which is due to  $\nu_1(a_{1g})$   $\text{AlO}_6$  (totally symmetric stretching mode). The depolarized modes the 438  $\text{cm}^{-1}$  and 332  $\text{cm}^{-1}$  can be assigned to  $\nu_2(e_g)$  and  $\nu_5(f_{2g})$ , respectively. Number, band intensity and polarization of the modes confirm the octahedral structure of the  $\text{AlO}_6$  unit. The

infrared active modes of the  $\text{AlO}_6$  unit ought not to coincide with the Raman modes according to the mutual exclusion rule, resulting from the centrosymmetry of the  $\text{AlO}_6$  octahedron. One infrared mode could be observed at  $598 \text{ cm}^{-1}$ , while the other mode could not be observed (the limit of the infrared spectrometer was at  $400 \text{ cm}^{-1}$ ). The mode at  $598 \text{ cm}^{-1}$  was assigned to  $\nu_3(\text{f}_{1u})$ . The second infrared active mode,  $\nu_4(\text{f}_{1u})$ , is expected at much lower wavenumbers. A summary of the Raman and infrared modes of  $\text{AlO}_6$  is given in Table 4.1. The mode  $\nu_1(\text{a}_{1g})$   $\text{AlO}_6$  of the hexaaquaaluminium(III) stays symmetric and shifts only slightly in a temperature range from 25 to  $125 \text{ }^\circ\text{C}$  (Rudolph, Mason and Pye, 2000).

The Raman spectroscopic results clearly show that over the applied concentration and temperature range the hexaaqua-aluminium (III) ion remains stable in chloride, and perchlorate solutions, and no inner-sphere or contact ion pairs are formed (Rudolph, Mason and Pye, 2000). In the sulfate system however, sulfate-water exchange is taking place in the first coordination sphere. Furthermore it is noteworthy to point out that in stoichiometric aluminium(III) salt solutions no spectroscopic sign of polynuclear-aluminiumhydroxo complexes is detected. These cationic complexes are rather formed in solutions with a high  $\text{OH}^-/\text{Al}^{3+}$  ratio. It has to be pointed out that our solutions are stoichiometric, rather acidic and without additional base (For detailed discussion about the formation of so called basic aluminium(III) salts (polyhydroxyaluminium(III) salts) see e.g. (Bertsch, 1989).

In aqueous stoichiometric aluminium(III) sulfate solutions one would expect the

same spectroscopic information as observed in aqueous  $\text{AlCl}_3$ ,  $\text{Al}(\text{ClO}_4)_3$  and  $\text{Al}(\text{NO}_3)_3$  solutions: the Raman active modes for  $\text{AlO}_6$  and the equivalent modes for the sulfate anion. Because concentrated aqueous aluminium(III) sulfate solution are very acid, formation of hydrogen sulfate should be taken into account. Before we start to discuss the vibrational spectra of aluminum sulfate solutions, the spectrum of the undisturbed sulfate anion and hydrogen sulfate will be analysed.

#### 5. 4. 2. $(\text{NH}_4)_2\text{SO}_4$ - solution spectra; the vibrational spectrum of unligated sulfate

The Raman spectra of aqueous  $(\text{NH}_4)_2\text{SO}_4$  - solutions have been studied because the sulfate anion does not form contact ion pairs with the spherical  $\text{NH}_4^+$  ion in aqueous solution and may be compared to sulfate in aqueous  $\text{Al}_2(\text{SO}_4)_3$  solution. If a polyatomic anion such as sulfate replaces water in the first coordination sphere of the cation, then marked changes occur in the spectrum of the ligated sulfate, so that it is possible to differentiate between the modes of the ligated and the unligated sulfate. Additionally, a shift or splitting of the metal aqua modes and the appearance of a metal-ligand vibration at low frequencies ( $100 - 400 \text{ cm}^{-1}$ ) should be detectable. In order to separate these effects we studied the unligated sulfate in the  $(\text{NH}_4)_2\text{SO}_4 - \text{H}_2\text{O}$  system to obtain information about the "free" sulfate, which was then compared to sulfate in  $\text{Al}_2(\text{SO}_4)_3$  solution. In Table 5.2 we give the correlation table for the point group  $T_d$ , the symmetry for the "free", undisturbed sulfate, with  $C_{3v}$ , and  $C_{2v}$  together with the band assignments of the sulfate modes.

The "free", undistorted  $\text{SO}_4^{2-}$  ion ( $T_d$  - symmetry) has nine modes of internal

vibrations having the representation  $\Gamma_{\text{vib}}(T_d) = a_1 + e + 2f_2$ . All modes of vibration are Raman active but in i.r. only the  $f_2$  modes are active.

The spectrum of a  $3.00 \text{ mol}\cdot\text{L}^{-1}$   $(\text{NH}_4)_2\text{SO}_4$  - solution (Figure 5.2.) shows the predicted four Raman-active bands for the tetrahedral  $\text{SO}_4^{2-}$ . The  $\nu_1(a_1) - \text{SO}_4^{2-}$  band centred at  $981.4 \text{ cm}^{-1}$  is totally polarised ( $\rho = 0.006$ ) whereas  $\nu_3(f_2) - \text{SO}_4^{2-}$ , entered at  $1110 \text{ cm}^{-1}$ , and the deformation modes  $\nu_4(f_2) - \text{SO}_4^{2-}$  at  $617 \text{ cm}^{-1}$  and  $\nu_2(e) - \text{SO}_4^{2-}$  at  $452 \text{ cm}^{-1}$ , are depolarised. A detailed discussion of the vibrational spectrum of sulfate in the  $(\text{NH}_4)_2\text{SO}_4$  -  $\text{H}_2\text{O}$  system can be found in previous publications (Rudolph, 1996; 1998; Rudolph and Pye, 1998, 2000 and Pye and Rudolph, 2001).

The  $\nu_1 - \text{SO}_4^{2-}$  band shape is symmetrical in both polarisation arrangements in the concentration range studied and it remains symmetrical up to  $200 \text{ }^\circ\text{C}$ . However, the band shape of  $\nu_1 - \text{SO}_4^{2-}$  band is not purely Lorentzian. The experimental band shape was fitted with a Gauss-Lorentz profile. At  $22 \text{ }^\circ\text{C}$ , this band has a Gauss-Lorentz factor of 0.735, which means the band has a fairly large Gaussian contribution, whereas at higher temperatures the  $\nu_1 - \text{SO}_4^{2-}$  band becomes more Lorentzian (at  $200 \text{ }^\circ\text{C}$  the shape factor, R is 0.898). The peak maximum of the  $\nu_1 - \text{SO}_4^{2-}$  band shifts to lower frequencies with increasing temperature ( $981.4 \pm 0.2 \text{ cm}^{-1}$  at  $25 \text{ }^\circ\text{C}$ ,  $979.8 \text{ cm}^{-1}$  at  $99 \text{ }^\circ\text{C}$  and  $977.5 \text{ cm}^{-1}$  at  $200 \text{ }^\circ\text{C}$  in the  $3.00 \text{ mol/L}$  solution). The frequency shifts upward with increasing concentration, with a linear dependency:  $\nu_{\text{max}} = 980.8 + 0.17 \cdot C_{\text{sulfate}}$ .

The FWHH broadens from  $3.50 \text{ cm}^{-1}$  to  $5.8 \text{ cm}^{-1}$  in the concentration range studied (FWHH =  $3.4 + 0.8 \cdot C_{\text{sulfate}}$ ). The relative molal intensity,  $S_{981}(\text{SO}_4^{2-})$  or relative molar

scattering coefficient is  $0.778 \pm 0.002$ . Within experimental error the S- value for the sulfate band is independent of temperature.

In the  $R_{iso}$  spectrum of  $(NH_4)_2SO_4$  solution, no sulfato complex formation is detectable. In the low frequency region only the restricted translation of the water molecules and the water-sulfate H-bonds is detected. Sulfate is known to form only slightly weaker H bonds than  $H_2O-H_2O$ , and this band is observed at slightly lower frequencies.

#### 5. 4. 3. $NH_4HSO_4$ aqueous solution, Hydrogen Sulfate Ion

Aqueous stoichiometric Al(III) solutions are very acidic and with the hydrolysis of aluminium(III) the formation of hydrogen sulfate is coupled because the second dissociation step of sulfuric acid is of medium strength. The Raman spectrum of  $HSO_4^-$  is strongly concentration and temperature dependent, and was measured over a broad temperature and concentration range by Rudolph, (1996). The Raman data of the vibration spectrum of  $HSO_4^-$  are presented in Table 5.3 and for a detailed description of the spectroscopic data we refer to the publication by Rudolph (1996).

#### 5. 4. 4. $Al_2(SO_4)_3$ aqueous solution spectra, sulfato complexes

We present the Raman spectra of a 0.98 M  $Al_2(SO_4)_3$  solution at 25 °C in Figure 5.3, at 58 °C in Figure 5.4 and at 106 °C in Figure 5.5. The  $R_{pol}$ ,  $R_{depol}$ , and  $R_{iso}$  scattering contributions are presented in panel A from 40 to 800  $cm^{-1}$  and in panel B from 40 to 1400  $cm^{-1}$  for the three Figures, respectively. The high quality Raman spectra in R format make it possible to gain insight into the formation of the aluminum(III) sulfato

complexes. In Figure 5.3 we clearly recognise the sulfate modes and the modes for the hexaaquaaluminium(III) cation as a shoulder at ca. 490  $\text{cm}^{-1}$  in the isotropic scattering,  $R_{\text{iso}}$  (cf. Figure 5.3A). Furthermore, the weak shoulder at ca. 1010  $\text{cm}^{-1}$  is clearly visible contributing only ca. 10 % of the band intensity of  $\nu_1(a_1)$  of (“free”) sulfate (cf. Figure 5.3B) besides the weak, broad mode at ca. 895  $\text{cm}^{-1}$  and a weak mode at 1054  $\text{cm}^{-1}$ .

Knowing the vibrational spectrum of hydrogen sulfate (cf. 4. 3 and discussions in Rudolph, 1996) these modes are assigned as  $\nu_2(a_1)$   $\text{HSO}_4^-$  and  $\nu_1(a_1)$   $\text{HSO}_4^-$ , respectively. At 58 °C, the Raman spectrum in Figure 5.4A, shows clearly the  $\nu_1(a_{1g})$   $\text{AlO}_6$  mode of  $[\text{Al}(\text{OH}_2)_6]^{3+}$  at 525  $\text{cm}^{-1}$  and the water modes in  $[\text{Al}^{3+}(\text{OH}_2)_5 \text{OSO}_3^{2-}]$ , the Al(III) pentaqua-sulfato complex at ca. 490  $\text{cm}^{-1}$  and in addition a weaker isotropic contribution at ca. 465  $\text{cm}^{-1}$ .

Furthermore, weak isotropic contributions at 255, and 355  $\text{cm}^{-1}$  are observable in  $R_{\text{iso}}$ , besides the strong contribution at 665  $\text{cm}^{-1}$ . The hydrogen sulfate modes  $\nu_2(a_1)$   $\text{HSO}_4^-$  and  $\nu_1(a_1)$   $\text{HSO}_4^-$ , at 58 °C in Figure 5.4B are clearly visible at 885  $\text{cm}^{-1}$  (this mode is temperature sensitive) and at 1054  $\text{cm}^{-1}$ , the intensity of these modes has increased with temperature. The isotropic contribution at 1010  $\text{cm}^{-1}$  on the low frequency side of  $\nu_1(a_1)$  of the “free” sulfate has also increased with temperature. This Raman spectrum presents the direct proof of the penetration of sulfate into the first coordination sphere of  $[\text{Al}(\text{OH}_2)_6]^{3+}$ .

At 106 °C (Figure 5.5A) in addition to the sulfate modes and the modes for  $[\text{Al}(\text{OH}_2)_6]^{3+}$ , modes are quite pronounced in the isotropic scattering contribution at 260  $\text{cm}^{-1}$ , 365  $\text{cm}^{-1}$  and a band complex with a maximum at 495  $\text{cm}^{-1}$ . This band complex has a low frequency contribution at 460  $\text{cm}^{-1}$  and at 525  $\text{cm}^{-1}$ , along with a small contribution of the  $\nu_1(a_{1g})$

$\text{AlO}_6$  mode of  $[\text{Al}(\text{OH}_2)_6]^{3+}$ . A weak isotropic scattering contribution at  $586\text{ cm}^{-1}$  is indicative for  $\nu_3(\text{e})\text{HSO}_4^-$ . In Figure 5.5B, the S-O stretching region, again the hydrogen sulfate modes are recognized at  $880\text{ cm}^{-1}$  and at  $1054\text{ cm}^{-1}$ . The modes for the ligated sulfate are at  $1010\text{ cm}^{-1}$ , and additionally a smaller intensity contribution at ca.  $1030\text{ cm}^{-1}$  and another weaker isotropic mode at  $1155\text{ cm}^{-1}$ . Clearly, the band of the ligated sulfate as well as the hydrogen sulfate modes increase with temperature, leading to the conclusion that both processes are entropically driven.

In order to make the band evolution of the isotropic modes described above clearer, we present  $R_{\text{iso}}$  spectra of a  $0.98\text{ M Al}_2(\text{SO}_4)_3$  solution in the temperature range from  $15$  to  $106\text{ }^\circ\text{C}$  in Figure 5.6A and 5.6B. The spectra in the wavenumber range from  $100$  to  $800\text{ cm}^{-1}$  are presented in Figure 5.6A and in the wavenumber range from  $800$  to  $1350\text{ cm}^{-1}$  in Figure 5.6B.

We extended the temperature range to much higher values, relevant for hydrothermal conditions and present a temperature profile of isotropic Raman spectra of a  $0.98\text{ M Al}_2(\text{SO}_4)_3$  solution up to  $184\text{ }^\circ\text{C}$ . In Figure 5.7 the temperature profile of the isotropic Raman spectra ( $800$  to  $1350\text{ cm}^{-1}$ , the S-O stretching region) of a  $0.98\text{ M}$  aqueous  $\text{Al}_2(\text{SO}_4)_3$  solution from  $25$  to  $184\text{ }^\circ\text{C}$  is presented. Figure 5.8 presents the spectrum of a  $0.98\text{ M}$  aqueous  $\text{Al}_2(\text{SO}_4)_3$  solution at  $184\text{ }^\circ\text{C}$ , the temperature of the evolution of the solid, along with the component bands from the nonlinear- least square fit. The results of this non-linear least square fit and the band assignments are presented in Table 5.4. From the isotropic Raman spectrum at  $184\text{ }^\circ\text{C}$  of a  $0.98\text{ mol/L Al}_2(\text{SO}_4)_3$  solution, presented in

Figures 5.7 and 5.8 the following results are given: I) The mode for “free” sulfate at 979.5  $\text{cm}^{-1}$  has almost disappeared. II) The hydrogen modes at 872  $\text{cm}^{-1}$  and 1044/1054  $\text{cm}^{-1}$  are now very intensive. III) In addition to the hydrogen sulfate modes, sulfate appears now as ligated sulfate with modes at 1010  $\text{cm}^{-1}$ , 1033  $\text{cm}^{-1}$ , 1054  $\text{cm}^{-1}$ , 1140  $\text{cm}^{-1}$  and a very weak, broad band at 1230  $\text{cm}^{-1}$ . IV) In the low wavenumber range, four isotropic modes are observed, which also increase with increasing temperature: modes at 260 and 366  $\text{cm}^{-1}$ , and modes in the S-O deformation range at 465 and 670  $\text{cm}^{-1}$  (cf. Figure 5.6).

In previous papers (Rudolph and Schönherr, 1991; Rudolph et al., 2000) we established the existence of 1:1 inner-sphere sulfato complex,  $[\text{Al}(\text{OH}_2)_5\text{OSO}_3^{2-}]$ , in equilibrium with the Al(III)-hexaaqua ion. The following equilibrium can be formulated as the last step of the Eigen-Wilkins-mechanism (cf. our discussions in previous papers (Rudolph, 1998, 2000 )):  $[\text{Al}^{3+}(\text{H}_2\text{O})_6 \cdot \text{SO}_4^{2-}] \rightleftharpoons [\text{Al}^{3+}(\text{H}_2\text{O})_5\text{OSO}_3^{2-}] + \text{H}_2\text{O}$  (7).

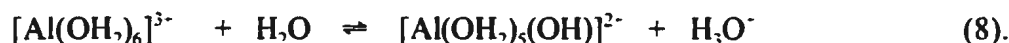
The degree of association was measured by Raman spectroscopy and 27-Al NMR as a function of concentration and temperature (up to 97 °C). 27-Al NMR spectroscopy allows the detection of the hexaaquaaluminium(III) and an aluminium species,  $[\text{Al}^{3+}(\text{H}_2\text{O})_5\text{OSO}_3^{2-}]$  3.3 ppm at higher field (Akitt et al., 1985; Rudolph and Schönherr, 1991). In the concentration range between 0.098- 0.98  $\text{mol} \cdot \text{L}^{-1}$  at 22 °C the concentration quotient for the association reaction,  $Q$ , has a constant value of  $0.13 \pm 0.01$ . The thermodynamic association constant and the enthalpy of formation for the contact ion pair were estimated to be  $K_A = 0.15 \pm 0.01$  and  $\Delta H^\circ = 28 \pm 2 \text{ kJ} \cdot \text{mol}^{-1}$ . The following reliable statement is given. At room temperature and below the sulfato complex occurs in low

concentration, this means most of the sulfate must occur in the second hydration sphere of the hexaaqua-aluminum(III) ion,  $[\text{Al}^{3+}(\text{H}_2\text{O})_6\text{SO}_4^{2-}]$  (about inner-sphere/outer-sphere complexes cf. for instance Rudolph et al., 1999). With increasing temperature the inner-sphere sulfato complex formation (diagnostic band at  $1010\text{ cm}^{-1}$ ) increases, indicating that the reaction is entropically driven.

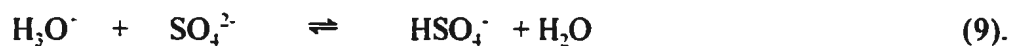
Besides the mode at  $1010\text{ cm}^{-1}$ , which has been previously assigned (Rudolph and Schönherr, 1991) as a sulfate ligand of a aluminum sulfato complex of possible  $C_{3v}$  symmetry, the isotropic modes at  $1033\text{ cm}^{-1}$ ,  $1140\text{ cm}^{-1}$  and at  $1230\text{ cm}^{-1}$  are newly detected modes of ligated sulfate (these modes are only observed above  $160\text{ }^\circ\text{C}$ ) due to a previously unreported sulfato complex species. This leaves the four modes at  $260$ ,  $366$ ,  $465$  and  $670\text{ cm}^{-1}$  to be assigned. The two modes at low wavenumbers, are most likely due to vibrations between  $\text{Al}^{3+}$  and the sulfate ligand, so called ligand modes and the modes at  $465$  and  $670\text{ cm}^{-1}$ , lying in the S-O deformation range of sulfate, are the bending modes of ligated sulfate. (Note, that the deformation modes of “free” sulfate,  $\nu_2(\text{e})$  and  $\nu_4(\text{f}_2)$  have no isotropic contributions.) We speculate that sulfate replaces another water molecule out of the first coordination sphere of a second  $[\text{Al}(\text{OH}_2)_6]^{3+}$  cation, at hydrothermal conditions, so that sulfate acts as a bidentate bridging ligand and even another water molecule of a third  $[\text{Al}(\text{OH}_2)_6]^{3+}$  could be replaced, so that sulfate would act as a tridentate bridging ligand as can be observed in the structure of alunite. This would account for the new polarized bands and for the similarity to sulfate in the hydronium alunite spectrum, discussed below. It should be noted that a bidentate bridging sulfate group has been

reported in  $[(\text{NH}_3)_4\text{Co}(\text{NH}_2\text{SO}_4)\text{Co}(\text{NH}_3)_4]$  (Nakamoto et al.(1957)).

It has been already pointed out that the hydrolysis of  $\text{Al}^{3+}$  becomes detectable above 25 °C and steadily increases with temperature (cf. Figure 5.6 and 5.7). The hydrolysis of  $[\text{Al}(\text{OH}_2)_6]^{3+}$  can be written according to:



The hydrolysis reactions in equation 8 is coupled with the sulfate ionization reaction:



As a result the degree of hydrolysis can be determined by measuring the equilibrium molalities of  $\text{HSO}_4^-$  and free  $\text{SO}_4^{2-}$ . In effect, sulfate acts as a probe that can be used to detect the hydrolysis of aluminum(III) as a function of temperature.

Raman spectroscopic studies on aqueous ammonium sulfate, published by one of us (Rudolph, 1996), have determined accurate molar scattering coefficients and values for the equilibrium quotient of reaction 9 at elevated temperatures. From quantitative Raman spectroscopic data (Rudolph, 1996), we were able to estimate the equilibrium quotient of mono-hydroxo-aluminum(III) according to eq. (8). Data for the 0.98 M (1.012 m)  $\text{Al}_2(\text{SO}_4)_3$  solution at 184°C yielded the approximate value of  $\text{p}Q_{11} = 2.0 \pm 0.5$ . Thermodynamic values for the  $\text{p}K_{11}$  of reaction (9) at 25°C are  $5.00 \pm 0.02$  at  $I = 0$  and at 185°C the  $\text{p}K_{11}$  value is  $1.5 \pm 0.1$  (Palmer and Wesolowski, 1993). More accurate Raman values of  $\text{p}Q_{11}$  might be obtained by using lower concentrations of sulfate in dilute aqueous  $\text{Al}(\text{ClO}_4)_3$  solutions. This procedure opens the possibility for determining hydrolysis constants at elevated temperatures and pressures with Raman spectroscopy by using sulfate

as a probe ion (cf. also Rudolph, Brooker and Tremaine, 1999).

It should be pointed out that the hydrolysis is also strongly influenced by the competing sulfato complex formation, which also increases with temperature, an entropically driven reaction. The principal equilibrium step for sulfato complex formation is according to eq. (7).

### 5. 5. Hydronium alunite

During our Raman measurement of a 0.98 M  $\text{Al}_2(\text{SO}_4)_3$  solution at 184°C a white precipitate was slowly formed and after the measuring cycle of ca. 40 minutes the amount of precipitate was quite substantial in amount and halted further measurements. A similar precipitate forms at 135°C from a dilute  $\text{Al}_2(\text{SO}_4)_3$  solution (0.098 M). The Raman spectrum of the white precipitate was measured *in situ* and the strongest band was detected at 1034  $\text{cm}^{-1}$ . After cooling the precipitate was characterized by XRD (search against the JCPDS (# 16-409)) and shown to be hydronium alunite,  $(\text{H}_3\text{O})\text{Al}_3(\text{SO}_4)_2(\text{OH})_6$ . The analytical results for H-alunite 20.5 % Al and 16.20 % S compare favourably with the theoretical values for  $(\text{H}_3\text{O})\text{Al}_3(\text{SO}_4)_2(\text{OH})_6$ , namely 20.527 % Al and 16.270 % S. The (hexagonal) unit cell parameters were determined with  $a = 7.0082(2) \text{ \AA}$  and  $b = 17.1377(2) \text{ \AA}$  and  $V = 729.01(2) \text{ \AA}^3$ . Our unit cell parameters are almost identical with the most recent published unit cell parameters for H-alunite (Stoffregen and Alpers, 1992).

There is only one published infrared spectrum of alunite, the pure potassium end member (Farmer, 1974). In Figure 5.9 the infrared and Raman spectra at 25°C for hydronium alunite are presented and the band assignments are given in Table 5.5. This

Raman spectrum has, to the best of our knowledge, not been reported. The vibrational spectral data presented are of diagnostic value to identify hydronium alunite, and the strongest Raman mode  $\nu_1\text{SO}_4^{2-}$  band  $1035 \pm 1 \text{ cm}^{-1}$  was used in detecting H-alunite *in situ*.

About the possible mechanism of the formation of hydronium alunite in stoichiometric solutions the following reaction may be written:



The formation of hydronium alunite results in an acidification of the supernatant and a conversion of sulfate into hydrogen sulfate. Measurements of the pH of the supernatant after precipitation of H- alunite has confirmed this. The pH dropped from 1.44 to 0.80. Raman spectroscopic measurement of the cooled supernatant shows that almost 50 % of the sulfate was converted into hydrogen sulfate.

From the precipitation reaction 10 and the following of the Raman spectra to hydrothermal conditions, the following conclusions may be drawn. Reaction 10 is a general equation and from our Raman spectroscopic investigations we know, that Al(III) is strongly hydrated and shows hydrolysis which increases with temperature (cf. equation 8). With the formation of hydronium ions, according to eq. 8 the formation of hydrogen sulfate is coupled according ( reaction 9) and both processes increase with increasing temperature. The six hydroxyl ions in H- alunite result from the hydrolysis of Al(III). Furthermore, in dilute aqueous  $\text{Al}_2(\text{SO}_4)_3$  solutions, e.g. 0.098 mol/L, the hydrolysis is enhanced and precipitation takes place at a lower temperature. For example a 0.098 mol/L  $\text{Al}_2(\text{SO}_4)_3$  solution, the H-alunite precipitation started at 135 °C. For much more dilute

solutions, the temperature of H-alunite formation is expected to be lower. A slight rise in pH should also increase as the H-alunite precipitates, but in solutions with a high  $\text{OH}^-/\text{Al}^{3+}$  ratio other basic aluminium sulfates may be formed (Bertsch, 1989). In short, the hydrolysis reaction of aluminum(III) delivers the  $\text{OH}^-$  ions and the sulfate buffers the hydronium ions formed. This fact is deduced from Raman spectroscopy and is furthermore supported by the results, that  $\text{Al}_2(\text{SO}_4)_3$  solutions with a large excess of sulfuric acid (above 4 M) do not show H-alunite formation (cf. results by Akitt et al., 1972) but rather soluble aluminium(III) complexes with sulfuric acid are formed. The Raman spectrum of the  $\text{Al}_2(\text{SO}_4)_3 - \text{H}_2\text{O}$  system shows furthermore, that aqua-hydroxy-aluminum(III) sulfato complexes are formed and it is possible to postulate preformed aqua-hydroxy-aluminum(III) - sulfato entities prior to H-alunite formation according to reaction 10. In the alunite structure, the sulfate anions form tridentate ligands which are bridged to three different Al(III) ions (for the alunite structure see Menchetti and Sabelli, 1976).

## 5. 6. Conclusions

i) At temperatures above 100 °C the hydrolysis reaction of the  $[\text{Al}(\text{OH}_2)_6]^{3+}$  is significant and  $\text{HSO}_4^-$  is formed in a corresponding reaction. The  $\text{p}Q_{11}$  values of the mono-hydroxo aluminum in both solutions were estimated.

ii) The degree of sulfato complex formation is also increased and complex species, most likely a bidentate and tridentate bridging sulfato complexes, are formed.

iii) Hydronium alunite is formed in stoichiometric aluminum sulfate solutions in the temperature range from 135 to 184°C under hydrothermal conditions.

iv) The formation of hydronium alunite is discussed in terms of the aluminum(III) hydrolysis, the corresponding formation of hydrogen sulfate and formation of sulfato complexes ions prior to hydronium alunite precipitation.

v) The i.r. and Raman spectra of hydronium alunite are reported and band assignments are given.

#### Acknowledgements

W. W. R. thanks for a scholarship from graduate studies of Memorial University NF, during the period 1997 till 1998. W. W. R. thanks also Dr. C. C. Pye, St. Mary's University, Halifax for helpful discussions and support.

Table 5.1: The  $\text{AlO}_6$  skeleton modes ( $\text{AlO}_6$  unit possesses  $O_h$  symmetry), Raman and i.r. spectroscopic frequencies in aqueous  $\text{Al}(\text{ClO}_4)_3$  and  $\text{AlCl}_3$  and solutions. (In these solutions no inner-sphere complexes are formed, while in  $\text{Al}_2(\text{SO}_4)_3$  solutions sulfato complex formation occurs).

assignment and activity	exper. frequencies ( $\text{cm}^{-1}$ ) in $\text{H}_2\text{O}$ 1)
$\nu_1(a_{1g})$ Ra	$525 \pm 1$ (0.003)
$\nu_2(e_g)$ Ra	$438 \pm 2$ (0.75)
$\nu_3(f_{1u})$ i.r.	$598 \pm 2$
$\nu_4(f_{1u})$ i.r.	not observed
$\nu_5(f_{2g})$ Ra	$332 \pm 2$ (0.75)
$\nu_6(f_{2u})$ -	not active

Note: in brackets the depolarization ratio is given.

1) W. W. Rudolph and S. Schönherr, Z. Phys. Chem. (Leipzig), **270** (1989) 1121.

Table 5.2: Correlation table for the point groups  $T_d$ ,  $C_{3v}$  and  $C_{2v}$ . Sulfate in undisturbed form (dilute aqueous  $(NH_4)_2SO_4$  solution), and two lower symmetry environments. The Raman and i.r. activities are given as well the numbers of Raman bands inclusive the number of polarized modes and the number of i.r. active modes coinciding with the Raman modes. The wavenumbers for the sulfate modes in undisturbed form ( $T_d$ ) are given in  $cm^{-1}$ .

$\nu$	$SO_4^{2-}$	$T_d$	$C_{3v}$	$C_{2v}$
$\nu_3$	1104	$f_2$ (Ra, i.r.)	$a_1$ (Ra, i.r.) + e (Ra, i.r.)	$a_1$ (Ra, i.r.) + $b_1$ (Ra, i.r.) + $b_2$ (Ra, i.r.)
$\nu_1$	980.7	$a_1$ (Ra)	$a_1$ (Ra, i.r.)	$a_1$ (Ra, i.r.)
$\nu_4$	613	$f_2$ (Ra, i.r.)	$a_1$ (Ra, i.r.) + e (Ra, i.r.)	$a_1$ (Ra, i.r.) + $b_1$ (Ra, i.r.) + $b_2$ (Ra, i.r.)
$\nu_2$	451	e (Ra)	e (Ra, i.r.)	$a_1$ (Ra, i.r.) + $a_2$ (Ra)
number of Raman active modes (in brackets the polarized bands)				
		4(1)	6(3)	9(4)
number of i.r. active modes (equal the number of coincidences with Raman bands)				
		2	6	8

Table 5.3: The assignment of the  $\text{HSO}_4^-$  modes, Raman band positions ( $\text{cm}^{-1}$ ), fwhh ( $\text{cm}^{-1}$ ), and degree of polarization of the hydrogen sulfate modes in 0.85 M  $(\text{NH}_4)\text{HSO}_4$  solution at 22 and 184 °C.

Assignment	22 °C	184 °C
$\nu_6(\text{a}_1) \text{HSO}_4^-$	422, -, dp	424, 50, dp
$\nu_3(\text{a}_1) + \nu_5(\text{e}) \text{HSO}_4^-$	586, -, pol	587, 32, 0.54
$\nu_2(\text{a}_1) \text{HSO}_4^-$	898, 46, 0.05	864, 50, 0.05
$\nu_1(\text{a}_1) \text{HSO}_4^-$	1053 <sup>a</sup> , 21.5, 0.014	1055, 13.0, 0.01
$\nu_4(\text{a}_1) \text{HSO}_4^-$	1202, 84, dp	1220, 86, dp

<sup>a</sup> At the low frequency side at  $1044 \text{ cm}^{-1}$  a shoulder is observable. For detailed explanation cf. Ref. 11.

Table 5.4: Parameters of the band components of the isotropic Raman spectrum of a 0.98 mol·L<sup>-1</sup> aqueous Al<sub>2</sub>(SO<sub>4</sub>)<sub>3</sub> solution at 184°C in the wavenumber region between 780 - 1350 cm<sup>-1</sup>. Compare also with Figure 8.

peak position (cm <sup>-1</sup> )	FWHH (cm <sup>-1</sup> )	R-factor	area	band assignment
872.0	60.5	0.82	67,53.0	$\nu$ S-OH (HSO <sub>4</sub> <sup>-</sup> )
979.5	14.9	0.69	2,788.0	$\nu_1$ SO <sub>4</sub> <sup>2-</sup> (free)
1010	38.0	0.86	28,194.0	SO <sub>4</sub> <sup>2-</sup> (complex)
1033	30.2	0.57	9,119.0	SO <sub>4</sub> <sup>2-</sup> (complex)
1044	74.0	0.72	6,114.0	$\nu_s$ SO <sub>3</sub> (HSO <sub>4</sub> <sup>-</sup> )
1054	16.5	0.92	16,057.0	$\nu_s$ SO <sub>3</sub> (HSO <sub>4</sub> <sup>-</sup> )
1141	46.2	0.72	4,930.0	SO <sub>4</sub> <sup>2-</sup> (complex)
1245	36.0	0.37	587.0	SO <sub>4</sub> <sup>2-</sup> (complex)

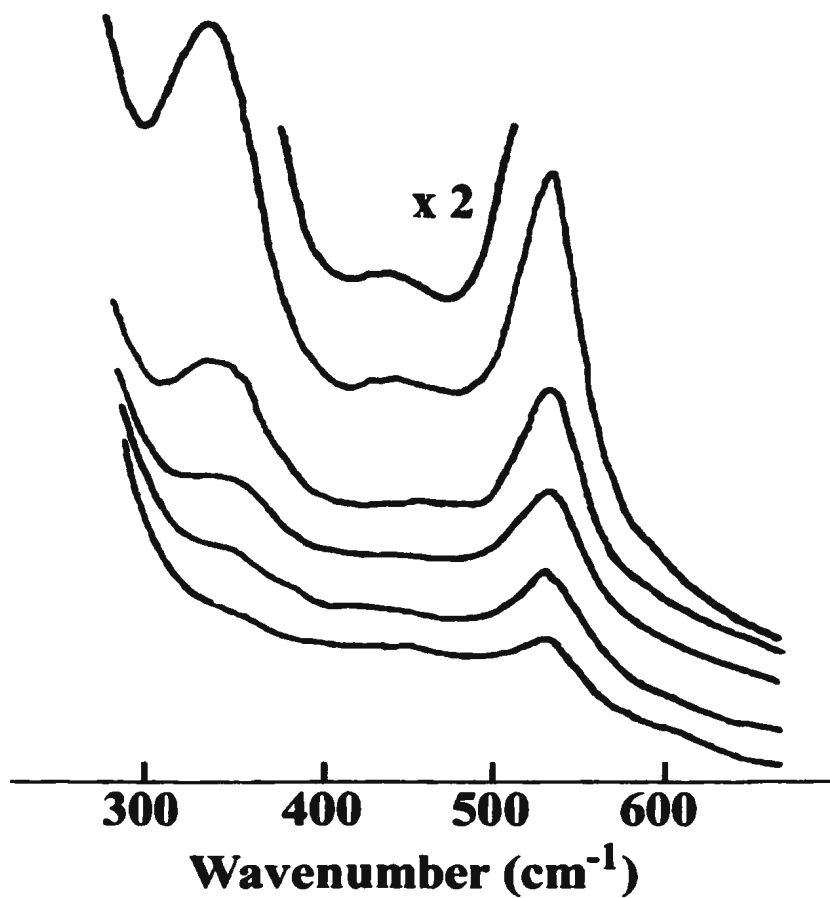
Table 5.5: Raman and infrared data for  $(\text{H}_3\text{O})\text{Al}_3(\text{SO}_4)_2(\text{OH})_6$  (hydronium alunite) at 25°C.\* Compare also with Figure 8.

Raman ( $\text{cm}^{-1}$ )**	infrared ( $\text{cm}^{-1}$ )**	band assignment
160 vw		
181 vw		
238 str-m,	240 w	
250 sh		
	285 m	$\text{AlO}_6$
352 m	350 str + 418 vw	$\text{AlO}_6$
383 m - str		$\text{AlO}_6$
488 str	490 w	$\nu_2 \text{SO}_4^{2-}$
504 m	515 sh, w	$\text{AlO}_6$
560 vvw + 590 vvw	592 str + 626 sh	$\text{AlO}_6$
648 str	666 str	$\nu_4 \text{SO}_4^{2-}$
880 vw, br	820 w, br	$\gamma \text{OH}$
1035 vstr	1033 vw	$\nu_1 \text{SO}_4^{2-}$
1072 m	1081 vstr	$\nu_3 \text{SO}_4^{2-}$
1110 w, br	1115 str, sh	$\text{H}_3\text{O}^+$
1161 w	1172 sh, m	$\delta \text{OH}$
1192 m	-	$\nu_3 \text{SO}_4^{2-}$
-	1237 vstr	$\nu_3 \text{SO}_4^{2-}$
-	1260sh	overtones $\text{SO}_4^{2-}$
1600, vvw, br	1615 m	$\text{H}_3\text{O}^+$
1635, vvw, br	1645 m	$\text{H}_2\text{O}$
-	1690 w,br	$\text{H}_2\text{O}$

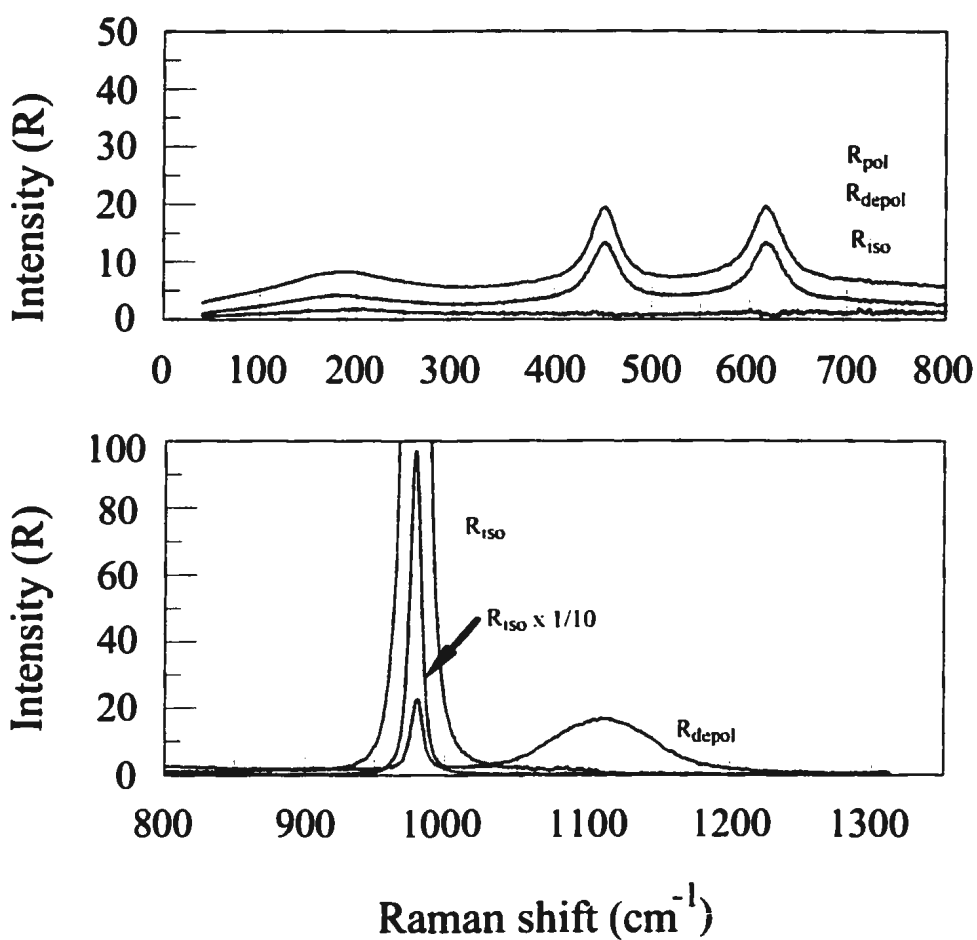
2250 vw, vbr	2190 w-m, vbr	H <sub>3</sub> O <sup>-</sup>
2700 vw, vbr	2700 vw, vbr	H <sub>3</sub> O <sup>-</sup>
3400 w, br, sh	3420 + 3200 w-vw, br	H <sub>2</sub> O
3478 w,br + 3500 w,br	3478 str, br + 3500 sh	stretch OH

\* Space group: R3m ( $D_{3d}^5$ ) with  $z = 3$ , where sulfate occupies  $C_{3v}$  site (No.166 of the International Tables).

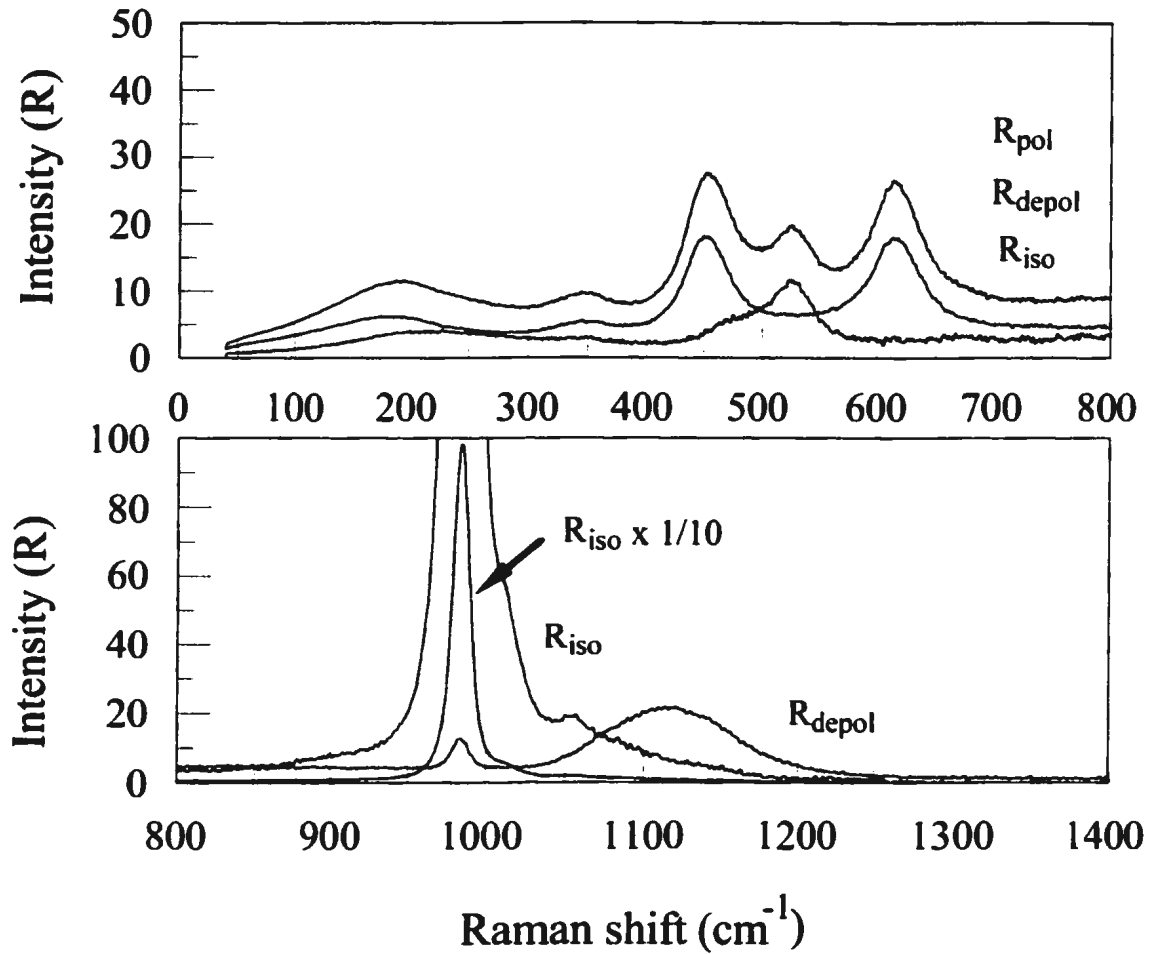
\*\* vvw = very, very weak, vw = very weak, w = weak, m = medium, str = strong, vstr = very strong, br = broad, and sh = shoulder.



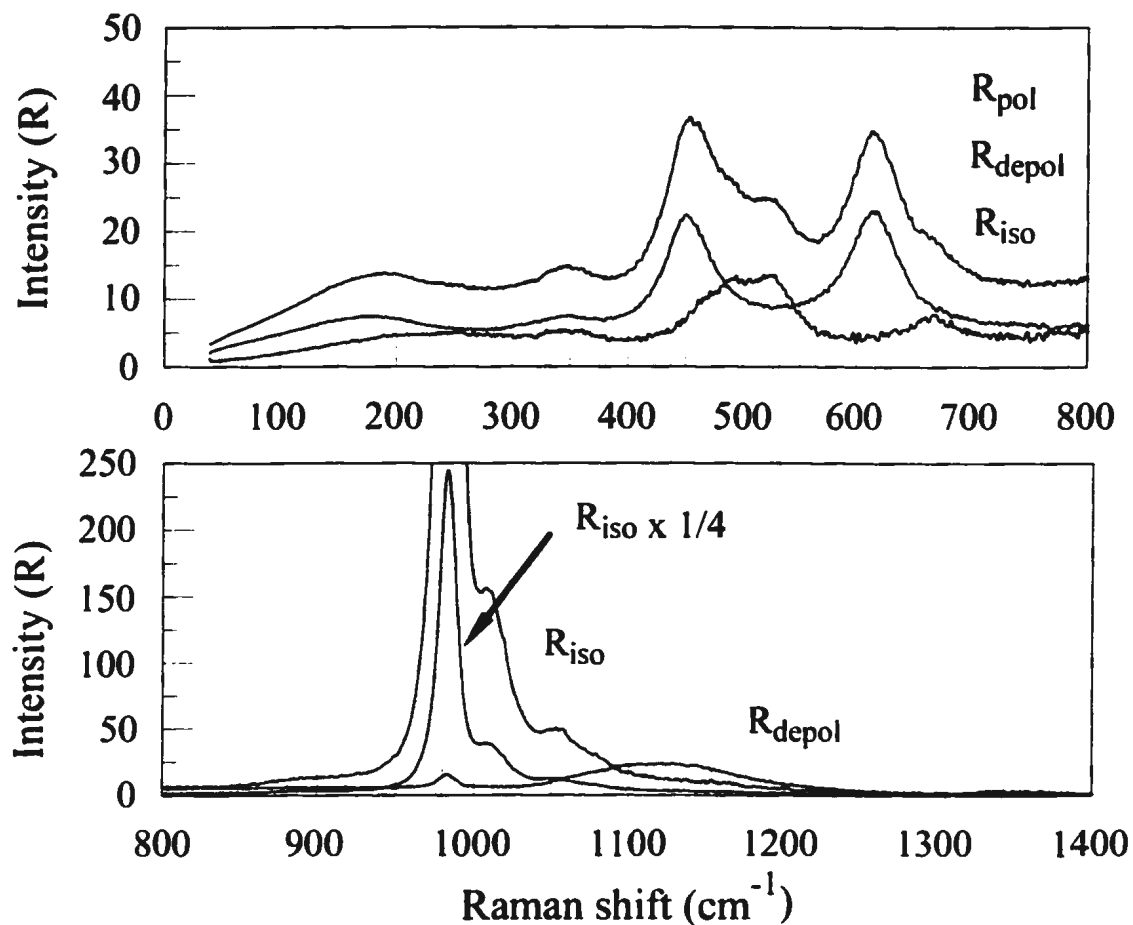
5.1. Polarized Raman spectra in I - format of aqueous  $\text{AlCl}_3$  solutions at  $22^\circ\text{C}$  in the wavenumber range from  $240$  to  $680\text{ cm}^{-1}$  ( $\text{AlO}_6$  modes:  $\nu_1(\text{a}_{1g}) = 525\text{ cm}^{-1}$ ,  $\nu_2(\text{e}_g) = 438\text{ cm}^{-1}$  and  $\nu_5(\text{f}_{2g}) = 332\text{ cm}^{-1}$ ). From top to bottom:  $3.14\text{ M}$ ;  $2.00\text{ M}$ ;  $1.50\text{ M}$ ;  $1.00\text{ M}$  and  $0.50\text{ M}$ . Note, that on top of the spectrum of the  $3.14\text{ M}$  solution, the weak mode  $\nu_2(\text{e}_g)$  is drawn with twice the intensity.



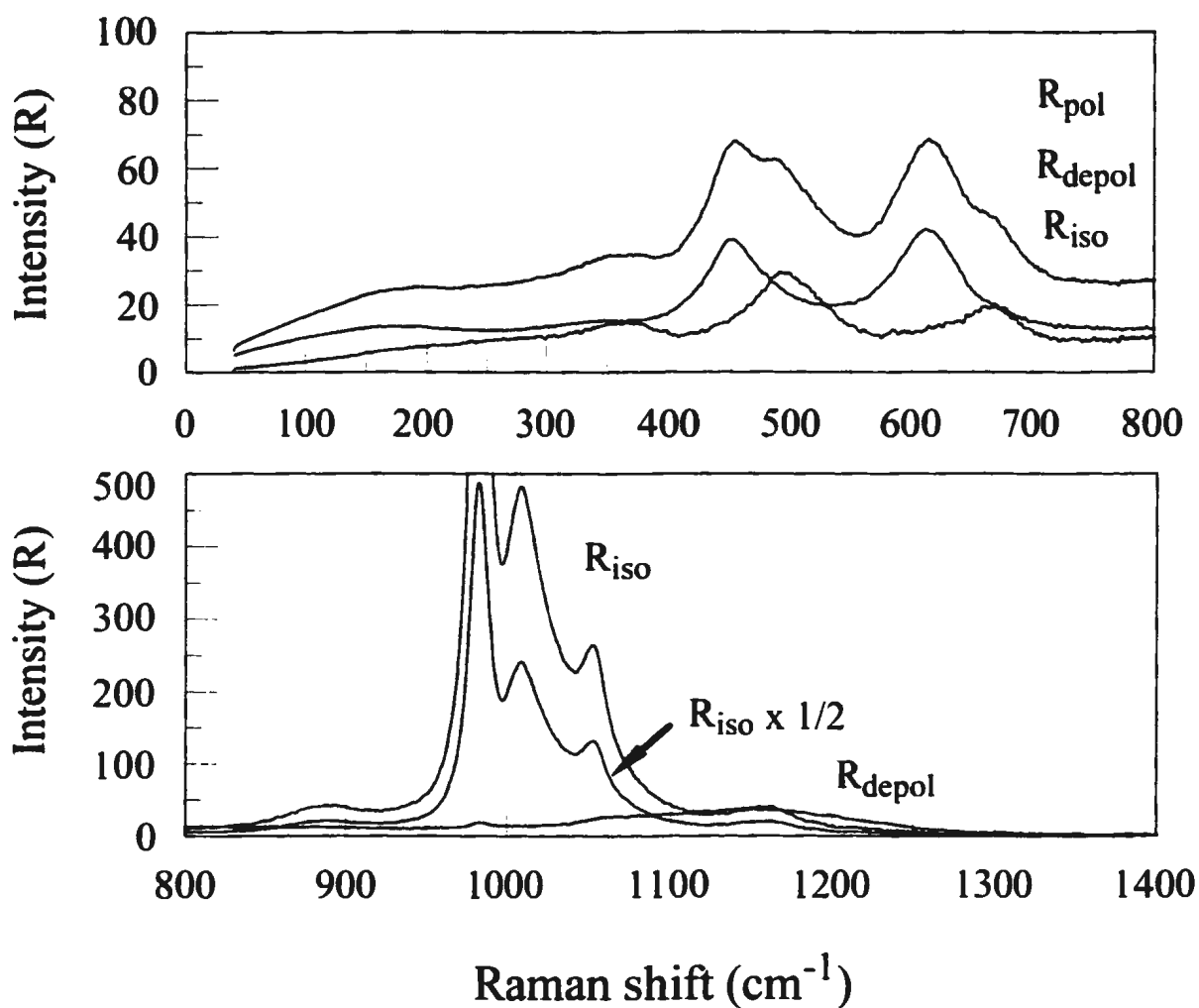
5.2. Raman spectrum of a 3.00 M aqueous  $(\text{NH}_4)_2\text{SO}_4$  solution at 22°C. Panel A gives the wavenumber range from 40 to 800  $\text{cm}^{-1}$  (deformation modes of sulfate). Panel B gives the wavenumber range from 800 to 1350  $\text{cm}^{-1}$  (S-O stretching modes). For explanations see text. In panel A the spectra in R format  $R_{\text{pol}}$ ,  $R_{\text{depol}}$  and  $R_{\text{iso}}$  are presented. In panel B only  $R_{\text{iso}}$  and  $R_{\text{depol}}$  are given for clarity. The mode  $\nu_1(a_1)$   $\text{SO}_4^{2-}$  at 981  $\text{cm}^{-1}$  is presented 1/10 of its size



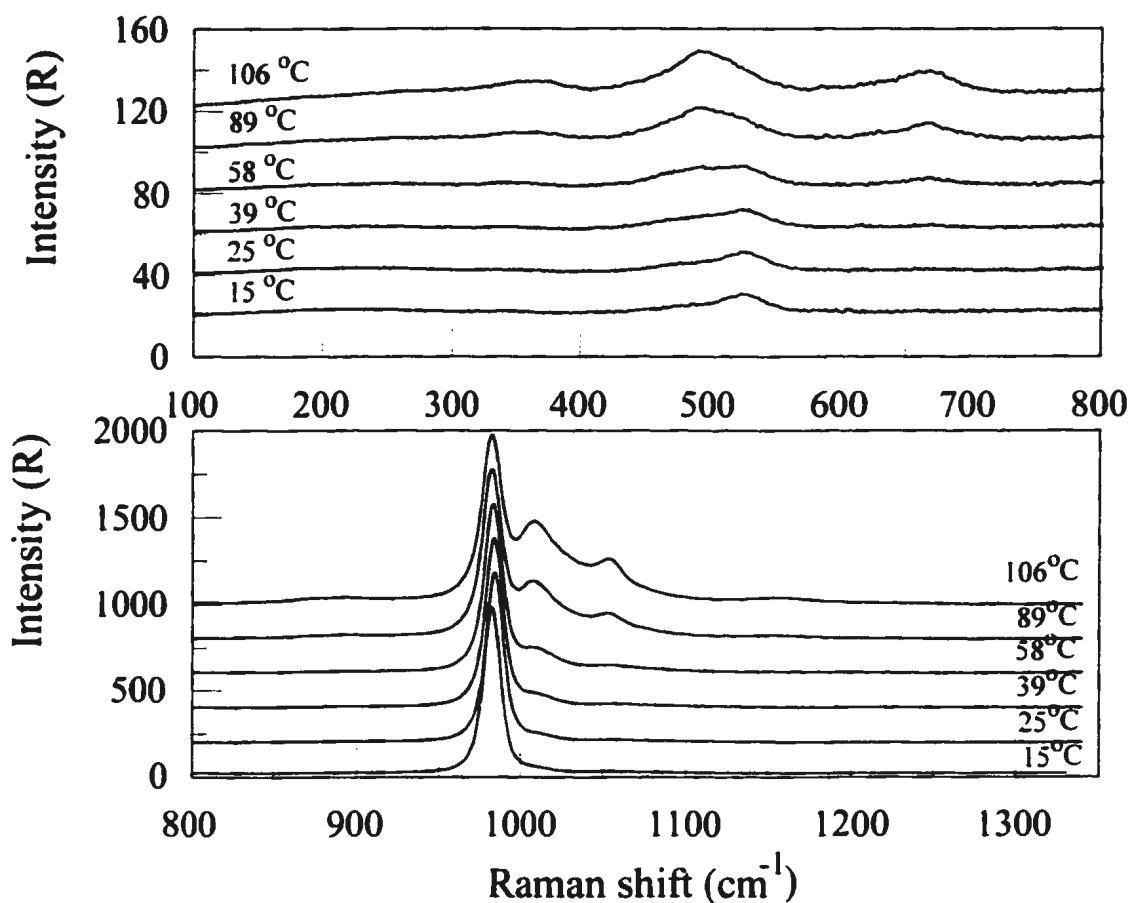
5.3. The Raman spectra (R- format) of an aqueous  $\text{Al}_2(\text{SO}_4)_3$  solution, 0.98 M, at 25°C. In panel A the wavenumber range from 40 - 800  $\text{cm}^{-1}$  is given. Note in the isotropic spectrum the mode  $\nu_1(a_{1g}) \text{AlO}_6$  at 525  $\text{cm}^{-1}$ , and the shoulder at the lower wavenumbers at ca. 480  $\text{cm}^{-1}$ . Panel B gives the wavenumber range from 800 - 1400. Note the shoulder at ca. 1011  $\text{cm}^{-1}$  (stemming from sulfato complex) and the weak mode at 1054  $\text{cm}^{-1}$  (mode  $\nu_1(\text{HSO}_4^-)$ )



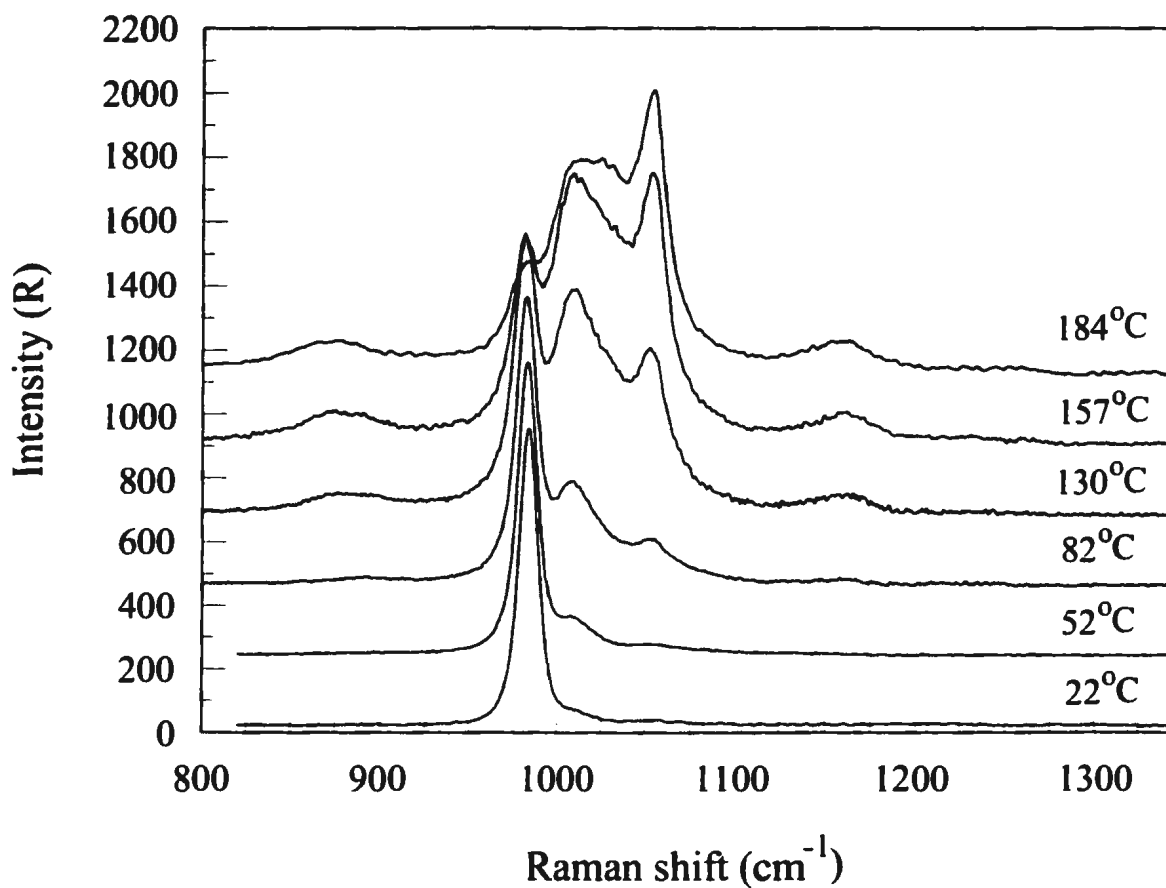
5.4. The Raman spectra (R- format) of an aqueous  $\text{Al}_2(\text{SO}_4)_3$  solution, 0.98 M, at 58°C. In panel A the wavenumber range from 40 - 800  $\text{cm}^{-1}$  is given. Note in the isotropic spectrum, that instead of a single mode  $\nu_1(a_{1g}) \text{AlO}_6$  at 525  $\text{cm}^{-1}$  a double band is observable (maxima at 525 and 490  $\text{cm}^{-1}$ ). The mode at 668  $\text{cm}^{-1}$  and 365  $\text{cm}^{-1}$  are indicative of the sulfato complex. Panel B gives the wavenumber range from 800 - 1400. Note at higher frequencies to the sulfate mode ( $\nu_1(e) - \text{SO}_4^{2-}$  at 983) the pronounced shoulder at ca. 1010  $\text{cm}^{-1}$  (sulfato complex) and the weaker mode at 1054  $\text{cm}^{-1}$  (hydrogen sulfate,  $\nu_1(a_1) (\text{HSO}_4^-)$ ). The weak broad mode at 892  $\text{cm}^{-1}$  is also indicative of hydrogen sulfate, namely  $\nu_2(a_1) (\text{HSO}_4^-)$



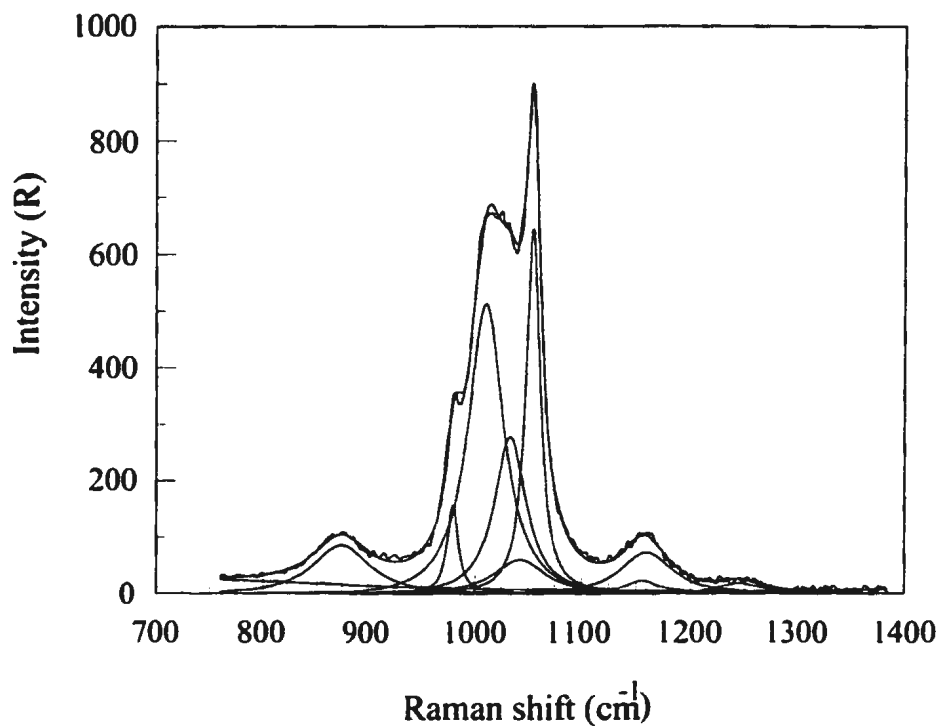
5.5. The Raman spectra (R- format) of an aqueous  $Al_2(SO_4)_3$  solution, 0.98 M, at 106°C. In panel A the wavenumber range from 40 - 800  $cm^{-1}$  is given. Note in the isotropic spectrum, that the mode at 525  $cm^{-1}$  ( $\nu_1(a_{1g}) AlO_6$ ) a mode at 490  $cm^{-1}$  is observable. The mode at 668  $cm^{-1}$  and 365  $cm^{-1}$  are indicative for the sulfato complex. In addition, a weak mode at 585  $cm^{-1}$  is observable, stemming from hydrogen sulfate, namely  $\nu_3(a_1)$  ( $HSO_4^-$ ). Panel B gives the wavenumber range from 800 - 1400. Note at higher frequencies to the sulfate mode ( $\nu_1(e) -SO_4^{2-}$  at 981.5) the pronounced shoulder at ca. 1010  $cm^{-1}$  (sulfato complex) and the weaker mode at 1054  $cm^{-1}$  (hydrogen sulfate,  $\nu_1(a_1)$  ( $HSO_4^-$ )). The weak broad mode at 886  $cm^{-1}$  is also indicative of hydrogen sulfate, namely  $\nu_2(a_1)$  ( $HSO_4^-$ ). The weak broad modes at 1155  $cm^{-1}$  and ca. 1250  $cm^{-1}$  are indicative for the sulfato complex



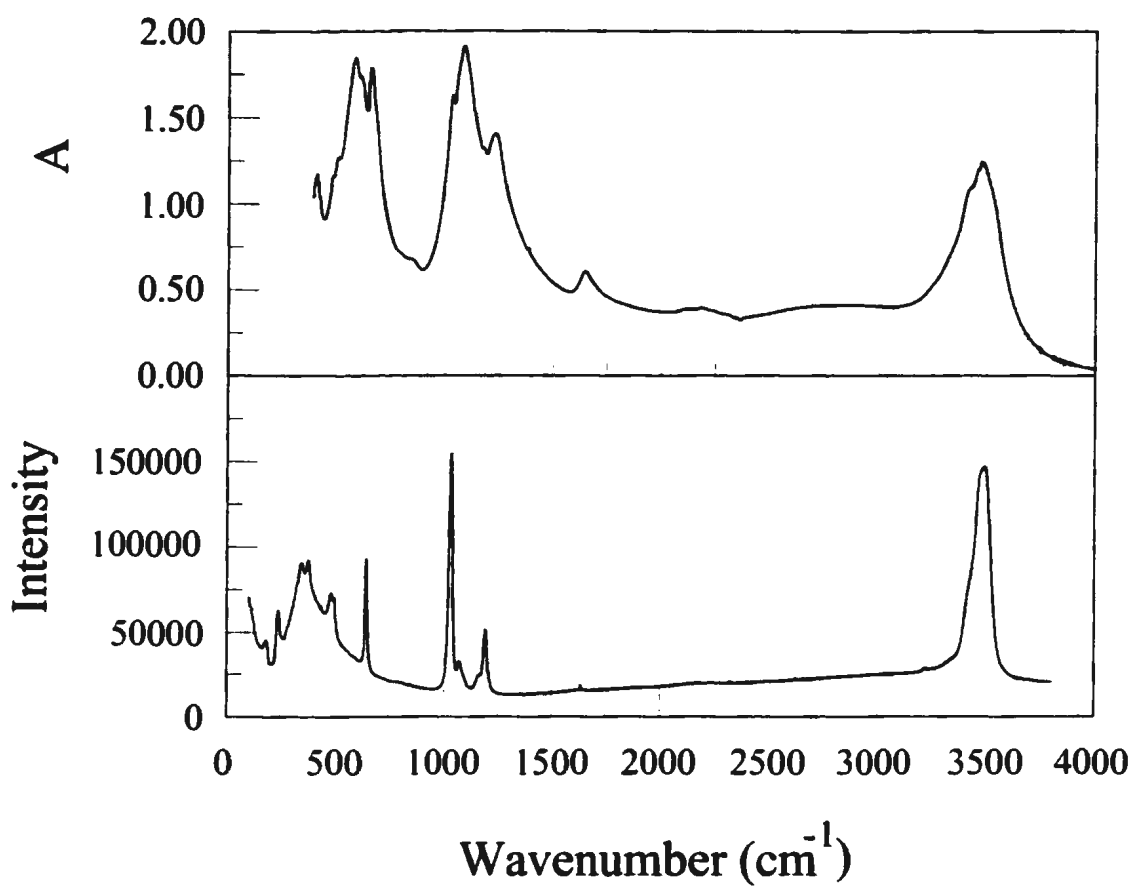
5.6. Temperature profile (15 °C to 106 °C) of the isotropic Raman spectra in R-format of an 0.98 M (1.012 m) aqueous  $\text{Al}_2(\text{SO}_4)_3$  solution. In panel A the wavenumber range from 40 - 800  $\text{cm}^{-1}$  is given. Note in the isotropic spectrum, that the mode at 525  $\text{cm}^{-1}$  ( $\nu_1(a_{1g}) \text{AlO}_6$ ) is disappearing successively with temperature increase and a new band at 490  $\text{cm}^{-1}$  is observable. The modes at 365  $\text{cm}^{-1}$ , 465  $\text{cm}^{-1}$  and at 668  $\text{cm}^{-1}$ , also indicative for the ligated sulfate, and are also rising with temperature. In the spectrum at 106 °C the hydrogen sulfate mode at 585  $\text{cm}^{-1}$ ,  $\nu_3(a_1)$  ( $\text{HSO}_4^-$ ) is observable. Panel B gives the wavenumber range from 800 - 1400. Note the mode of "free" sulfate,  $\nu_1(e) - \text{SO}_4^{2-}$ , at 984  $\text{cm}^{-1}$  shifting slightly with temperature from 984  $\text{cm}^{-1}$  at 15 °C to 981.5  $\text{cm}^{-1}$  at 106 °C. The modes indicative for ligated sulfate at 1010  $\text{cm}^{-1}$ , 1030  $\text{cm}^{-1}$  (shoulder), 1155  $\text{cm}^{-1}$  and 1250  $\text{cm}^{-1}$  increase in intensity continuously with temperature. The modes of  $\text{HSO}_4^-$ , at 1054  $\text{cm}^{-1}$  (with a shoulder at 1044  $\text{cm}^{-1}$ ) and at 896  $\text{cm}^{-1}$  (this mode is strongly temperature dependent) increase also with temperature



5.7. Temperature profile of the isotropic Raman spectra in R-format of an 0.98 M (1.012 m) aqueous  $\text{Al}_2(\text{SO}_4)_3$  solution from room temperature (22 °C) to 184 °C, the temperature alunite is precipitating. The wavenumber range from 800- 1350  $\text{cm}^{-1}$  is given. The explanation under panel B , Figure 6, is applicable here as well. Note that the free sulfate disappeared almost completely at 184 °C, transformed into ligated sulfate and hydrogen sulfate.



5.8. Isotropic Raman spectrum in R- format of a 0.98 M (1.012 molal)  $\text{Al}_2(\text{SO}_4)_3$  solution at 184 °C at 760 - 1380  $\text{cm}^{-1}$ . In addition, the synthetic band profile is given, as well as, the component bands and the baseline. Note the component at 870  $\text{cm}^{-1}$  and 1044/1054  $\text{cm}^{-1}$ , which are due to  $\text{HSO}_4^-$ . The unligated sulfate mode at 978  $\text{cm}^{-1}$  has almost disappeared. The other modes at 1010, 1033, 1154 and 1245  $\text{cm}^{-1}$  are due to the ligated sulfate.



5.9. Overview infrared and Raman spectrum of  $(\text{H}_3\text{O})\text{Al}_3(\text{SO}_4)_2(\text{OH})_6$  at 25°C. In the upper panel the i.r spectrum is given whilst in the lower panel the Raman spectrum is given

## 5. 7. References

- Akitt, J. W., Greenwood, N. N. and Khandelwal, B. L., 1972. "Aluminium-27 Nuclear Magnetic Resonance Studies of Sulphato-complexes of the Hexa-Aquo Aluminium Ion". *J. C. S. Dalton*, 1226-1229.
- Akitt, J. W., Farnsworth, J. A. and Letellier, P., 1985. "Aluminium-27 Nuclear Magnetic Resonance Studies of Sulphato-complex formation". *J. Chem. Soc., Faraday Trans. I.*, 81, 193 -201.
- Bertsch, P. M., (1989) "Aqueous Polynuclear Aluminium Species". Ch. 4, in "The Environmental Chemistry of Aluminum", Editor: G. Sposito, CRC Press, Boca Raton, Florida, 87 - 115.
- Brooker, M. H., Faurkov Nielsen, O. and Praestgaard, E., 1988. "Assessment of correction procedures for reduction of Raman spectra", 19, 71- 78.
- Farmer, V. C., 1974." *The Infrared Spectra of Minerals*". Mineralogical Society, London.
- Finch, C., 1993. "Methods of water analysis by inductively coupled plasma-emission spectrometry". *Current Research*. Newfoundland Department of Mines and Energy, Geological Survey Branch, Report 93-1, 435 - 441.
- Harris, W. E. and Kratochvil, B. *An Introduction to Chemical Analysis*". Saunders College Publishing, Philadelphia, 1981), p. 75, p. 203.
- Lükewille, A. and Prenzel, J.. 1993. Reconstruction of water acidification in a forested catchment, western Harz Mountains, Germany". *Applied Geochem.*, Suppl. Issue

No.2, 131 - 134.

Menchetti, S. and Sabelli, C., 1976. "Crystal chemistry of the alunite series: crystal structure refinement of alunite and synthetic jarosite". *N. Jb. Miner. Mh.*, 406 - 417.

Nakamoto, K., Fujita, J., Tanaka, S. and Kobayashi, M., 1957. "Infrared Spectra of Metallic Complexes. IV. Comparison of the Infrared Spectra of Unidentate and Bidentate Metallic Complexes". *J. Am. Chem. Soc.* **79**, 4904 - 4908.

Palmer, D. A. and D. J. Wesolowski, D. J., 1993. "Aluminum speciation and equilibria in aqueous solution: III. Potentiometric determination of the first hydrolysis constant of aluminum (III) in sodium chloride solutions to 125 ° C". *Geochim. Cosmochim. Acta*, **57**, 2929-2938.

Pye, C. C. and Rudolph, W. W., 2001, "An ab initio and Raman investigation of sulfate ion hydration", *J. Phys. Chem. A*, **105**, 905 - 912.

Rudolph, W. W. and Schönherr, S., 1989. "Raman- und Infrarotspektroskopische Untersuchungen an konzentrierten Aluminiumsalzloesungen"., *Z. Phys. Chem. (Leipzig)*, **270**, 1121-1134.

Rudolph, W. W. and Schönherr, S., 1991. "Raman- und Infrarotspektroskopische Untersuchungen an konzentrierten Aluminiumsalzloesungen". *Z. Phys. Chem. (München)*, **172**, 31-48.

Rudolph, W. W., 1996. "Structure and dissociation of the hydrogen sulphate ion in aqueous solution over a broad temperature range: a Raman study". *Z. Phys. Chem.*,

194, 73-96.

- Rudolph, W. W., 1998. "Hydration and water-ligand replacement in aqueous cadmium(II) sulfate solution: A Raman and infrared study". *J. Chem. Soc., Faraday Trans.*, **94**, 489-499.
- Rudolph, W. W., Brooker, M. H. and Tremaine, P. R., 1999. "Raman- and Infrared Spectroscopic Investigations of Aqueous ZnSO<sub>4</sub> Solutions from 8°C to 165 °C: Inner- and Outer-Sphere Complexes". *Z. Phys. Chem.*, **209**, 181 - 207.
- Rudolph, W. W., Brooker, M. H. and Tremaine, P. R., 1999. "Raman Spectroscopy of Aqueous ZnSO<sub>4</sub> Solutions under Hydrothermal Conditions: Solubility, Hydrolysis and Sulfate Ion Pairing". *J. Sol. Chem.* **28**, No. 5. 621-630.
- Rudolph, W. W. and Pye, C. C., 1999. "Zinc(II) Hydration in Aqueous Solution: A Raman Spectroscopic Investigation and An *ab initio* Molecular Orbital Study of Zinc(II) water Clusters". *J. Sol. Chem.* **28**, No. 9. 1045-1070.
- Rudolph, W. W. and Pye, C. C., 2000. "Aqueous Solution Chemistry of Scandium(III) Studied by Raman Spectroscopy and *ab initio* Molecular Orbital Calculations". *J. Sol. Chem.* **29**, No. 10. 1045-1070.
- Rudolph, W. W., Mason, R. and Pye, C. C., 2000. "Aluminium(III) hydration in aqueous solution. A Raman spectroscopic investigation and an *ab initio* molecular orbital study of aluminium(III) water clusters". *Phys. Chem. Chem. Phys.*, **2**, 5030 - 5040.
- Scott, K., 1987. "Solid solution in, and classification of, gossan-derived members of the

- alunite family, Northwest Queensland Australia". *Amer. Mineral.*, **72**, 178 - 187.
- Stoffregen, R. E. and Alpers, Ch. N., 1992. "Observations on the unit-cell dimensions, H<sub>2</sub>O content, and  $\delta$ D values of natural and synthetic alunite". *Am. Mineral.*, **77**, 1092-1098.
- Vogel, A. I., 1961. "A Text-Book of Quantitative Inorganic Analysis". Third Edition, Longman, London.
- Zotov, A. V., 1971. "Dependence of the composition of alunite on the temperature of its formation". *Geochemistry International.*, **1**, 71 - 75.

## 6. Studies on synthetic alunites: synthesis and X-ray characterization.

Wolfram W. Rudolph and Roger Mason

### 6. 1. Abstract

Stoichiometric end member alunites, alunite  $[\text{KAl}_3(\text{SO}_4)_2(\text{OH})_6]$ , natroalunite  $[\text{NaAl}_3(\text{SO}_4)_2(\text{OH})_6]$ , ammonioalunite  $[(\text{NH}_4)\text{Al}_3(\text{SO}_4)_2(\text{OH})_6]$ , rubidium alunite  $[\text{RbAl}_3(\text{SO}_4)_2(\text{OH})_6]$  and hydronium alunite  $[(\text{H}_3\text{O})\text{Al}_3(\text{SO}_4)_2(\text{OH})_6]$  have been synthesized under hydrothermal conditions together with samples of the  $\text{K}^+ - \text{H}_3\text{O}^+$  solid solution series over the entire compositional range. A so called basic gallium sulfate (BGS) of the alunite type was also synthesized and compared with the hydronium alunite structure. These alunites were characterized by chemical methods and by powder X-ray diffraction (XRD).

Alunites with different monovalent cations in A site (i.e.  $\text{Na}^+$ ,  $\text{K}^+$ ,  $\text{NH}_4^+$ ,  $\text{Rb}^+$  and hydronium) are described and the unit cell parameters for the rhombohedral space group R-3m (# 166) with (hexagonal cell dimensions)  $a$  and  $c$  were determined. The  $c$  parameter increases with increasing effective ionic radius of cation in the A site, whereas the  $a$  parameter is relatively unchanged. The effects of substitution on the unit cell parameters are rationalized in terms of the structural arrangements of the alunite structure. The unit cell parameters of BGS were determined and compared with the unit cell parameters of hydronium alunite.

## 6. 2. Introduction

Minerals of the alunite - jarosite group have the general formula  $AB_3(SO_4)_2(OH)_6$ , where A is  $H_3O^+$ ,  $Na^+$ ,  $K^+$ ,  $Rb^+$ ,  $Ag^+$ ,  $Tl^+$ ,  $NH_4^+$ ,  $1/2 Ca^{2+}$  or  $1/2 Pb^{2+}$  and B is  $Al^{3+}$  (alunite group) or  $Fe^{3+}$  (jarosite) (Scott, 1987). Members of these groups are isostructural, belonging to the hexagonal space-group R-3m (Menchetti and Sabelli 1976 and Szymanski 1985). Basic gallium sulfate, although not a naturally occurring member of the alunite group, is isostructural with that group and is very similar to (hydronium) alunite (Johansson, 1963).

In this paper we deal exclusively with members of the alunite group and with basic gallium sulfate, which we call, informally, "hydronium gallunite". Alunite, sensu stricto,  $[KAl_3(SO_4)_2(OH)_6]$  is one of the most abundant minerals of the alunite-jarosite group (Scott, 1987) and is formed over a wide temperature range (ca. 20 to 400 °C) as a secondary mineral produced from Al-rich minerals (e.g. feldspars) in oxidizing, sulfur-rich environments. There is an extensive solid solution series among A site ions (Scott, 1987 and Stoffregen and Alpers, 1992). Complete solid solution has also been demonstrated between alunite and jarosite, the substitution in B site ( $Al^{3+} \rightleftharpoons Fe^{3+}$ ), (Parker, 1962; Brophy at al., 1962; Härtig at al., 1984), and may exist for all alunite - jarosite type of minerals. Little information is available about the crystallographic effects of these substitutions (Stoffregen and Alpers, 1992).

The variation in alunite unit-cell dimensions with substitution of  $Na^+$  for  $K^+$ , which is another common chemical variation in alunite, has been studied using synthetic

and natural alunite samples by Parker (1962) and by Stoffregen and Alpers (1992).

Gallium accompanies iron (III) and aluminium (III) in its compounds and recently, natural jarosite samples with approximately 1000 to 3000 ppm gallium replacing iron (III) in the B site, were described by Dutrizac et al. (1986). Aslanian et al. (1982) describe the isomorphous substitution of  $\text{Al}^{3+}$  and  $\text{Ga}^{3+}$  ions in the alunite structure of synthetic compounds.

This paper is primarily concerned with the substitution of  $\text{H}_3\text{O}^+$  (hydronium ion, or oxonium<sup>2</sup> ion) for  $\text{K}^+$ , which is a common chemical variation in alunite [ $\text{K}_{1-x}(\text{H}_3\text{O})_x\text{Al}_3(\text{SO}_4)_2(\text{OH})_6$ ] (with  $x = 0$  to 1). We present chemical and XRD data on synthetic alunite samples of end member and intermediate composition in the solid solution series from  $\text{K}^+ - \text{H}_3\text{O}^+$ . Hydronium gallunite was also synthesized and studied in order to compare it with hydronium alunite.

## 6. 3. Experimental Section

### 6. 3. 1. Synthesis of alunite samples

Synthesis conditions are important in producing stoichiometric samples and consequently we explain in some detail the hydrothermal synthesis applied, starting from the stock solutions used, their chemical analysis and proceeding to the description of the hydrothermal synthesis and subsequent chemical characterization of the products.

---

<sup>2</sup>

Hydronium and oxonium are synonymous terms for  $\text{H}_3\text{O}^+$ . Oxonium is the preferred chemical term, but in the mineralogical literature hydronium is favoured, and the mineral name for  $(\text{H}_3\text{O})\text{Al}_3(\text{SO}_4)_2(\text{OH})_6$  is hydronium alunite. The term hydronium for  $\text{H}_3\text{O}^+$  has been used throughout the paper.

Alunites were prepared from commercial grade  $\text{Al}_2(\text{SO}_4)_3 \cdot 18 \text{H}_2\text{O}$  after further purification.  $\text{Al}_2(\text{SO}_4)_3 \cdot 18 \text{H}_2\text{O}$  was precipitated with p.a. (pro analysi) ethanol from the aqueous solution, dried over  $\text{CaCl}_2$  and used to prepare an  $\text{Al}_2(\text{SO}_4)_3$  stock solution. The Al(III) content of the stock solution was determined by colorimetric titration with standard EDTA and xylenol orange as an indicator (Vogel, 1961). The sulfate content was verified by titration with standardized  $\text{Ba}(\text{ClO}_4)_2$  solution using Thorin, 2-(2-dihydroxy-3,6-disulfo-1-naphthylazo) benzene arsonic acid, as an adsorption indicator (Harris and Kratochvil, 1981). Before titration, the solution was passed through a column with a cation exchanger Dowex 50W-X8. The eluate was then titrated with the standardized  $\text{Ba}(\text{ClO}_4)_2$  solution. This elution technique prevented co-precipitation of Al(III) with the  $\text{BaSO}_4$  (Harris and Kratochvil, 1981). The stock solution was 0.98 M (1.012 m). The solution densities were determined with a standardized 5 ml pycnometer at 20°C. The stock solution was filtered through a 0.45 micron Millipore filter. Commercial-grade  $\text{K}_2\text{SO}_4$ ,  $\text{Na}_2\text{SO}_4$ ,  $(\text{NH}_4)_2\text{SO}_4$  and  $\text{Rb}_2\text{SO}_4$  (p.a. quality) were used for synthesis. The starting solutions for alunite synthesis were prepared by weight.

We carried out synthesis under hydrothermal conditions in 45 ml Teflon lined bombs. The optimal temperature conditions for producing stoichiometric alunite were determined in preliminary studies. Synthesis temperatures of 190 and 205 °C were chosen and the synthesis was maintained for up to approximately 1200 hours in order to improve crystallinity and to reach equilibrium. Temperatures above 250 °C have to be avoided, because above this temperature boehmite,  $\gamma\text{-AlO}(\text{OH})$ , is formed (cf. Stoffregen and

Cygan, 1990). The hydrothermal synthesis conditions of solid solutions in the  $\text{H}_3\text{O}^+ - \text{K}^+$  series (run # A007 to A014) are presented in Table 6.1. Alunite end members,  $[(\text{H}_3\text{O})\text{Al}_3(\text{SO}_4)_2(\text{OH})_6]$ ,  $[\text{KAl}_3(\text{SO}_4)_2(\text{OH})_6]$ ,  $[\text{NaAl}_3(\text{SO}_4)_2(\text{OH})_6]$ ,  $[(\text{NH}_4)\text{Al}_3(\text{SO}_4)_2(\text{OH})_6]$ , and  $[\text{RbAl}_3(\text{SO}_4)_2(\text{OH})_6]$  have been synthesized and are also included in Table 6.1. Two alunite samples (run # A001 and A002) have also been synthesised in a preliminary study in order to determine optimal conditions for synthesis. After quenching the reaction vessel in ice water, the crystalline alunite samples were isolated and washed with bidistilled water and dried at 160 °C for 6 h. The solid products were cooled in a desiccator and stored for further investigation. Synthesis of H- alunite,  $[(\text{H}_3\text{O})\text{Al}_3(\text{SO}_4)_2(\text{OH})_6]$ , alunite,  $[\text{KAl}_3(\text{SO}_4)_2(\text{OH})_6]$  and natroalunite ( $[\text{NaAl}_3(\text{SO}_4)_2(\text{OH})_6]$ ), were carried out twice in order to check the synthesis procedure and the complete analytical procedure (from the acid digestion and analytic procedure) and to establish that stoichiometric compounds were produced.

In order to compare the hydronium alunite (H-alunite) to a sample where the substitution of the B site was changed, a gallium analog of the (hydronium) alunite type was synthesized hydrothermally (# G001). 3.137 g gallium(III) sulfate was dissolved in 29.215g water and 0.147 g sulfuric acid (99%, p.a.) was added. The synthesis temperature was kept at 200 °C in a 45 ml Teflon lined vessel for 1024 h. The H-gallunite was washed twice with distilled water and dried at 140 °C for 6 h. The weight of the H-gallunite produced was 1.595 g.

### 6. 3. 2. Analytical methods

The chemical analysis of alunite species was carried out on samples digested in 4 M HCl (Baker, ultrapure) in a Teflon lined beaker mantled with a steel jacket at 120 °C over night. The aluminum, potassium and sulfur content was determined with inductively coupled plasma optical emission spectroscopy (ICP -OES). The instrument used for all analyses of Al, S, Na, and K was an ARL 3520 sequential ICP-OES. For more details about the wet chemical procedure and ICP-OES see Finch, 1993. Two independent measurements (from acid digestion to ICP OES measurement) were made.

In order to verify the stoichiometry of the alunite end members thermoanalytical investigations have been carried out (Dr. Peer Schmidt, TU Dresden, Institut für Anorganische Chemie). The thermogravimetric studies were performed in an atmosphere of air with a thermal analyser of Fa. Netzsch, STA 409. Measurements were taken from 25 to 1100 °C with a heating rate of 10 K/min. In addition to the problem of non-stoichiometry addressed by numerous authors (Parker, 1962; Brophy et al., 1962 and Ripmeester et al., 1986), there is an unresolved problem of "excess water" in the alunite-jarosite structure, discussed by Kubisz (1970), Härtig et al. (1984) and Ripmeester et al. (1986). Although the term "excess water" is not clear in the literature quoted above, we do understand this water can be removed from the alunite samples without destroying the structure and should not be confused with water stemming from OH<sup>-</sup>, or in hydronium alunite from H<sub>3</sub>O<sup>+</sup>. This "excess water" is not part of the stoichiometry of alunites. From thermoanalytical studies (Bomhammel et al., 1987), it is known that hydronium alunite

does not decompose below 200 °C, and that the decomposition temperature is a function of the potassium content in the alunite samples of the alunite-hydronium alunite solid solution series.

The alunite samples were prepared for powder X-ray diffraction by spreading it as a slurry (in acetone) on a glass slide. Powder XRD patterns of the solids were collected using a Rigaku RU-200 automated X-ray diffractometer using Cu-K $\alpha$  radiation with an accelerating voltage of 40 KeV and a filament current of 100 mA. The scans were obtained over the  $2\theta$  range from 13 - 90 ° at a scan speed of 2.500 deg/min. For precise unit cell parameter determinations the alunites were mixed with Si (refined silicon, National Bureau of Standards, NBS Standard reference, material No. 57) as an internal standard. Hexagonal-rhombohedral unit cell refinements were obtained with a regression diagnostics program written by Holland and Redfern (1997) based on 15 - 20 reflections.

Morphological investigations were performed with a scanning electron microscope. Each sample was suspended in absolute ethanol and then mounted on an Al metal stub. After drying at room temperature, the samples were coated with gold using an Edwards S150A sputter coater equipped with an argon gas supply for purging.

The majority of the morphological studies of the alunites were carried out with a Hitachi S570 scanning electron microscope operating at an accelerating voltage of 20 keV. The microscopic working distances ranged between 15 and 23 mm, with magnifications up to 11,000x, depending on the height and quality of the crystals, as well as on the efficiency of the gold coating. SEM micrographs of the solids were recorded on a Polaroid type 665

positive/negative film using a Polaroid camera attached to the scanning electron microscope.

#### 6. 4. Results

Details of starting solutions and synthesis conditions are given in Table 6.1. Two alunite samples (run # A001 and A002, Table 6.1) were synthesised in a preliminary study to find the optimal conditions for the synthesis of stoichiometric compounds. The hydrothermal synthesis conditions used for these samples and for the preparation of end members,  $[(\text{H}_3\text{O})\text{Al}_3(\text{SO}_4)_2(\text{OH})_6]$ ,  $[\text{KAl}_3(\text{SO}_4)_2(\text{OH})_6]$ ,  $[\text{NaAl}_3(\text{SO}_4)_2(\text{OH})_6]$ ,  $[(\text{NH}_4)\text{Al}_3(\text{SO}_4)_2(\text{OH})_6]$ , and  $[\text{RbAl}_3(\text{SO}_4)_2(\text{OH})_6]$ , and solid solutions in the  $\text{H}_3\text{O}^+ - \text{K}^+$  series (run # A007 to A014) are presented in Table 6.1. Analytical results for members of the solid solution series  $\text{K}^+ - \text{H}_3\text{O}^+$  (specimens A014 to A007) are given in Table 6.2. Thermogravimetical data on end member alunites,  $[(\text{H}_3\text{O})\text{Al}_3(\text{SO}_4)_2(\text{OH})_6]$ ,  $[\text{KAl}_3(\text{SO}_4)_2(\text{OH})_6]$ ,  $[\text{NaAl}_3(\text{SO}_4)_2(\text{OH})_6]$ ,  $[(\text{NH}_4)\text{Al}_3(\text{SO}_4)_2(\text{OH})_6]$ , and  $[\text{RbAl}_3(\text{SO}_4)_2(\text{OH})_6]$  are presented in Table 6.3. Table 6.4 contains unit cell parameters for the end members and Table 6.5 contains cell parameters for the solid solution between  $[(\text{H}_3\text{O})\text{Al}_3(\text{SO}_4)_2(\text{OH})_6]$  and  $[\text{KAl}_3(\text{SO}_4)_2(\text{OH})_6]$ .

##### 6. 4. 1. Chemical characterization, thermal analysis and morphological studies of the alunite crystal powders

Powder XRD patterns of the solids indicate that only members of the alunite group were precipitated and that each experiment produced only a single solid phase.

Examination of the SEM photographs (Figure 6.1) shows that the alunite samples

produced consist of particles ranging in size from 8 to 10  $\mu\text{m}$ .

A comparison of the ratio of potassium to aluminium in the starting solution and in the solids shows that potassium is preferentially incorporated into the structure (Table 6.2). In solutions with a K : Al ratio higher than 1 : 3, stoichiometric alunite (i.e. K : Al = 1:3) is formed (A014 and A013, Table 6.2). When the solution composition K : Al = 1 : 3, an alunite with K:Al < 1 : 3 is formed. By adjusting the solution composition we were thus able to prepare end member alunite (i.e. K-alunite) that does not contain hydronium. Similarly, adjustment of the chemistry of the starting solutions allowed intermediate members of the  $[\text{K}_{1-x}(\text{H}_3\text{O})_x\text{Al}_3(\text{SO}_4)(\text{OH})_6]$  solid solution series to be synthesised. For the intermediate compounds of the solid solution series,  $[\text{K}_{1-x}(\text{H}_3\text{O})_x\text{Al}_3(\text{SO}_4)(\text{OH})_6]$ , the hydronium content in the A site was calculated as the difference, namely  $1 - X_K = X_{\text{H}_3\text{O}}$

Experiments without potassium in the starting solution produced a solid phase that was identified as hydronium alunite using powder XRD. The amount of excess water is very minute and is of the order of 0.5 wt %, which is lost in the temperature range from 38 to 203  $^{\circ}\text{C}$  determined with thermogravimetric analysis (compare results in Table 6.3).

The compounds of the solid solution with  $X_K < 1$ , including the pure hydronium end member, contain only slight amounts of excess water in their structures, presumably in the A site. Infrared spectra (to be published) show the same trend. The amount of excess water is of the order of 0.2 to 1.0 wt %.

The pH values of the sulfate solution prior to the precipitation of alunite was about 2.2, but after complete precipitation, the pH had decreased to 1.09 to 0.60 in the

supernatants (Table 6.1) with the lowest pH for the pure alunite end member and a higher value for the H- alunite end member. The final pH values of the supernatant of alunites intermediate in composition are between the values of these two end members.

Stoichiometric end members natroalunite (mole ratio Na:Al:SO<sub>4</sub> ratio = 1: 2.99: 2.00), ammonioalunite (mole ratio NH<sub>4</sub>: Al : SO<sub>4</sub> = 1 : 2.98 : 2.00) and rubidium alunite (mole ratio Rb:Al:SO<sub>4</sub> ratio = 1: 2.98: 2.00) were prepared as detailed in Table 6.2. Their stoichiometry (by wet chemical analysis) compares very well with the ideal 1 : 3: 2 (A site: Al : SO<sub>4</sub>). The amount of excess water found is small and is of the order of 0.5 wt % lost in the temperature interval from 38 to ca. 500 °C as determined by thermogravimetric analysis (compare results in Table 6.3).

The stoichiometry for hydronium gallunite was also determined using wet chemical analysis and the mole ratio Ga : SO<sub>4</sub> was found to be 2.01 : 3.00 and the wt % gallium found in H- gallunite (ideal formula (H<sub>3</sub>O)Ga<sub>3</sub>(SO<sub>4</sub>)<sub>2</sub>(OH)<sub>6</sub>), f.w. 522.351) was 40.1 (ideal wt % Ga = 40.042) and the wt % sulfur 12.204 (ideal wt % sulfur 12.277). Almost no additional water was detected in the H-gallunite. Our synthetic H-gallunite compares to the synthetic product described by Johansson (1963).

#### 6. 4. 2. Unit cell parameters

The unit cell parameters *a* and *c*, the ratio *c/a*, the volume of the unit cell and the crystallographic densities are presented in Table 6.4 for the alunite end members H-alunite, H-gallunite, Na-alunite, alunite, NH<sub>4</sub>-alunite and Rb-alunite.

The isomorphous replacement of the univalent cation changes the *c* parameter

significantly (ca. 7%) as the ionic radius of the cation increases in the series  $\text{Na}^+$ ,  $\text{K}^+$ ;  $\text{NH}_4^+$ ,  $\text{Rb}^+$  while the  $a$  parameter changes to a much lesser degree. Changes in the  $a$  parameter, although in the same direction, are much smaller (ca. 0.4 % difference between natroalunite and Rb-alunite). Hydronium alunite, which has the highest  $a$  parameter is out of sequence.

Substituting the trivalent cation  $\text{Ga}^{3+}$  for  $\text{Al}^{3+}$  in hydronium alunite, results in the end member hydronium gallunite. Comparing H-alunite and H-gallunite (Table 6.4) there is only a slight increase in  $c$  parameter (ca. 0.2 %) but a significant increase in  $a$  parameter (ca. 2.5 %). This suggests that the substitutions in the A and B site can be distinguished on the basis of their effects on the cell parameters.

In Table 6.5 the unit cell parameters  $a$  and  $c$ , the ratio  $c/a$ , the volume of the unit cell and the crystallographic densities are presented for the compounds of the solid solution series  $[(\text{H}_3\text{O},\text{K})\text{Al}_3(\text{SO}_4)_2(\text{OH})_6]$  including the two end members H-alunite (0 %K) and alunite (100 % K). The ratio of the unit-cell dimensions,  $c/a$ , for 6 synthetic alunite samples of intermediate composition  $0 < X_K < 1$ , along with the two end-members ( $X_K = 1$ ,  $X_K = 0$ ) are plotted as a function of  $X_K$  in Figure 6.2. The variation in  $a$  across this binary is approximately the same size as the typical standard error (95 % confidence interval) on  $a$  and thus not significant. The data plot in Figure 6.2 on the straight line connecting alunite and H-alunite follows Vegard's Law.

## 6. 5. Discussion

In order to facilitate discussion of the chemical and unit cell parameter data we present a brief discussion of the alunite structure.

### 6. 5. 1. Structural Arrangements in Alunite

The first crystal structure of alunite was assigned to the acentric space group  $R\bar{3}m$  ( $C_{3v}^5$ ) on the basis of a positive pyroelectric test by Hendricks (1937), although the reported structural coordinates displays a centre of symmetry. Later crystal structure refinement data revealed, that the space group for the alunite-jarosite structure has to be assigned to a centrosymmetric space group  $R\bar{3}m$  ( $D_{3d}^5$ ) by Wang et al. (1965) and Menchetti and Sabelli (1976), with  $z = 3$  ( in the hexagonal unit cell). In the alunite structure, the sulfur forms tetrahedra and the aluminum forms octahedra which are corner-linked (Figure 6.3). The structure is made up of tetrahedral-octahedral-tetrahedral (T-O-T) layers. The aluminum octahedron is slightly distorted, being formed by four OH groups and two oxygen atoms from two different  $SO_4$  tetrahedra. Each aluminum atom lies in a symmetry centre.

The sulfur atoms lie on the trigonal axis and are surrounded by three basal oxygen atoms (O(2)) and the apical oxygen (O(1)), which also lies on the threefold axis. The apical oxygen, O(1) is somewhat special (no close contact to other cations) and forms H-bonds to OH (cf. Menchetti and Sabelli (1976)). Wang et al. (1965) described this S-O bond as almost "doubly" bonded. The univalent cations ( $Na^+$ ,  $K^+$ ,  $H_3O^+$  etc.) are surrounded by twelve anions, namely six oxygen atoms, O(2), and six OH groups, which are nearly at the same distance from the cation.

### 6. 5. 2. Chemical Composition

Our synthesis conditions (Table 6.1) were designed to produce stoichiometric alunites using very long reaction times and optimal temperatures. The substitution of  $\text{H}_3\text{O}^+$  for  $\text{K}^+$  is of special importance, because most of the natural and synthetic alunites described in the literature contain  $\text{H}_3\text{O}^+$  in smaller or larger quantities (Parker 1962, Ripmeester et al. 1986 Dutrizac and Kaiman 1976, Altaner et al. 1988). In some earlier experiments, the substitution of hydronium ion for  $\text{K}^+$  is obscured by a deficiency in alkalis and an excess in  $\text{H}_2\text{O}$  content compared to the expected stoichiometric composition (Ripmeester et al., 1986). The nonstoichiometric water has been attributed to the presence of  $\text{H}_3\text{O}^+$  but may also reflect other forms of "excess water" (Ripmeester et al., 1986). Our data show that, only with careful attention to synthesis conditions, can nonstoichiometry in alunites (lack of alkali metal ions and aluminium deficiency) be avoided (compare for instance the synthesis conditions of jarosite type compounds by Dutrizac and Kaiman, 1976). Similarly, careful analysis is required to establish the precise stoichiometry of the phases produced.

From thermogravimetric analysis of the end member alunites (Table 6.3), three characteristic temperature intervals can be observed. First, the breakdown of the alunite structure accompanied by loss of water from OH (or hydronium), which is preceded by a small loss of adsorbed water, step 1 in Table 6.3. Second, the beginning of  $\text{SO}_3$  loss, and third, the final step of  $\text{SO}_3$  loss. The breakdown of the alunite structure in  $[(\text{H}_3\text{O})\text{Al}_3(\text{SO}_4)_2(\text{OH})_6]$ ,  $[\text{KAl}_3(\text{SO}_4)_2(\text{OH})_6]$ ,  $[\text{NaAl}_3(\text{SO}_4)_2(\text{OH})_6]$ ,  $[(\text{NH}_4)\text{Al}_3(\text{SO}_4)_2(\text{OH})_6]$

, and  $[\text{RbAl}_3(\text{SO}_4)_2(\text{OH})_6]$  is at ca. 423 (mean value cf. Table 6.3), 558, 544, 500 and 530°C, respectively. These temperatures represent the real stability limits of the alunite end members (cf. e.g. Bomhammel et al., 1987).

### 6. 5. 3. Unit cell parameters of alunites

There have been many measurements of alunite unit cell parameters published in the past: we assemble them in Table 6.6 for comparison with our results (Tables 6.4 and 6.5) for end member natroalunite, alunite, ammonioalunite, Rb-alunite and H-alunite.

Considering first the data for alunite *sensu stricto*, the range in *a* varies from 6.97 to 7.014 Å and that in *c* is from 17.13 to 17.38 Å. At the extrema of these ranges we suggest that the data were collected either on material that was synthesised under conditions that would not lead to a stoichiometric product (e.g. Härtig et al., 1984) or on natural material that was not of end-member composition (e.g. Menchetti & Sabelli, 1976). In some cases it is clear that the material studied did not correspond to ideal alunite stoichiometry (e.g. Ripmeester et al., 1986), whereas in others the authors did not report chemical compositions (e.g. Wang et al., 1965). It is particularly noteworthy that in samples that were grown under conditions chosen to produce a stoichiometric alunite, and in which stoichiometry was confirmed by analysis, the results are very consistent (Stoffregen & Alpers, 1992; this work). The most common problem encountered in producing a stoichiometric alunite is the incorporation of excess water. Stoffregen and Alpers (1992) also pointed out the importance of synthesis conditions on resulting stoichiometric alunite products and consequently on reliable unit cell parameters.

Turning to H-alunite, the values measured for the end member (Table 6.4) lie in the middle of the ranges reported in the literature. We note that all the determinations were made on synthetic material, with attendant problems of incorporation of excess water. As described above, we took care to remove excess water by heating the samples to 190°C and we believe the relatively simple relationship between  $c/a$  and  $X_K$  (Fig. 6.2) suggests that our hydronium bearing alunites are stoichiometric.

Unit-cell parameters published by Stoffregen and Alpers (1992) for the synthetic alunite end-members (natroalunite and potassium - alunite) formed at 250 and 450 °C agree with our data within  $2\sigma$  for  $c$  and  $a$  parameters, whereas the sample formed at 150°C has significant larger  $a$  and smaller  $c$  and  $V$ . These results are similar to older data published by Parker (1962) for synthetic alunite formed at 100 °C, which showed an increase in  $c$  and a decrease in  $a$  after heating the samples in air for 1 h at 300 °C. Parker (1962) attributed this shift in unit-cell dimensions to the loss of non-OH water during heating.

As has been described in the above section, the isomorphous replacement of the univalent cation results in varying the  $c$  parameter, while the  $a$  parameter changes to a much lesser degree. Menchetti and Sabelli (1976) on the other hand did not observe a change in the  $a$  parameter by substituting the univalent cation, most likely due to their non-stoichiometric product used (cf. our discussion in the experimental section). The isomorphous replacement in the A position ( $\text{Na}^+$ ,  $\text{K}^+$ ,  $\text{NH}_4^+$ ,  $\text{Rb}^+$  and  $\text{H}_3\text{O}^+$ ) results in a widening of the 12-fold coordination polyhedra, and a subsequent increase of the inter-sheet distance ( $c$  parameter). This is due to the increasing size of the ionic radii of each of

the cation in twelvefold coordination ( $\text{Na}^+ = 1.39 \text{ \AA}$ ,  $\text{K}^+ = 1.64 \text{ \AA}$ ,  $\text{NH}_4^+ > 1.69 \text{ \AA}$  and  $\text{Rb}^+ = 1.73 \text{ \AA}$ ; Kahn and Baur, 1972 and Shannon, 1976). The  $1.69 \text{ \AA}$  value represents the ionic radius of  $\text{NH}_4^+$  in ninefold coordination (Kahn and Baur, 1972) and therefore, the effective ionic radius of  $\text{NH}_4^+$  in twelvefold coordination must be larger than  $1.69 \text{ \AA}$ . The axial ratio  $c/a$  for natroalunite, alunite, ammonioalunite and Rb-alunite as a function of the effective ionic radius for  $\text{Na}^+$ ,  $\text{K}^+$ ,  $\text{NH}_4^+$  and  $\text{Rb}^+$ , respectively is presented in Figure 6.4. The influence on the length of the  $a$  parameter is small but still measurable. The increase of the  $a$  parameter with increase in the ionic radius going from  $\text{Na}^+$ ,  $\text{H}_3\text{O}^+$ ,  $\text{K}^+$ ,  $\text{NH}_4^+$  to  $\text{Rb}^+$  shows one exception namely in hydronium alunite, which has the highest  $a$  parameter (cf. results in Table 4) although its ionic radius is almost as large as  $\text{K}^+$ .

Rubidium, with the largest ionic radius of the univalent cations studied is incorporated into the A site of the crystal structure. The effective ionic radius of  $\text{Cs}^+$  in 12-fold coordination is  $1.88 \text{ \AA}$  (Shannon and Prewitt, 1969). In jarosite it is reported that caesium ion does not fit the A-site (Fairchild, 1933) and from this analogy we speculate that cesium cannot be incorporated into the alunite structure.

In order to understand the effects of substitution of Ga(III) in the B site it is instructive to consider the effects of substitution of  $\text{Fe}^{3+}$  for  $\text{Al}^{3+}$  (Menchetti and Sabelli, 1976). The length of the  $a$  parameter is directly related to the B-OH bond length. If B is Al (Al-OH =  $1.879 \text{ \AA}$ ) the  $a$  parameter is  $6.9826(2) \text{ \AA}$  (our value from Table 6.4) but lengthens to  $7.315 \text{ \AA}$  if B is  $\text{Fe}^{3+}$  (Fe-OH =  $1.975 \text{ \AA}$ ; Menchetti and Sabelli, 1976). On the other hand, together with variation of the B-OH bond length, the B-O(2) bond length is

also influenced, that is  $\text{Al-O}(2) = 1.947 \text{ \AA}$  and  $\text{Fe-O}(2) = 2.058 \text{ \AA}$ . Consequently the thickness of the T-O-T layer (Figure 6.3) also expands or contracts. We might expect that the  $c$  parameter should also expand or contract, but in reality this is not what is happening (Menchetti and Sabelli, 1976). The octahedra are arranged in layers of octahedra with tetrahedra above and below. Changes in the dimension of the octahedra with chemical substitution are accommodated, in the  $c$  dimension, by changes in the interpenetration of the octahedra and tetrahedra sheets. For a detailed discussion of this phenomenon compare the results published by Menchetti and Sabelli (1976).

Comparing H-alunite and H-gallunite, there is only a slight increase in  $c$  parameter but a significant increase in  $a$  parameter. This is due to the bigger Ga-OH bond length (Ga-OH bond is equal to  $1.952 \text{ \AA}$ ; Johansson, 1963) compared to the Al-OH bond length equal of  $1.879 \text{ \AA}$  (this bond length is measured for alunite, no data for hydronium alunite are available, but the Al-OH bond length should be comparable for the two alunite species). If B is Al (Al-OH =  $1.879 \text{ \AA}$ ) the  $a$  parameter is  $7.0080(2) \text{ \AA}$ , while it lengthens to  $7.1846(5) \text{ \AA}$  if B is occupied by  $\text{Ga}^{3+}$  (compare our unit cell data in Table 4). On the other hand together with the B-OH variation the bond length B-O(2) also varies, namely  $\text{Al-O}(2) = 1.947 \text{ \AA}$  and  $\text{Ga-O}(2) = 2.017 \text{ \AA}$  (Johansson, 1963). The arguments are used to explain the structural effects of substituting  $\text{Fe}^{3+}$  for  $\text{Al}^{3+}$  in the alunite-jarosite structure, and hold also for substituting  $\text{Ga}^{3+}$  for  $\text{Al}^{3+}$  in the hydronium alunite-hydronium gallunite structure.

## 6. 6. Conclusions

1. Careful synthesis and chemical analysis are required in order to prepare and

characterize stoichiometric end member alunites.

2. There exists complete solid solution between alunite and hydronium alunite.

Potassium is incorporated preferentially into the solid phase upon precipitation from aqueous solution at approximately 200 °C. Members of the solid solution can be prepared by suitable adjustment of solution composition. The ratio of the unit cell parameters  $c/a$  follows Vegard's rule.

3. With an increase in the effective ionic radius of the cation occupying the A site in the series from  $\text{Na}^+$ ,  $\text{K}^+$ ,  $\text{NH}_4^+$  to  $\text{Rb}^+$ , there is a large increase in the  $c$  unit cell parameter accompanied with a small increase in the  $a$  parameter.

4. Hydronium gallunite was hydrothermally synthesized and the unit cell parameters determined. Substitution of the B site in the alunite results in an increase in  $a$  parameter and only in a slight increase in the  $c$  parameter compared to the hydronium alunite end member.

#### Acknowledgements

W. W. R. thanks for a scholarship from graduate studies of Memorial University NF, during the period 1997 to 1998. Furthermore, W. W. R. thanks Mr. Chris Finch, Department of Mines and Energy, Newfoundland for the use of his ICP-OES instrument and for assistance with the measurements. For the thermal measurements W. W. R. thanks Dr. Peer Schmidt, TU Dresden, Institut fuer Anorganische Chemie. R. M. thanks NSERC for support in the early stages of this project and Memorial University for support in the later stages.

**Table 6.1: Synthesis conditions for two alunites synthesised prior to the systematic study (# A001 and A002) the hydronium alunite/alunite solid solution series (# A007 to A014) and end member alunites (hydronium alunite (H-alunite), natroalunite, alunite, ammonioalunite and rubidium alunite (Rb-alunite)).**

Run no. Alunite sample	Starting solution Compositions				synthesis conditions			yield (g)	pH supern.
	A <sub>2</sub> SO <sub>4</sub> # (g)	Al <sub>2</sub> (SO <sub>4</sub> ) <sub>3</sub> (g)	H <sub>2</sub> O (g) (total)	pH	T (°C)	p (bar)	time (h)		
A001 alunite	0.270		30.230	-	180	10	56	0.930	-
A002 H-alunite	0	1.86	30.500	-	180	10	56	0.260	-
A007 H-alunite	0	2.2031	38.490	2.27	190	12.9	504	0.569	1.09
A008	0.0632	2.1910	37.870	2.26	190	12.9	504	0.769	0.98
A009	0.1091	2.1968	38.206	2.26	190	12.9	504	0.770	0.97
A010	0.1704	2.1970	37.849	2.25	190	12.9	504	1.010	0.80
A011	0.2765	2.2067	37.876	2.25	190	12.9	504	1.443	0.62
A012	0.3829	2.2030	37.912	2.24	190	12.9	504	1.605	0.61
A013	0.5859	2.1990	38.030	2.23	190	12.9	504	1.627	0.61

A014 alunite	0.850	2.1942	38.016	2.23	190	12.9	504	1.708	0.60
A015 * H-alunite	0	2.220	38.001	-	190	12.9	792	0.520	-
A022 natroalunite	0.8061	2.2147	38.248	2.22	190	12.9	792	1.583	0.62
A023 natroalunite	0.7692	2.2132	20.947	2.23	188	12.6	1200	1.532	0.52
A043 ammonioalu- nite	0.6474	2.2021	36.200	2.24	200	15	1008	1.482	0.62
A044 ** alunite	1.9665	4.8647	35.133	2.48	200	15	1128	3.866	0.42
1.80 A045 ** alunite	2.6422	4.9093	35.092	2.47	200	15	1128	3.707	0.37
A048 H-alunite	0	4.1769	35.1850	1.90	200	15	1200	1.269	0.82
A049 H-alunite	0	4.1900	35.1850	1.90	200	15	1200	1.269	0.81
A051 Rb-alunite	3.3320	2.4300	36.456	2.20	205	16.8	1128	1.900	0.74

# A = Na<sup>+</sup>, K<sup>+</sup>, NH<sub>4</sub><sup>+</sup> or Rb<sup>+</sup>, respectively; \* plus 0.164 g H<sub>2</sub>SO<sub>4</sub> (96.78 %); \*\* A044 plus 0.187 g KOH and A045 plus 0.168 g KOH

Table 6.2: Analytical results for the analysis of hydronium alunite/alunite solid solution series. Also shown is the mole ratio K : Al in synthetic alunite and in solution prior to the precipitation of alunite.

sample	%Al	%S	%K	$X_K$	% excess water	mole ratio K:Al in solid	mole ratio K:Al in starting solution
A007	20.520	16.200	-	0	2.8	0 : 3	0 : 3
A008	20.055	15.865	3.620	0.372	2.5	0.372 : 3	0.1701 : 3
A009	18.990	15.560	6.470	0.674 <sub>6</sub>	2.4	0.675 : 3	0.2925 : 3
A010	18.900	15.500	7.065	0.740	1.2	0.740 : 3	0.4568 : 3
A011	18.900	15.280	8.580	0.905	0.4	0.905 : 3	0.7380 : 3
A012	19.400	15.400	9.280	0.978	0.2	0.978 : 3	1.0240 : 3
A013	19.544	15.482	9.438	1	0.1	1 : 3	1.5694 : 3
A014	19.550	15.500	9.440	1	0.1	1 : 3	2.2812 : 3

Table 6.3: Thermogravimetric data on the endothermic reactions for endmember aluites, H-alunite, alunite, Na-alunite, NH<sub>4</sub>-alunite and Rb-alunite.

A007, H-alunite				
TG-interval	Tmin /°C	Tmax /°C	Tpeak /°C	Δ TG /wt %
1	38	203.4		0.45
2	203.4	375.4	350.3	7.77
3	375.4	477.8	409.3	3.98
4	477.8	545.2	509.4	4.42
5	545.8	679.5		2.78
6	679.5	798.6	780	14.09
7	798.6	901.6	880.4	22.06
8	901.6	984.7		5.06
9	984.7	1100.5		0.36
A014, alunite				
1	32	498.0		1.00
2	498.0	599.5	557.6	12.93
3	599.5	727.5		2.24
4	727.5	851.2	817.6	21.61
5	851.2	1102.0		5.25
A023, Na-alunite				
1	32	477.8		1.10
2	477.8	581.0	543.7	13.72
3	581.0	695.4		1.42
4	695.4	848.1	782.6	26.56
5	848.1	1096.5		2.72
A043, NH <sub>4</sub> -alunite				

**Table 6.3: Thermogravimetric data on the endothermic reactions for endmember alunites, H-alunite, alunite, Na-alunite, NH<sub>4</sub>-alunite and Rb-alunite.**

1	32	369.2		0.16
2	369.2	539.8	500.5	18.23
3	539.8	655.1		3.43
4	655.1	787.1		6.34
5	787.1	857.3	820	13.13
6	857.3	907.9	892	11.82
7	908.4	1100.1	957.5	8.27
<b>A051, Rb-alunite</b>				
1	38	420.8		0.8
2	420.8	569.0	529.5	12.0
3	569.0	746.00		4.0
4	746.0	849.0	814.6	18.40
5	849.0	1100.0	1047.2	5.0

Table 6.4: Determined unit cell parameters and crystal data for hydronium alunite, hydronium gallunite, alunite, natroalunite, ammonioalunite and Rb-alunite.

Sample	Run no.	a (Å)	c (Å)	V (Å <sup>3</sup> )	c/a	D(x) (g/cm <sup>3</sup> )
H-alunite	A007	7.0080 (2)	17.136 (1)	728.83 (6)	2.44551	2.695
H-gallunite	G001	7.1846 (5)	17.169 (2)	767.50 (8)	2.38969	3.390
Na-alunite	A023	6.9711 (2)	16.670 (1)	701.57 (6)	2.39130	2.827
alunite	A014	6.9826 (2)	17.332 (1)	731.84 (6)	2.48217	2.820
NH <sub>4</sub> -alunite	A043	6.9965 (8)	17.840 (6)	756.33 (10)	2.54984	2.590
Rb-alunite	A051	6.9975 (5)	17.855 (3)	757.14 (8)	2.55169	3.030

Table 6.5: Mol ratio  $X_K$ , unit cell parameters,  $a$  and  $c$ , ratio  $c/a$ , unit-cell volume and crystallographic density for synthetic alunites of the general formula  $(H_3O,K)Al_3(SO_4)_2(OH)_6$ .

Run no.	$X_K$	$a$ (Å)	$c$ (Å)	$c/a$	Volume (Å <sup>3</sup> )	density (g/cm <sup>3</sup> )
A007	0	7.0080	17.136	2.44551	728.83	2.695
A008	0.372	6.9970	17.204	2.45877	729.43	2.748
A009	0.675	6.9960	17.265	2.46784	731.81	2.775
A010	0.740	6.9970	17.282	2.46992	732.74	2.781
A011	0.905	6.9940	17.306	2.47441	733.12	2.802
A012	0.978	6.9850	17.32	2.47960	731.83	2.816
A013	1.00	6.9835	17.331	2.48171	731.98	2.819
A014	1.00	6.9826	17.332	2.48217	731.83	2.820

Table 6.6: Unit cell parameters and unit cell volume taken from the literature for end member alunites: alunite, H-alunite, Na-alunite, NH<sub>4</sub>-alunite and the basic gallium salt of the alunite type (H<sub>3</sub>O)Ga<sub>3</sub>(SO<sub>4</sub>)<sub>2</sub>(OH)<sub>6</sub>.

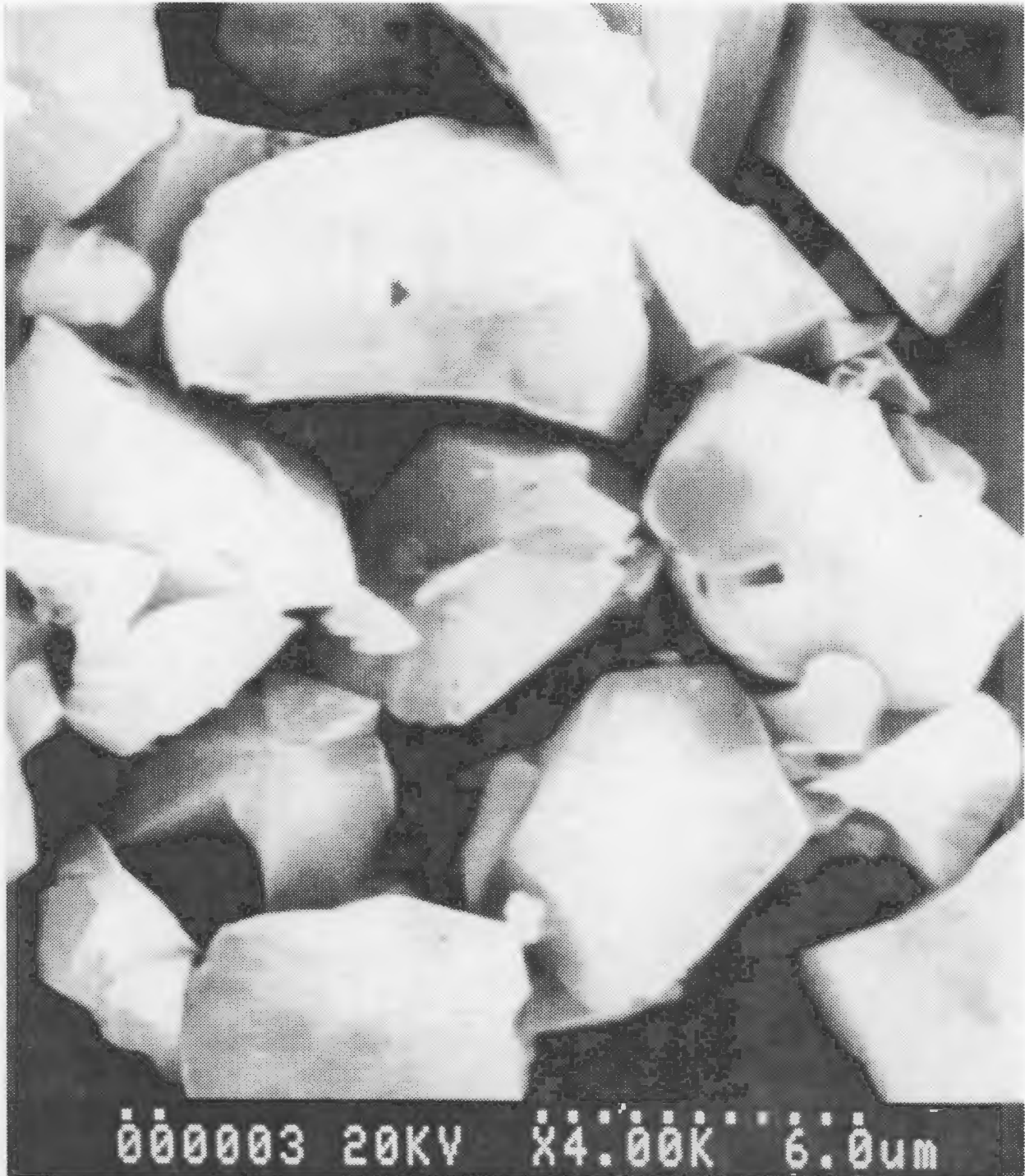
sample	a (Å)	c (Å)	V (Å <sup>3</sup> )	description	literature
alunite	6.97	17.38	-	-	Hendricks (1937)
alunite	7.013 6.982	17.14 17.32	- -	not heat teated heated at 300°C for 1 h	Parker (1962)
alunite	6.98	17.29	-	-	Brophy et al.(1962)
alunite	6.970	17.27	-	-	Wang et al. (1965)
alunite	6.98	17.34	-	-	Kubisz (1970)
alunite	6.995	17.301	-	natural sample	Menchetti and Sabelli (1976)
alunite	7.012	17.13	-	synthetic sample	Härtig et al. (1984)
alunite	7.003	17.16	728.8	Synthetic sample K deficiency	Ripmeester et al. (1986)
alunite	7.0000(2) 6.9831(5) 6.9810(1)	17.180(7) 17.334(2) 17.331(4)	729.1(4) 732.03(9) 731.5(2)	synthetic samples heated at: 150 °C 250 °C 450 °C	Soffregen and Alpers (1992)

Table 6.6: Unit cell parameters and unit cell volume taken from the literature for end member alunites: alunite, H-alunite, Na-alunite, NH<sub>4</sub>-alunite and the basic gallium salt of the alunite type (H<sub>3</sub>O)Ga<sub>3</sub>(SO<sub>4</sub>)<sub>2</sub>(OH)<sub>6</sub>.

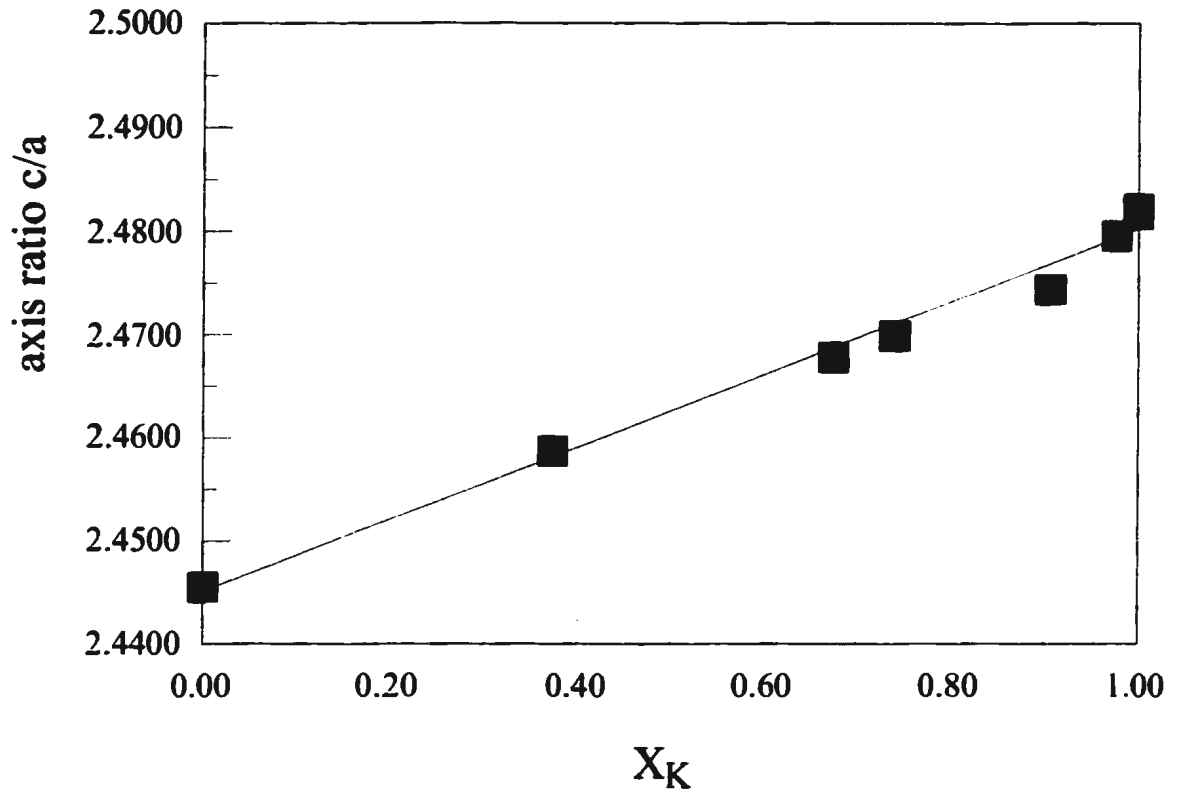
H-alunite	7.03	17.15	-	synthetic sample	Davey et al. (1963)
H-alunite	7.01	17.18	-		Kubisz (1970)
H-alunite	7.006(1)	17.130(11)	728.16	Synthetic sample	Ossaka et al. (1982)
H-alunite	7.006(4)	17.15(1)	729.0	In D <sub>2</sub> O	Ripmeester (1986)
H-alunite	7.005(2)	17.114(7)	727.2(4)	synthetic sample	Soffregen and Alpers (1992)
Na-alunite	6.990(2)	16.905(12)		natural sample (Na <sub>58</sub> K <sub>42</sub> )Al <sub>3</sub> (SO <sub>4</sub> ) <sub>2</sub> (OH) <sub>6</sub>	Okada et al. 1982
Na-alunite	6.982	16.737	706.58	natural sample	Schoch et al. 1989
Na-alunite	6.9990(8) 6.9823(5) 6.9786(7)	16.690(3) 16.700(2) 16.696(3)	708.0(2) 705.1(1) 704.2(2)	synthetic sample heated at: 150 °C 250 °C 450 °C	Soffregen and Alpers (1992)
NH <sub>4</sub>	7.013(1)	17.885(50)	760.5(3)	natural sample	Altaner et al. 1988
basic gallium salt	7.18	16.96	-	synthetic sample (4.1 % H <sub>2</sub> O)	Tananaev et al. 1967

**Table 6.6: Unit cell parameters and unit cell volume taken from the literature for end member alunites: alunite, H-alunite, Na-alunite, NH<sub>4</sub>-alunite and the basic gallium salt of the alunite type (H<sub>3</sub>O)Ga<sub>3</sub>(SO<sub>4</sub>)<sub>2</sub>(OH)<sub>6</sub>.**

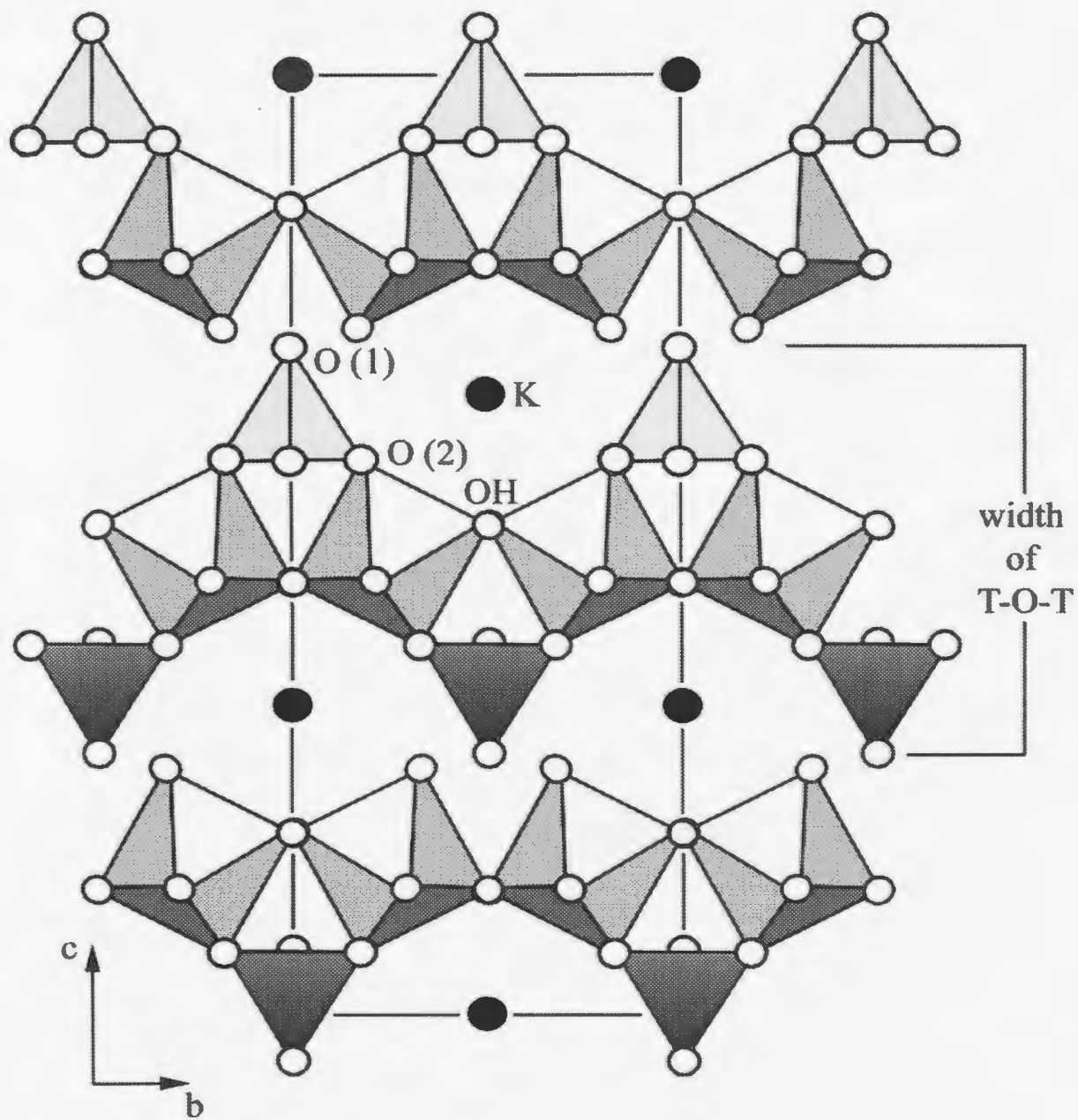
basic gal- lium salt	7.178	17.17	766	synthetic sample	Johansson, 1962
-------------------------	-------	-------	-----	------------------	-----------------



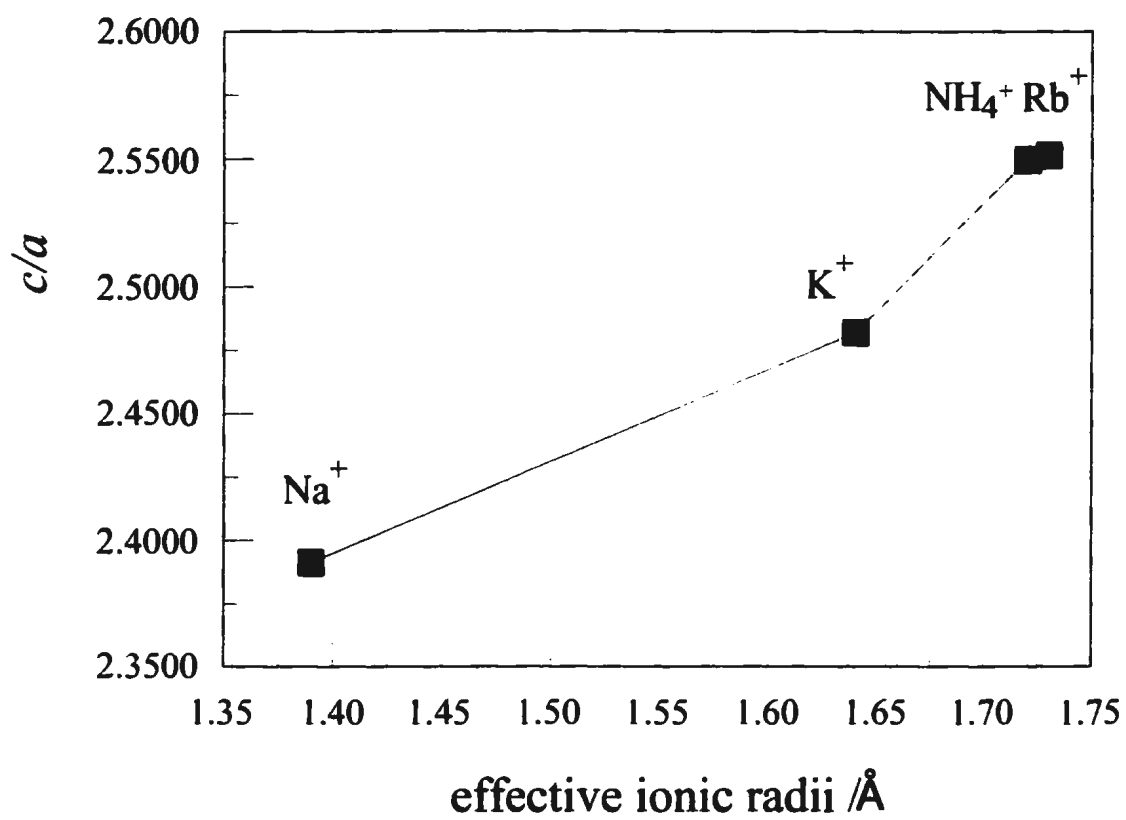
6.1. SEM photograph of synthetic alunite. Scale bar is 6  $\mu\text{m}$ . This image was obtained with a Hitachi S570 scanning electron microscope using an accelerating voltage of 20 keV and a current of 100 nA



6.2. The axis ratio  $c/a$  for the alunite - hydronium alunite solid solution series as a function of the mole fraction  $X_K$ .



6.3. Drawing of the interpenetration of T-O-T layers for alunite.



6.4. The axis ratio  $c/a$  for natroalunite, alunite, ammonioalunite and rubidium-alunite as a function of the effective ionic radius of Na<sup>+</sup>, K<sup>+</sup>, NH<sub>4</sub><sup>+</sup>, and Rb<sup>+</sup>.

## 6. 7. References

- Altaner, St. P., Fitzpatrick, J. J., Krohn, M. D., Bethke, P. M. Hayba, D. O. Goss, J. A. and Brown, Z. A., 1988. "Ammonium in alunite". *Amer. Miner.* 73, 145- 152.
- Aslanian, S. O., Apostolov, D. E. And Yordanov, Y. A., 1982. "Isomorphous Substitution of  $Al^{3+}$  and  $Ga^{3+}$  ions in the alunite structure". 35, No. 8, 1093-1096.
- Bomhammel, K., Naumann, R. and Paulik, F., 1987. "Thermoanalytical and calorimetric investigations on the formation and decomposition of some alunites". *Thermochim Acta*, 121, 109 - 119.
- Brophy, G. P., Scott, E. S. and Snellgrove, R.A., 1962. "Sulfate studies II Solid solution between alunite and jarosite". *Amer. Miner.*, 47, 112- 126.
- Davey, P. T., Lukaszewski, G. M. and Scott, T. R., 1963. "Thermal decomposition of basic aluminium sulphate,  $3Al_2O_3 \cdot 4SO_3 \cdot 9H_2O$ ". *Aust. J. Appl. Sci.*, 14, 137-154.
- Dutrizac, J. E. and Kaiman, S., 1976. "Synthesis and properties of jarosite-type compounds". *Can. Min.* 14, 151-158.
- Dutrizac, J. E. Jambor, J. L. and Chen, T. T., 1986. "Host minerals for the gallium-germanium ores of the apex mine, Utah". *Economic Geol.*, 81, 946 - 950.
- Fairchild, J. G., 1933. "Artificial jarosites. The separation of potassium from cesium". *Amer. Miner.*, 18, 543-547.
- Finch, C., 1993. "Methods of water analysis by inductively coupled plasma-emission spectrometry". *Current Research. Newfoundland Department of Mines and Energy, Geological Survey Branch, Report 93-1*, 435 - 441.

- Harris, W. E. and Kratochvil, B., 1981. *An Introduction to Chemical Analysis*, Saunders College Publishing, Philadelphia, p. 75, p. 203.
- Härtig, C., Brand, P. and Bohmhammel, K., 1984. "Fe-Al- Isomorphie und Strukturwasser in Kristallen vom Jarosit-Alunit-Type". *Z. Anorg. Allg. Chemie.*, 508, 159-164.
- Hendricks, S. B., 1937. "The crystal structure of alunite and the jarosites". *Amer. Miner.*, 22, 773-784.
- Holland, T. J. B. and Redfern, S. A.T., 1997. "Unit cell refinement from powder diffraction data: the use of regression diagnostics". *Mineral. Mag.*, 61, 65 - 77.
- Johansson, G., 1963. "On the crystal structure of a basic gallium sulfate related to alunite". *Arkiv kemi*, 20, 343-352.
- Kahn, A.A. and Baur, W. H., 1972. "Salt hydrates: VIII The crystal structure of sodium ammonium orthochromate dihydrate and magnesium diammonium bis (hydrogen orthophosphate) tetrahydrate and a discussion of the ammonium ion". *Acta Cryst.*, B28, 683 - 693.
- Menchetti, S. and Sabelli, C., 1976. "Crystal chemistry of the alunite series: crystal structure refinement of alunite and synthetic jarosite". *N.Jb. Miner. Mh.*, 406- 417.
- Okada, K., Hirabayashi, J., and Ossaka, J., 1982. "Crystal structure of natroalunite and crystal chemistry of the alunite group". *N. Jb. Miner. Mh.*, 534-540.
- Ossaka, J., Hirabayashi, J., Okada, K. and Harada, J., 1982. "Crystal data for  $3\text{Al}_2\text{O}_3 \cdot 4\text{SO}_3 \cdot 9\text{H}_2\text{O}$ ". *J. Appl. Cryst.*, 15, 353-354.
- Parker, R. L., 1962. "Isomorphous substitution in natural and synthetic alunite". *Amer.*

- Miner.*, 47, 127- 136.
- Ripmeester, J. A., Ratcliffe, Ch. I., Dutrizac, J. E., and Jambor, J. L., 1986. "Hydronium in the alunite-jarosite group" ., *Can. Miner.*, 24, 435-447.
- Schoch, A. E., Beukes, G. J., Van der Westhuizen, W. A. and De Bruijn, H., 1989. "Natroalunite from Koenabib, Pofadder district, South Africa". *S. Afr. J. Geol.*, 92, 20 - 28.
- Scott, K. M., 1987. "Solid solution in, and classification of, gossan-derived members of the alunite-jarosite family, northwest Queensland, Australia". *Amer. Miner.*, 72, 178 - 187.
- Shannon, R. D., 1976. "Revised effective ionic radii and systematic studies of interatomic distances in halides and chalcogenides". *Acta Cryst.* A32, 751 - 767.
- Stoffregen, R. E. and Cygan, G. L. 1990. "An experimental study of Na-K exchange between alunite and aqueous sulfate solutions". *Amer. Miner.*, 75, 209-220.
- Stoffregen, R. E. and Alpers, Ch. N., 1992. "Observations on the unit-cell dimensions, H<sub>2</sub>O content, and δD values of natural and synthetic alunite". *Amer. Miner.*, 77, 1092-1098.
- Szymanski, J. T., 1985. "The crystal structure of plumbojarosite Pb[Fe<sub>3</sub>(SO<sub>4</sub>)<sub>2</sub>(OH)<sub>6</sub>]<sub>2</sub>". *Can. Mineral.*, 23, 659 - 668.
- Tananaev, I. V., Kuznetsov, V. G. And Bolshakova, N. K., 1967. "Basic gallium salts of the alunite type". *Russ. J. Inorg. Chem. (Engl. Edition)* Vol.12, No.1, 28 -30.
- Vogel, A. I., *A Text-Book of Quantitative Inorganic Analysis*, Third Edition, Longman,

London 1961.

Wang, R., Bradley, W. F. and Steinfink, H., 1965. "The crystal structure of alunite". *Acta Cryst.* 18, 249 - 252.

## 7. Raman and infrared absorption studies on synthetic alunites.

Wolfram W. Rudolph and Roger Mason

### 7. 1. Abstract

Stoichiometric end member alunite  $[\text{KAl}_3(\text{SO}_4)_2(\text{OH})_6]$ , hydronium alunite  $[(\text{H}_3\text{O})\text{Al}_3(\text{SO}_4)_2(\text{OH})_6]$  and samples of the solid solution series over the entire compositional range from  $\text{K}^+$  to  $\text{H}_3\text{O}^+$  have been synthesized under hydrothermal conditions and characterized by Raman and infrared spectroscopy. Vibrational analysis has been applied in order to investigate the different types of chemical species in these alunites, particularly hydrogen-oxygen species, the sulfate anions and the  $\text{AlO}_2(\text{OH})_4$  unit. Deuterated samples  $[\text{KAl}_3(\text{SO}_4)_2(\text{OD})_6]$ , and  $[(\text{D}_3\text{O})\text{Al}_3(\text{SO}_4)_2(\text{OD})_6]$  have been prepared to facilitate the identification of O-H/O-D vibrations and to make assignments more reliable.

### 7. 1. Introduction

The alunite group comprises basic sulfates of ideal composition  $\text{AB}_3(\text{SO}_4)_2(\text{OH})_6$ , where A is  $\text{H}_3\text{O}^+$ ,  $\text{Na}^+$ ,  $\text{K}^+$ ,  $\text{Rb}^+$ , etc. and  $\text{B} = \text{Al}^{3+}$ . Compounds in which the B site is occupied by  $\text{Fe}^{3+}$  belong to the jarosite group of minerals. Together, the alunite and jarosite groups constitute the alunite-jarosite supergroup (Scott, 1987).

In this paper we deal exclusively with members of alunite group. Alunite, sensu stricto,  $[\text{KAl}_3(\text{SO}_4)_2(\text{OH})_6]$ , is one of the most abundant minerals of the isostructural alunite-jarosite group (Scott, 1987) and is formed over wide temperature range (ca. 20 to

400 °C) as a secondary phase from Al-rich minerals (e.g. feldspars) in oxidizing, sulfur-rich environments. There is extensive solid solution among A site ions (Scott, 1987 and Stoffregen and Alpers, 1992). Complete solid solution has also been demonstrated between alunite and jarosite, the substitution in B site ( $\text{Al}^{3+} \rightleftharpoons \text{Fe}^{3+}$ ), (Parker, 1962; Brophy et al., 1962; Härtig et al., 1984), and may exist for all alunite - jarosite species.

Alunites have been characterized by X-ray, chemical and thermal methods (Parker, 1962, Slansky, 1973, Menchetti and Sabelli, 1976, Pysiak and Glinka, 1981, Ripmeester et al. 1986). However, there are discrepancies in the results because some of the synthetic samples not only contain a deficiency of A site ions, but also contain "excess" (non-stoichiometric) water (Parker, 1962; Ripmeester et al. 1986; Rudolph and Mason). In addition, there is doubt as to the space group to which alunite group compounds belong. Vibrational spectroscopic investigations should allow the proof or disproof of the existence of three different types of hydrogen - oxygen species in alunites, namely  $\text{OH}^-$ ,  $\text{H}_3\text{O}^+$  and possibly  $\text{H}_2\text{O}$ . We present Raman and infrared spectra taken on well characterized synthetic alunite samples of end member and intermediate composition in the solid solution series from  $\text{K}^+$  to  $\text{H}_3\text{O}^+$ , using deuterated samples of  $[\text{KAl}_3(\text{SO}_4)_2(\text{OD})_6]$ , and  $[(\text{D}_3\text{O})\text{Al}_3(\text{SO}_4)_2(\text{OD})_6]$  to facilitate the identification of the hydrogen (deuterium) -oxygen species. We use the results to establish the space group of stoichiometric alunite compounds.

### 7. 3. Experimental Section

#### 7. 3. 1. Synthesis of alunite samples

Details of the method of synthesis and characterisation by X-ray diffraction are described in a previous paper (Rudolph and Mason, 2001). Deuterated samples for the present study were prepared from a deuterated  $\text{Al}_2(\text{SO}_4)_3$  stock solution 1.03 mol/L (deuteration degree approximately 98 %) and 99.9 %  $\text{D}_2\text{O}$  and 99.0 % sulfuric acid- $\text{d}_2$  (both chemicals from Cambridge Isotope Laboratory, Andover, MA, USA). The starting solutions for alunite synthesis were prepared by weight. The hydrothermal synthesis was carried out in thick walled quartz tubes (wall thickness 1 mm) 1 inch in diameter and an approximate total volume of 18 ml.

#### 7. 3. 2. Analytical and spectroscopic methods

Chemical analysis of the deuterated species were made applying procedures detailed by Rudolph and Mason, 2001. Most Raman spectra were measured at TU Mining Academy Freiberg, Saxony, Institute of Theoretical Physics. The Raman spectra were also excited with the 514.5 nm line of a Spectra Physics Argon ion laser with a laser power of about 20 mW in order to avoid sample heating. The scattered light was analysed with a triple monochromator T64000 (Jobin Yvon) equipped with holographic gratings (1800 lines/mm) and detected by a cooled charge-coupled device. The wavenumber scale of the spectrometer was calibrated by comparison with the emission lines of a neon lamp. The spectra were collected at 298 K in the additive mode of the spectrometer with a spectral resolution of  $1.2 \text{ cm}^{-1}$ . A few Raman spectra on alunite, and hydronium alunite were

measured at Memorial University of Newfoundland, Department of Chemistry using a scanning Rhenishaw Model 1000 Raman spectrometer; these samples were also excited with the 514.5 nm laser line at 20 mW (Spectra Physics Argon ion Laser, Model 263). Spectra measured using different instruments gave identical results.

The KBr pressed pellet technique was employed as the standard method of sample preparation. The alunite samples were heated to 160 °C before infrared absorption measurements in order to remove adsorbed water. A mixture of 1.0 % by weight of sample was mixed with dried spectroscopic-grade KBr ground in an agate mortar until a homogeneous fine-grained powder was obtained. Pellets were prepared immediately in a Perkin-Elmer disk press using 250 to 300 mg of the sample mix. The infrared absorption spectra were measured with a Matson Polaris FT-IR spectrometer (Department of Chemistry, MUN) in transmission mode in the wavenumber range from 400 to 4000  $\text{cm}^{-1}$ . Sixteen to thirty two scans were taken. The resolution was about 4  $\text{cm}^{-1}$ . Hydronium alunite was also measured with a Perkin-Elmer 283 double beam dual-grating infrared absorption spectrometer (Department of Chemistry, MUN) in the 250 to 4000  $\text{cm}^{-1}$  region using air in the reference beam path. The Perkin-Elmer 283 model infrared spectrometer was used in order to extend the low wavenumber region.

An especially rapid method (2 to 3 minutes) for collecting infrared absorption spectra of minerals is the attenuated total reflection (ATR) technique. Infrared spectra in the wavenumber range from 600 to 4000  $\text{cm}^{-1}$  were measured with a Bruker FT-IR spectrometer IFS 66, Germany. A Golden Gate Single reflection Diamond ATR cell

(Manufacturer: Graseby Specac INC. Fairfield, CT, U.S.A.) was used as the sample accessory cell. In the accessory a 2 mm x 2 mm square diamond crystal is used which is brazed onto a tungsten carbide disc leaving of 0.6 mm x 0.6 mm sample square. On the micro sample a reproducible pressure is applied through a clamp mechanism between the diamond crystal and the sapphire window. The ATR spectrum was transformed into an absorption spectrum with the help of the so called ATR correction function. Diamond possesses an absorption region between 1900 to 2300  $\text{cm}^{-1}$  which has to be taken into account when interpreting the OH deformation/stretching mode region. These spectra were measured at the institute of polymer research. The senior author would like to thank Dr. D. Fischer, IPF, Dresden, Germany, for the use of his FT-IR spectrometer and for helpful comments.

Alunites in the  $\text{H}_3\text{O}^+ - \text{K}^+$  solid solution series, including the two end members  $[(\text{H}_3\text{O})\text{Al}_3(\text{SO}_4)_2(\text{OH})_6]$  and  $[\text{KAl}_3(\text{SO}_4)_2(\text{OH})_6]$  were also measured using the diffuse reflectance technique. Diffuse reflectance spectra of alunite samples were measured with a Diffuse Reflection Attachment, Praying Mantis (Harrick Scientific Corporation, Ossining NY, U.S.A.). The same FT-IR spectrometer was used as for the ATR measurements. This method is, like ATR, a surface method but the penetration depth is much greater (10 to 500  $\mu\text{m}$ ). The alunite sample (10 mg) was mixed with 200 mg KBr and placed in the sample cup of the reflectance cell. The diffuse reflectance spectrum has been converted to a absorption like spectra using the Kubelka-Munck function.

## 7.4. Results

### 7.4.1. Chemical characterization and morphological studies of the alunite crystal powders

Examination of the SEM photographs shows that the alunite samples are polycrystalline particles, ranging in size from 8 to 10  $\mu\text{m}$  (Rudolph and Mason, 2001). The absence of unidentified peaks in XRD indicates that no other crystalline phases are present in the precipitate at detectable levels.

Analytical results on synthesized alunite samples of the solid solution series  $\text{K}^+ - \text{H}_3\text{O}^+$  (specimens A014 to A007), taken from Rudolph and Mason, 2001, are compiled in Table 7.1. Wet chemical analysis yielded a composition of the alunite end members very close that of "ideal" alunite with a  $\text{K}:\text{Al}:\text{SO}_4$  ratio of 1:2.99:2.00 compared to the ideal 1:3:2 ratio. The measured stoichiometry indicates that the synthesised alunite contains no hydronium substitution or non-stoichiometric water. This is particularly important for the studies of the vibrational spectra (see below) because the stoichiometry and homogeneity of the phases exert a controlling influence on those spectra.

The composition of the deuterated alunite samples (A029 and A030) was found to be almost of ideal composition  $\text{K} : \text{Al} : \text{S} = 1 : 3 : 2$  and the degree of deuteration was found to be greater than 98 %. The deuterium alunite showed the ratio  $\text{Al} : \text{S} = 3 : 2$ , but the degree of deuteration was less than 65 %. The deuterated alunite sample (d-alunite-d) exchanged D with H quite rapidly during handling and storage and was therefore stored airtight in a sealed glass bottle. The D/H ratio was determined by measuring the band areas

of the OD and OH stretching modes. Its noteworthy, that  $[\text{KAl}_3(\text{SO}_4)_2(\text{OH})_6]$  crystal powder does not exchange D with H as rapidly. This behaviour was also described by Kubisz, (1972) for a similar deuterium compound,  $[(\text{D}_3\text{O})\text{Fe}_3(\text{SO}_4)_2(\text{OH})_6]$ .

#### 7. 4. 2. Vibrational spectroscopic results on synthetic alunites

We begin by presenting the vibrational spectra (Raman and infrared) for alunites and discuss these data taking into account the results from the factor group analysis (FGA) and from general spectroscopic considerations as discussed below. Raman and infrared spectroscopic data for alunite,  $\text{KAl}_3(\text{SO}_4)_2(\text{OH})_6$ , and alunite-d,  $\text{KAl}_3(\text{SO}_4)_2(\text{OD})_6$  are compiled in Table 7.2. The overview Raman and infrared spectra for the alunite end member is presented in Figure 7.1. The assignments of the Raman and infrared absorption modes are given in Table 7.2, and although a detailed discussion of the modes is given below, a few remarks should be made. The sulfate modes (cf. Rudolph, 1996) can be assigned, using the substitution of H by D in alunite, because deuteration causes a large shift of the  $\delta$  and  $\gamma$  OH modes, while sulfate modes do not shift at all or only slightly (compare Figure 7.2). The Raman spectrum of the OH region for  $\text{KAl}_3(\text{SO}_4)_2(\text{OH})_6$  is compared with the OD stretching region of  $\text{KAl}_3(\text{SO}_4)_2(\text{OD})_6$  in Figure 7.3. The stretching mode  $\nu$  OH shows a double mode and the substitution of D for H results in a large shift of  $\nu$  OH (a doublet) from  $3507/3480 \text{ cm}^{-1}$  to  $2592/2571 \text{ cm}^{-1}$ . The ratio  $\nu$  OH/ $\nu$  OD is with 1.353 smaller than the theoretical value 1.414 due to the anharmonicity of the O-H bond (see discussion below).

The Raman and infrared spectroscopic data for H-alunite and d-alunite-d together

with the assignment of the vibrational modes are compiled in Table 7.3. The slight shift of the sulfate modes and the OH modes distinguishes H-alunite from alunite. The most remarkable difference between H-alunite and alunite consists in the OH stretching region, because of the hydronium ion modes. The Raman and infrared absorption spectrum for the pure H-alunite end member are presented in Figure 7.4.

The Raman spectra of the solid solution series from alunite to hydronium alunite ( $[\text{K}_{1-x}(\text{H}_3\text{O})_x\text{Al}_3(\text{SO}_4)_2(\text{OH})_6]$ ,  $(0 \leq x \leq 1)$ ; samples A014 to A007) are presented in Figure 7.5 A (wavenumber range from 100 to 1300  $\text{cm}^{-1}$ ) and Figure 7.5 B (wavenumber range from 3275 to 3720  $\text{cm}^{-1}$ ). The Raman spectroscopic data are compiled in Table 7.5. The infrared spectra (ATR-spectra) for the alunites of these solid solution series are presented in Figure 7.6 A and 7.6 B in the wavenumber range from 600 - 1300  $\text{cm}^{-1}$  and in the wavenumber range from 2800 - 3800  $\text{cm}^{-1}$ , respectively. The infrared spectroscopic data are compiled in Table 7.6.

## 7. 5. Discussion

Before discussing the assignment of vibrational modes of the crystals to the modes observed in Raman and infrared spectra it is necessary to present, briefly, the structure of alunite, as known from X-ray diffraction measurements.

### 7. 5. 1. Structure of alunite

Alunite crystallizes in the centrosymmetric space group  $R\bar{3}m$  ( $D_{3d}^5$ ), with  $Z=3$  (in the hexagonal unit cell) (Wang et al., 1965; Menchetti and Sabelli, 1976). The sulfur forms tetrahedra and the aluminum octahedra, the two kinds of coordination polyhedra being

corner-linked (Figure 7.7). The structure is made up of tetrahedral-octahedral-tetrahedral (T-O-T) layers. The aluminum octahedron is slightly distorted, being formed by four OH groups and two oxygen atoms from two different  $\text{SO}_4$  tetrahedra. Each aluminium atom lies on a centre of symmetry. The sulfur atoms lie on the trigonal axis and are surrounded by three basal oxygen atoms (O(2)) and one apical oxygen (O(1)) which also lies on the threefold axis. The apical oxygen, O(1) is somewhat special (no close contact to other cations) and has been variously described as H-bonded to OH (Menchetti and Sabelli, 1976) or “doubly” bonded to S (Wang et al., 1965).

The univalent cations ( $\text{Na}^+$ ,  $\text{K}^+$ ,  $\text{H}_3\text{O}^+$  etc.) are surrounded by twelve anions, namely six oxygen atoms, O(2), and six OH groups, which are nearly at the same distance from the cation.

#### 7. 5. 2. Assignment of the vibrational modes

The vibrational spectra of solids are governed by the crystal structure, which determines the local symmetry of the ions and the space group (factor group). In order to understand the vibrational modes it is first necessary to establish how many modes there should be, before making assignments. Factor group analysis (FGA) is used to establish the number of modes and their activity in Raman and infrared spectra. For centrosymmetric crystals we can make use of the so called mutual exclusion rule which states, that vibrational modes active in the Raman effect are forbidden in infrared and vice versa. Consequently, if the vibrational model of a crystal can be described in the framework of the harmonic approximation, a comparison of the corresponding infrared and Raman

modes allows one to determine if the crystal has a centre of inversion. Although the more recent structure determinations on alunite (Wang et al., 1965; Menchetti and Sabelli, 1976) suggests that it belong to space group R-3m, the older literature favoured the acentric group R3m (Hendricks, 1937) and the optical second harmonic examination on alunite (Loiacono et al., 1982) has been interpreted to imply an acentric space group. FGA provides a sensitive test of symmetry when the results are compared with spectral data. FGA is particularly valuable for poorly crystallized crystals, which are synthesized (or found) only in a microcrystalline form (like the alunites described) and therefore single crystal analysis is not possible.

#### 7. 5. 2. 1. Factor group analysis

Detailed discussion of the FGA can be found in Decius and Hexter (1977), Ross (1972) and Ferraro and Nakamoto (1994). The vibrational modes may be divided into internal and external modes, the former being vibrations about the centre of mass of a molecule/molecular ion, such that the centre of mass itself remains fixed in position. These modes in crystals are frequently similar in number and type to those found in isolated molecules of the same kind. External modes involve translational and rotational motions of whole molecules. For these modes, the centre of mass of the molecules move, but the centre of the mass of the unit cell remains constant with respect to the neighbouring unit cells. Analysis of the internal modes is especially suitable for treatment using the correlation method, which begins with an analysis of the vibrational modes of the undisturbed molecule (e.g. free sulfate) and is completed by taking into account the effects

of the symmetry environment of the ion as incorporated in a crystal structure. We are especially interested in the internal modes of sulfate and hydroxyl ions and therefore apply the correlation method.

In the zero wave vector approximation,  $k \approx 0$  (modes near the centre of the Brillouin zone)  $3nZ$  modes are to be expected, where  $n$  stands for the number of atoms in the formula unit and  $Z$  stands for the number of formula units in the unit cell. At  $k \approx 0$  the three acoustic modes have vanishing frequencies leaving  $3nZ-3$  optical modes. The distribution of the optical branch frequencies, their distribution, symmetry classification, and optical activity can be enumerated only from a consideration of the unit cell (instead of the entire crystal). Symmetry classification of the  $k \approx 0$  modes can therefore be accomplished by taking into consideration the factor group of the crystal, which is isomorphous with one of the 32 crystallographic point groups. In the case of alunite, the crystallographic point group is  $-3m (D_{3d})$  (ditrigonal-scalenoedric). The factor group represents the group formed by the symmetry elements contained in the smallest unit cell, the Bravais cell. The formal treatment of the factor group analysis follows the procedure published by Fateley, Dollish, McDevitt and Bentley (1974).

In the case of alunite type structures  $n = 26$  and with only one formula unit occupying the unit cell,  $Z = 1$  (rhombohedral unit cell), results in 78 phonon branches arising from normal modes of 2  $SO_4$ , 6 OH, and 3Al and K. The site symmetry for K is  $D_{3d}$ , for Al  $C_{2h}$ , for  $SO_4$   $C_{3v}$ , and for OH  $C_s$ . From these factor group normal modes we have to subtract 3 acoustic modes (characters  $A_{2u}$  and  $E_u$ ) which are at essential equal to zero

wavenumbers for  $k \approx 0$ , which leaves 75 vibrational modes. The results of the factor group analysis are given in Table 6. The site symmetry for the two sulfates is  $C_{3v}$  and this means that the local field acting on the two sulfate modes is lower than their symmetry in the “free” state ( $T_d$ ). In the unit cell the two sulfate modes couple with each other and this results in 12 modes, out of which only six are infrared active and six are Raman active. From simple enumerations of the numbers of the internal modes for sulfate, 18 normal modes are expected but because of degeneracy only 12 modes are observed. The  $A_{1g}$  and  $E_g$  modes are Raman active, while the modes with character  $A_{2u}$  and  $E_u$  are infrared active. The space group  $D_{3d}$  in other words gives rise to the mutual exclusion of Raman and IR modes as mentioned previously. The correlation diagram in Figure 8 presents the symmetry properties of the sulfate modes in alunite for space group  $R\bar{3}m$  ( $D_{3d}^5$ ). The 6 internal modes for the  $OH^-$  group result in 4 modes with  $\Gamma_v(OH^-) = A_{1g} + E_g + A_{2u} + E_u$ , again only the vibrational modes with the subscript g (gerade) are Raman active and the modes with the subscript u (ungerade) are IR allowed.

Assuming the acentric space group  $R\bar{3}m$  ( $C_{3v}^5$ ) for alunite, the correlation of the 2 x 9 normal modes for sulfate should also result in 12 modes (6 with character E), but for this space group model all the twelve modes are Raman and infrared active (break down of the mutual exclusion rule).

#### 7. 5. 2. 2. Band Assignment

Their vibrational frequencies and assignments are shown in Table 7.2 to 7.5 respectively. In general a good agreement is observed between the number and type of

internal motions predicted by factor group analysis and observed experimentally. Sulfate modes can be unequivocally assigned. Furthermore the vibrational modes in the Raman effect have slightly different frequencies compared with the infrared modes. This is direct evidence for the centrosymmetric space group R-3m (# 166) proposed by Wang et al. and Menchetti and Sabelli (1976). The report on the deviation of the space group for alunite from the centrosymmetric space group may be explained by a nonstoichiometric alunite composition (cf. synthesis of alunites) often reported for synthetic alunites. It is noteworthy that the vibrational refinement of space group ambiguities is a valuable tool in mineralogy.

Studying of the deuterated compounds enables us to distinguish the modes due to the sulfate anions from those of the hydroxyl anions, because the latter shift to lower frequencies in deuterated compounds. Because of anharmonicity of the bonds the shift of  $\nu$  O-H/ $\nu$  O-D is 1.36 and for  $\delta$ O-H/ $\delta$  O-D is 1.32 to 1.30 rather than theoretically expected 1.414 (Ryskin, 1975).

Both the number and distribution of vibrational modes of the sulfate molecule between Raman and infrared spectra confirm the space group of alunite compounds to be R-3m. The vibrational modes of OH in the Raman effect have different frequencies compared with the infrared modes. The stretching mode of the OH group, showing a doublet structure, is observed at 3480 and 3507  $\text{cm}^{-1}$  in the Raman and in infrared at 3486 and 3514  $\text{cm}^{-1}$  (cf. results in Table 7.2). This is further evidence for the centrosymmetric space group R-3m. The  $\nu$  OH mode in deuterated alunite,

$\text{KAl}_3(\text{SO}_4)(\text{OH})_6$ , which contains ca. 2 % H (decoupled OH oscillator) is found at  $3493 \text{ cm}^{-1}$  in both Raman and infrared spectrum. This demonstrates that the doublet of  $\nu$  OH is caused by coupling of the OH oscillators and is not caused through different site symmetry of the OH groups. We attribute reported deviations of alunite from the centrosymmetric space group R-3m to nonstoichiometry owing to inadequate methods of synthesis (see Rudolph and Mason, 2001 for a more complete discussion).

The hydroxyl ions have in the isolated molecular state  $C_{2v}$  symmetry and possess only one fundamental mode. The corresponding mode lies in alkali metal hydroxides in the range from  $2800$  to  $3700 \text{ cm}^{-1}$  (cf. for instance Siebert, 1966). If attached to another ion, such as  $\text{Al}^{3+}$ , as in alunite, these Al-O-H modes show next to the  $\nu$  AlO-H mode (stretching mode) additional modes, namely  $\delta$ AlO-H (deformation mode) and  $\gamma$ AlO-H (out of plane deformation mode) (cf. Ryskin, 1975). The rhombohedral unit cell contains six  $\text{OH}^-$  ions in equivalent  $C_2$  positions. In the crystal structure these OH units may couple. The position of the O-H stretching mode is expected around  $3500 \text{ cm}^{-1}$  by analogy to  $\nu$  O-H in boehmite (Ryskin, 1975). Its position depends on several factors, firstly, the strength of the Al-OH bond and secondly the strength of the hydrogen bond formed with the  $\text{O}_1$  sulfate oxygen ( $\text{Al-O-H} \cdots \text{O}_1\text{S}(\text{O}_{11})_3$ ) and thirdly from the nature of the cation in the A site ( $\text{Na}^+$ ,  $\text{K}^+$ ,  $\text{H}_3\text{O}^+$  etc.). The deformation mode  $\delta$  O-H may be easily confused with the S-O modes if the spectra of deuterated alunites are not available. The characteristic wavenumber region for this mode is in the range from  $1150$  to  $1000 \text{ cm}^{-1}$  (Ryski, 1975). The characteristic wavenumber of the out of plane deformation mode of O-H,  $\gamma$  O-H can

be found in the region between 800 to 600  $\text{cm}^{-1}$  and may be easily overlooked.

Modes in the range from 300 to 700  $\text{cm}^{-1}$ , which do not belong to sulfate, must come from the  $\text{AlO}_6$  unit in the alunite structure (cf. Structural discussion), because the influence of the monovalent cation is found to be of lesser importance. Support for this conclusion can be found in the vibrational spectra of oxides and hydroxides of Al in which Al-O modes, are found between 700 and 300  $\text{cm}^{-1}$ . In this spectral region the analogy to  $\text{AlO}_6$  in crystalline  $\text{AlCl}_3 \cdot 6 \text{H}_2\text{O}$  is clear. In this compound vibrational modes between 600 and 440  $\text{cm}^{-1}$  have been attributed to Al-O stretching vibrations and those between 440 and 300  $\text{cm}^{-1}$  to Al-O bending vibrations (Kiss et al., 1980). The characteristic wavenumbers for compounds with  $\text{AlO}_6$  units of the hexaaquaaluminium(III) ion like in  $\text{AlCl}_3 \cdot 6\text{H}_2\text{O}$  (cf. Rudolph et al., 2000), corundum (Moenke, 1962) and in aluminiumoxyhydroxides such as boehmite or diaspore (Ryskin, 1975; Kiss et al., 1980) can be used to assign the corresponding modes in alunite.

The hydronium modes in H-alunite are broad and weak and cannot be unequivocally assigned. This topic has been addressed several times, but satisfactory interpretation is still pending. Neutron scattering data are warranted. The pyramidal hydronium ion possesses  $C_{3v}$  symmetry in the free state and the characteristic modes are given in Table 7 (Wilkins et al. 1974, Williams, 1976). Only one  $\text{H}_3\text{O}^+$  ion ( $D_{3d}$  site) is present in the rhombohedral cell of hydronium alunite. Its located below sulfate tetrahedra and has twelve neighbours: six  $\text{O}_{11}$  oxygens and six O-H<sup>+</sup> ions (Johansson, 1963). It is most likely that the hydronium ion is oriented statistically, forming three normal or bifurcated

hydrogen bonds. The vibrational modes of the  $\text{H}_3\text{O}^+$  ion are very much influenced by the nature of the crystal site and by the nature of the cation-anion interactions (Jones et al., 1989). The translational modes (T) lie at about 100 to 300  $\text{cm}^{-1}$  and the librational modes ( $\tau(\text{H}_3\text{O}^+)$  and  $\rho(\text{H}_3\text{O}^+)$ ) in the wavenumber region of about 500 to 800  $\text{cm}^{-1}$  (Jones et al., 1989). It should be noted that the modes of the  $\text{H}_3\text{O}^+$  ion are broad and of medium to weak intensity in the infrared absorption. The  $\text{H}_3\text{O}^+$  modes, especially the diagnostic mode  $\nu_2(\text{H}_3\text{O}^+)$  at 950 - 1140  $\text{cm}^{-1}$ , is overlapped by S-O modes, which are much more intense. In the Raman effect the  $\text{H}_3\text{O}^+$  modes are very weak and in some cases not detectable due to overlap by other modes (sulfate).

The sulfate modes and OH modes are directly influenced by the change in the monovalent ion in A position. The  $\nu_1(\text{SO}_4)$  mode in alunite at 1025  $\text{cm}^{-1}$  is approximately 9  $\text{cm}^{-1}$  lower than in hydrogen alunite. The tendency for the OH modes is opposite, namely OH stretching in alunite is ca. 15 - 20  $\text{cm}^{-1}$  higher than in hydronium alunite. These are diagnostic wavenumbers and can be used as a fingerprint for alunite and hydronium alunite.

## 7. 6. Conclusions

1. Stoichiometric end member alunites were hydrothermally synthesized and were characterized by wet chemical analysis, XRD and ICP OES, and infrared and Raman spectroscopy.

2. Alunite/hydronium alunite solid solution specimens were synthesized and characterized with wet chemical methods and ICP OES, and infrared and Raman

spectroscopy.

3. The infrared and Raman spectra of the alunite end members have been measured and assignments have been made.

4. Deuterated alunite samples allowed the unequivocal assignment of the OH/OD internal vibrations and the internal modes of the sulfate.

5. The use of vibrational spectroscopy in order to refine the space group for alunite showed clearly that the alunite belongs to the centrosymmetric space group R-3m ( $D_{3d}^5$ ).

#### Acknowledgements

W. W. R. thanks for a scholarship from graduate studies of Memorial University NF, during the period 1997 to 1998. Furthermore, W. W. R. would like to thank Dr. Dieter Fischer, IPF, Dresden, Germany and Dr. Gert Irmer, TU Mining Academy Freiberg/Saxony, Germany for the use of their spectrometer (IPF: FT-IR Bruker IFS 66, TU Bergakademie Freiberg: Raman spectrometer Jobi Yvonne T 64000) and for their helpful discussions.

Table 7.1: Analytical results for alunite/hydronium alunite solid solution series.

sample	%Al	%S	%K	$X_K$	mole ratio K:Al in solid
A014	19.550	15.500	9.440	1	1 : 3
A013	19.544	15.482	9.438	1	1 : 3
A012	19.400	15.400	9.280	0.978	0.978 : 3
A011	18.900	15.280	8.580	0.905	0.905 : 3
A010	18.900	15.500	7.065	0.740	0.740 : 3
A009	18.990	15.560	6.470	0.674 <sub>6</sub>	0.675 : 3
A008	20.055	15.865	3.620	0.372	0.372 : 3
A007	20.520	16.200	-	0	0 : 3

Table 7.2: Raman and infrared data for  $KAl_3(SO_4)_2(OH)_6$  (alunite) and  $KAl_3(SO_4)_2(OD)_6$  (alunite-d) at 25°C.

Raman		i.r.		band assign.
alunite	alunite-d	alunite	alunite-d	
163 vw	164 vw			
184 vw	182 vw			
235 m - str	235 m - str			
258 w	258 w			
347 m	343 m			$AlO_6$
382 m-str	362 m-str			
	416 w		415 m	$\gamma$ OD
		424 m		$AlO_6$
483 str	492 str	489 w	495 w, sh	$\nu_2 SO_4^{2-}$
509 m	497 m-str, sh			$AlO_6$
		524 m	508 m	$AlO_6$
562 m	-	-		$\gamma$ OH
609 w	578 w	598 sh, w + 625 str	605 m	$AlO_6$
652 str	648 sh + 654 str	665 sh + 681 str	660 str	$\nu_3 SO_4^{2-}$
-	838 w		845 str + 885 str, br	$\delta$ OD
-			-	$\gamma$ OH
982 vw	985 vw		990 w	combination : 2 x $\nu_2$ $SO_4^{2-}$

1024 vstr	1025 vstr	1026 m	1024 m	v <sub>1</sub> SO <sub>4</sub> <sup>2-</sup>
		1055 m, sh	1055 w	?
1077 m	1116 m-str	1081.5 vstr	- 1116 vstr	v <sub>3</sub> SO <sub>4</sub> <sup>2-</sup>
		~ 1130 sh, m	1145 sh, m	combination :v <sub>2</sub> SO <sub>4</sub> <sup>2-</sup> + v <sub>4</sub> SO <sub>4</sub> <sup>2-</sup>
1152 w	-	1161 str		δ OH
1186 m	1187 str	1220 str	1210 vstr	v <sub>3</sub> SO <sub>4</sub> <sup>2-</sup>
		1250sh	-	overtone SO <sub>4</sub> <sup>2-</sup>
		2118 vw + 2180 vw -	2135 vw 2230 vw 2350 vw	combination :2 x v <sub>3</sub> SO <sub>4</sub> <sup>2-</sup>
3480 str + 3506 str	2571 str + 2592 str	3484 str + 3508 sh	2576 str, br + 2596 str	v OH/OD
-	3481 vw	-	3492 vw	v OH

vw = very weak, w = weak, m = medium, str = strong, vstr = very strong, br = broad, and sh = shoulder.

Table 7.3: Raman and infrared data for  $(\text{H}_3\text{O})\text{Al}_3(\text{SO}_4)_2(\text{OH})_6$  (H-alunite) at 25°C.

Raman	infrared	band assignment
160 vw		
181 vw		
238 str-m,	240 w	
250 sh		
	285 m	
352 m	350 str + 418 vw	$\text{AlO}_6$
383 m - str		$\text{AlO}_6$
488 str	492 w	$\nu_2 \text{SO}_4^{2-}$
504 m	516 sh, w	$\text{AlO}_6$
560 vvw + 590 vvw	592 str + 626 sh	$\text{AlO}_6$
648 str	666 str	$\nu_4 \text{SO}_4^{2-}$
880 vw, br	820 w, br	$\gamma \text{OH}$
1035 vstr	1033 vw	$\nu_1 \text{SO}_4^{2-}$
1072 m	1081 vstr	$\nu_3 \text{SO}_4^{2-}$
1110 w, br	1115 str, sh	$\delta \text{H}_3\text{O}^+$
1161 w	1172 sh, m	$\delta \text{OH}$
1192 m	-	$\nu_3 \text{SO}_4^{2-}$
	1237 vstr + 1260sh	overtones $\text{SO}_4^{2-}$
1600, vvw, br	1615 m	$\delta \text{H}_3\text{O}^+$
1639, vvw, br	1645 m	$\delta \text{H}_2\text{O}$
-	1690 w, br	$\delta \text{H}_2\text{O}$
2250 vw, vbr	2190 w-m, vbr	$\nu \text{H}_3\text{O}^+$

2700 vw, vbr	2700 vw, vbr	v H <sub>3</sub> O <sup>-</sup>
3400 w, br, sh	3420 + 3200 w-vw, br	v H <sub>2</sub> O
3478 w, br 3500 w, br	3480 str, br 3500 sh	v OH v OH

very weak, vw = very weak, w = weak, m = medium, str = strong, vstr = very strong, br = broad, and sh = shoulder.

Table 7.4: Raman data for alunite solid solution series from the pure potassium end member to H-alunite,  $\bar{v} = 298$  K.

A014	A013	A012	A011	A010	A009	A008	A007	Assgn.
163 s	163	163	163	163	162.5	162	161.5	
235 s	235	235	235	235	235	235	238	
258 w	258	258	258	258	258	256	250 sh	
347 w	347	347	347	347	347	348	352	
382 m	382	382	382	382	382	383	384	$\nu \text{AlO}_6$
483 str	483	483	483	484	485	486	488	$\nu_2 \text{SO}_4^{2-}$
509 m	509	508	508	508	507	505	504	$\nu \text{AlO}_6$
562 m	562	562	562	562	561	560	560 vw	$\gamma \text{OH}$
607 w	606	606	606	606	606	606	590 vw	$\nu \text{AlO}_6$
652 str	652	652	652	652	652	651	648	$\nu_4 \text{SO}_4^{2-}$
1024	1024	1024	1024	1025	1027	1029	1035	$\nu_1 \text{SO}_4^{2-}$

Table 7.4: Raman data for alunite solid solution series from the pure potassium end member to H-alunite,  $\bar{V} = 298$  K.

A014	A013	A012	A011	A010	A009	A008	A007	Assgn.
1077	1077	1077	1077	1077	1077	1076	1072	$\nu_3 \text{SO}_4^{2-}$
1152	1052	1052	1052	1053	1054	1055	1161	$\delta \text{OH}$
1186	1186	1186	1186	1186	1187	1190	1192	$\nu_3 \text{SO}_4^{2-}$
						1636	1639	
							2190	
							2250	
							3100	
							3425	
3480	3480	3480	3479	3480	3480	3479	3478	$\nu \text{OH}$
3507	3506	3506	3507	3506	3508	3504	3501	$\nu \text{OH}$

Table 7.5: Infrared data (ATR) for alunite solid solution series from the pure potassium end member to H-alunite,  $\bar{V} = 298$  K.

A014	A013	A012	A011	A010	A009	A008	A007	Assgn.
626 m	626	626	626	626	626	624	624	
681 str	680	680	680	680	678	665	664	$\nu_4 \text{SO}_4^{2-}$
1025.5	1025.5	1026	1026	1026	1027	1032	1034.5	$\nu_1 \text{SO}_4^{2-}$
1081.5	1077	1077	1077	1077	1077	1076	1082	$\nu_3 \text{SO}_4^{2-}$
1160	1052	1052	1052	1053	1054	1055	1161	$\delta \text{OH}$
1220	1220	1220	1220	1121	1222	1128	1231	$\nu_3 \text{SO}_4^{2-}$
					1645	1643	1643	
							1690	
							2250	
							2850	
							3150	
							3425	

Table 7.5: Infrared data (ATR) for alunite solid solution series from the pure potassium end member to H-alunite,  $\bar{U} = 298$  K.

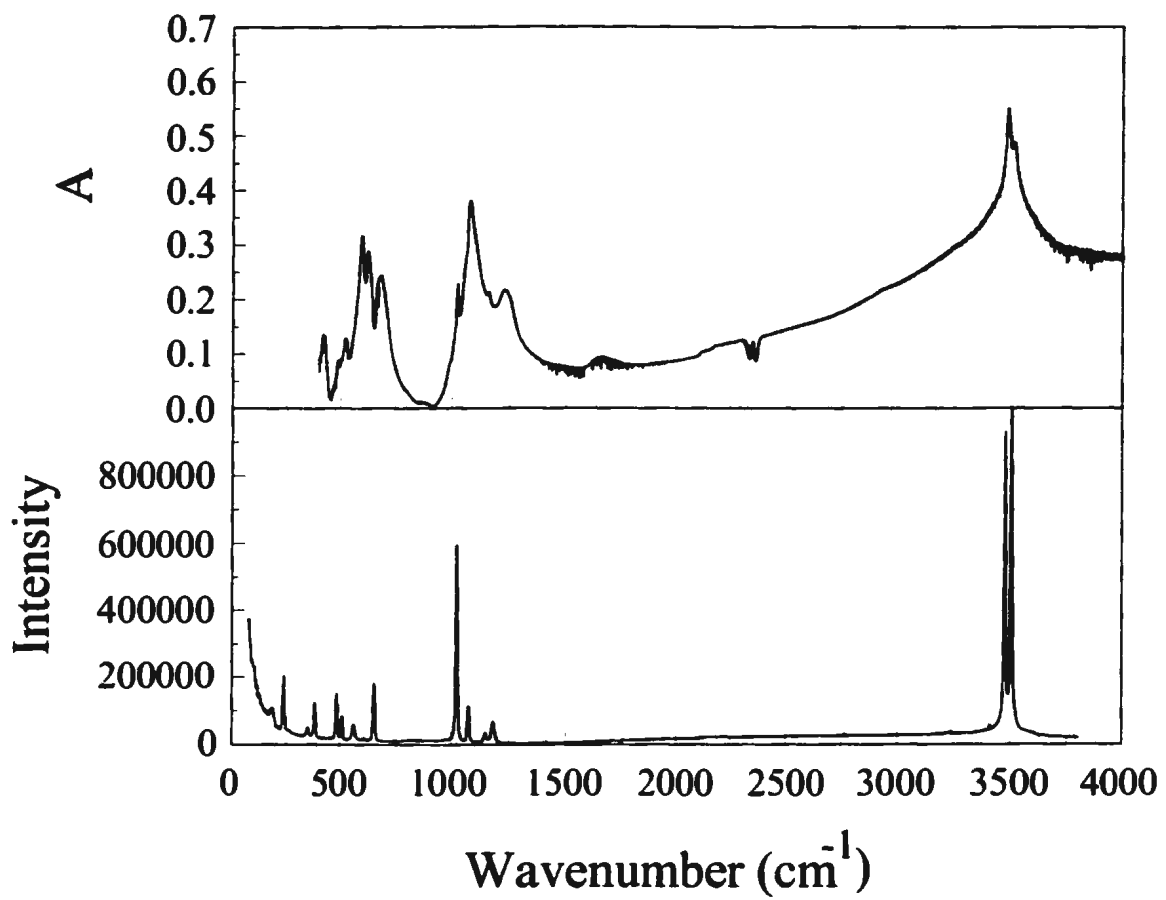
3483.5	3483	3484	3484	3480	3480	3479	3475	v OH
3506	3506	3506	3507	3506	3508	3505	3505 sh	v OH

Table 7.6 : Factor group analysis for alunite ( $D_{3d}^5$ ).

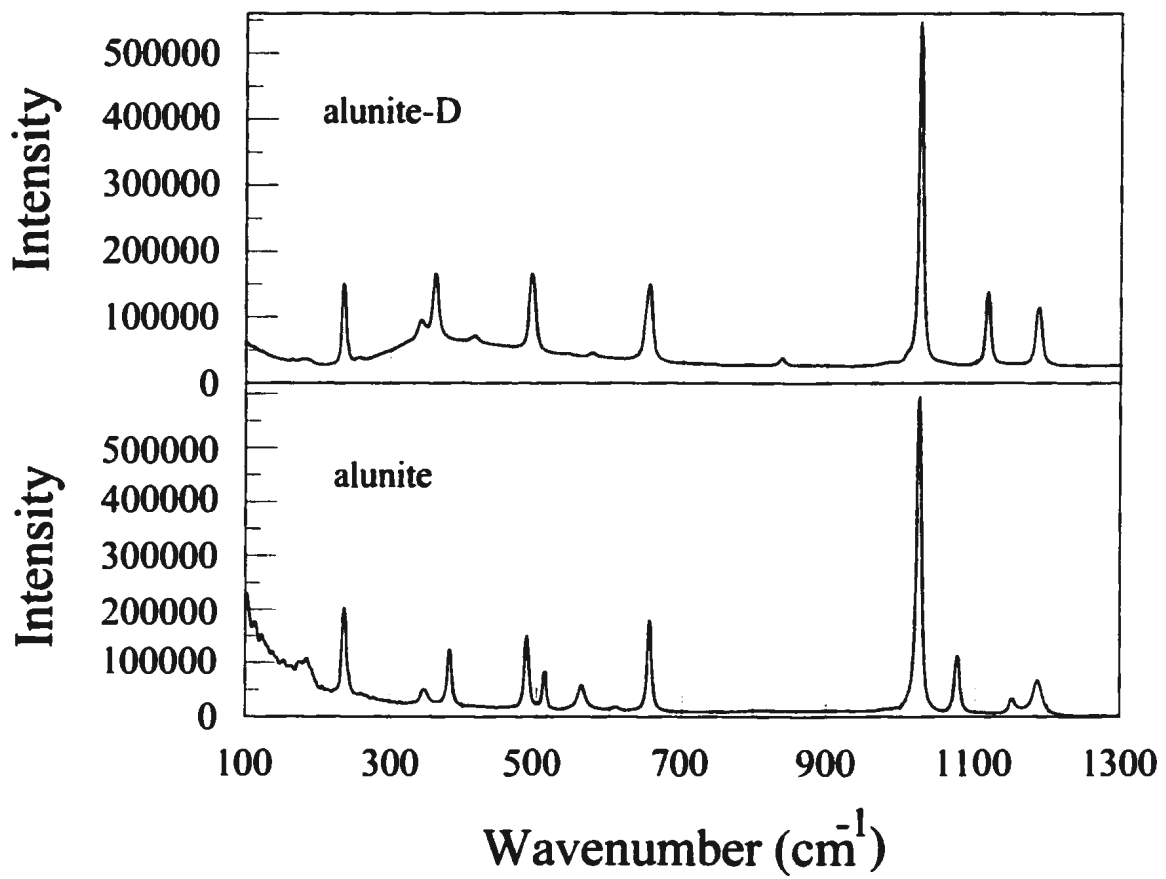
$D_{3d}$	total modes	acoustic modes	internal modes		librations		K	translations			activity
			$SO_4$	OH	$SO_4$	OH		Al	$SO_4$	OH	
$A_{1g}$	9		3	1		1			1	2	Ra
$A_{2g}$	2				1					1	-
$E_g$	11		3	1	1	1			1	3	Ra
$A_{1u}$	3				1			1		1	-
$A_{2u}$	13	1	3	1		1	1	2	1	2	i.r.
$E_u$	16	1	3	1	1	1	1	3	1	3	i.r.

Table 7.7: Characteristic internal vibrations (in  $\text{cm}^{-1}$ ) of  $\text{H}_3\text{O}^+$ .

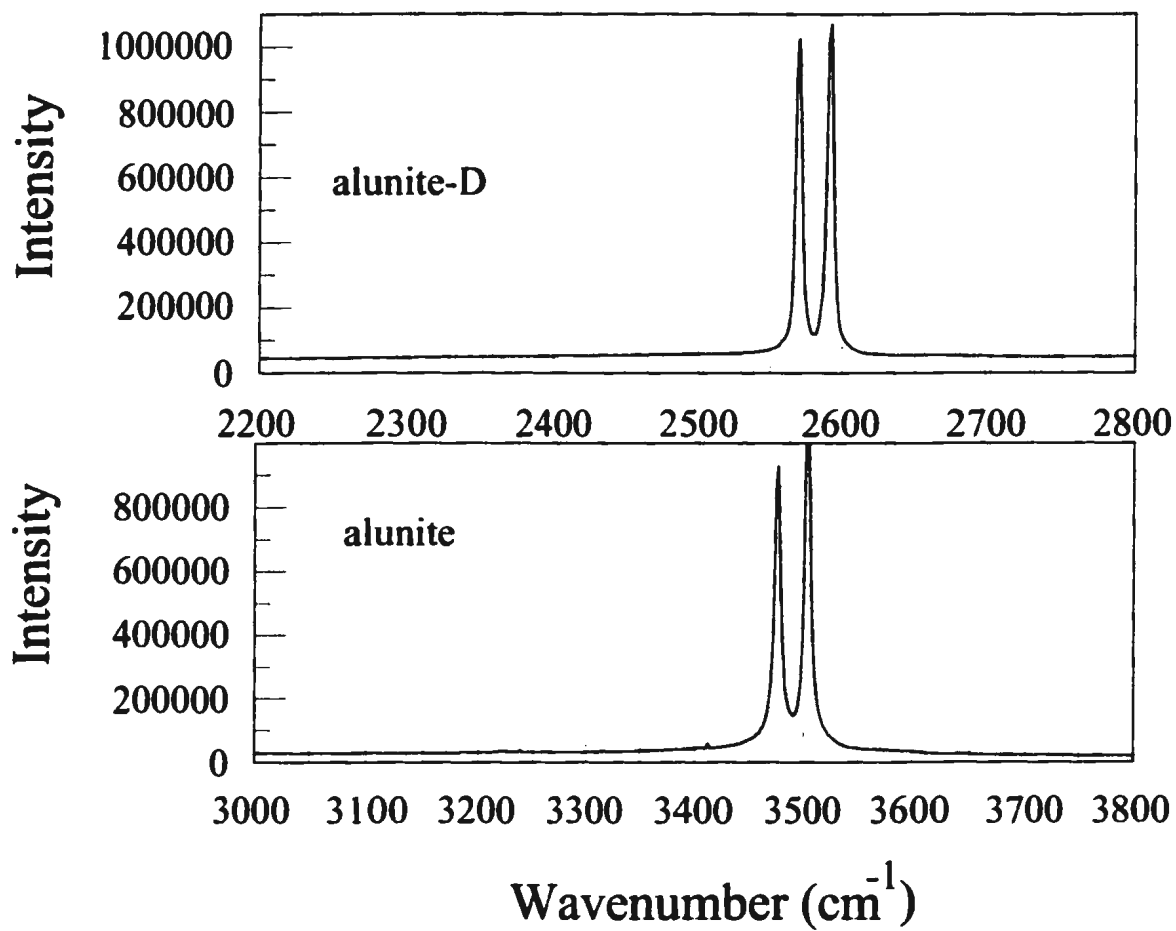
Mode	frequency range	description
$\nu_2(\delta_s)$	950-1140	this mode is used as the diagnostic mode, but is often obscured by other internal modes
$\nu_4(\delta_{as})$	1650-1720	may be obscured by $\delta(\text{H-O-H})$
$\nu_1(\nu_s)$	2460-3380	broad and weak
$\nu_3(\nu_{as})$	2460-3380	broad and weak



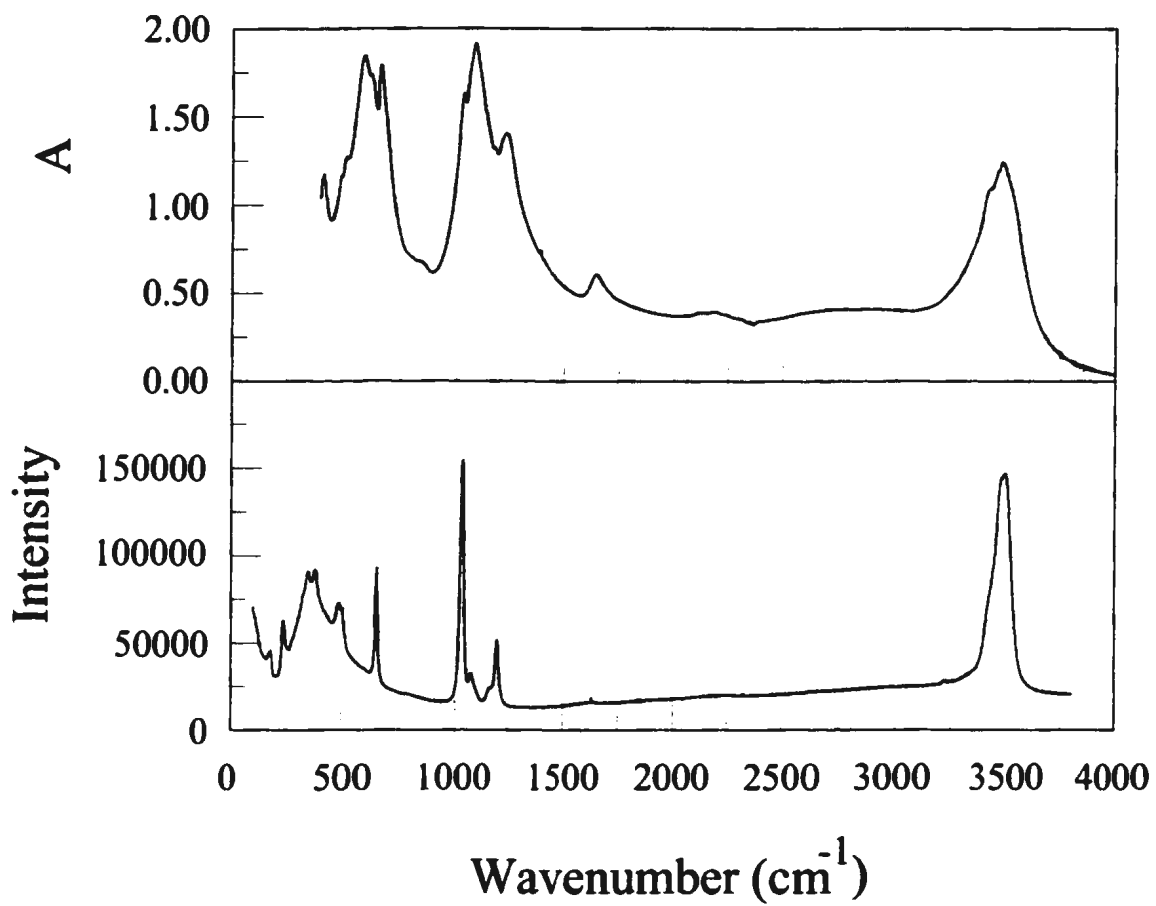
7.1 Raman and infrared spectrum of alunite at 25 °C. Upper panel: infrared spectrum; lower panel: Raman spectrum.



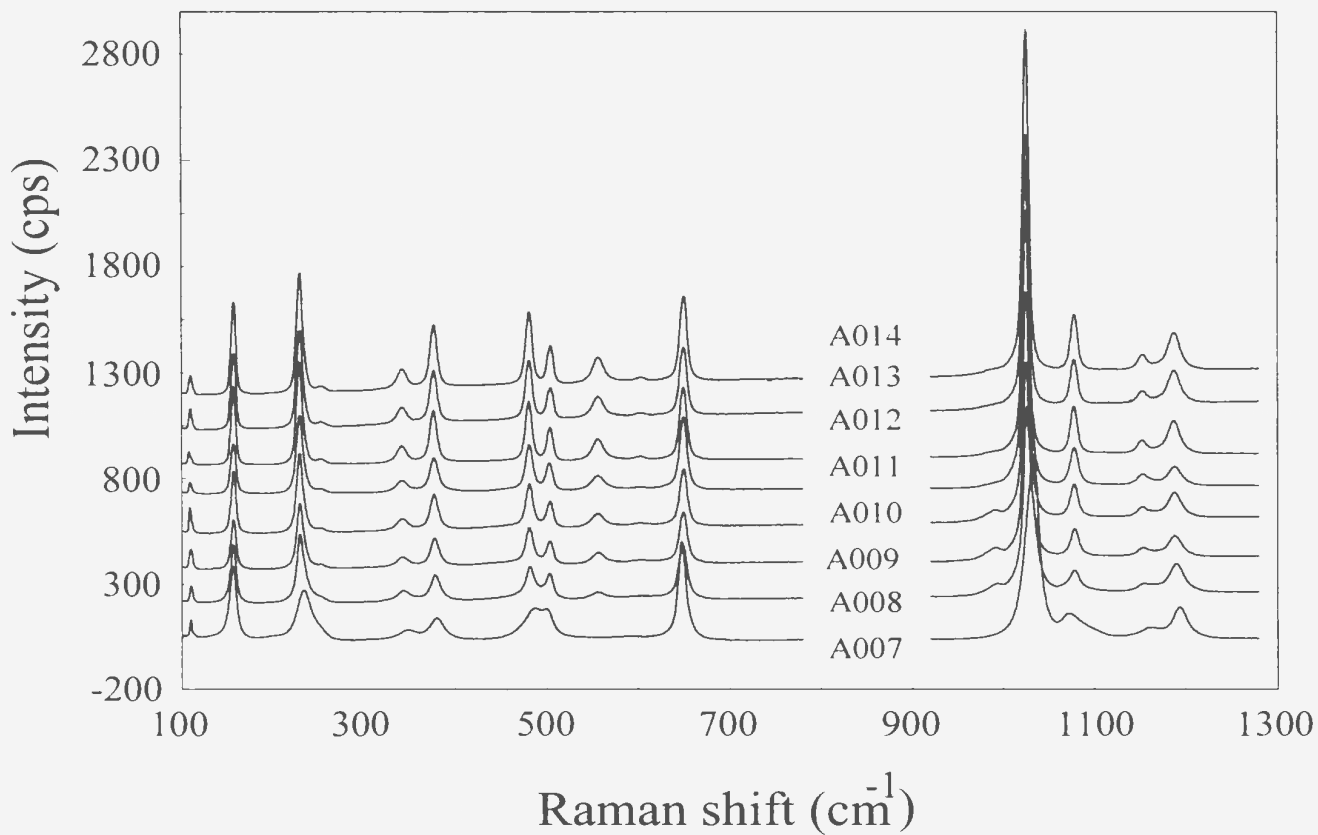
7.2. Raman spectra of alunite and alunite-d at 25 °C in the wavenumber range from 100 to 1300 cm<sup>-1</sup>.



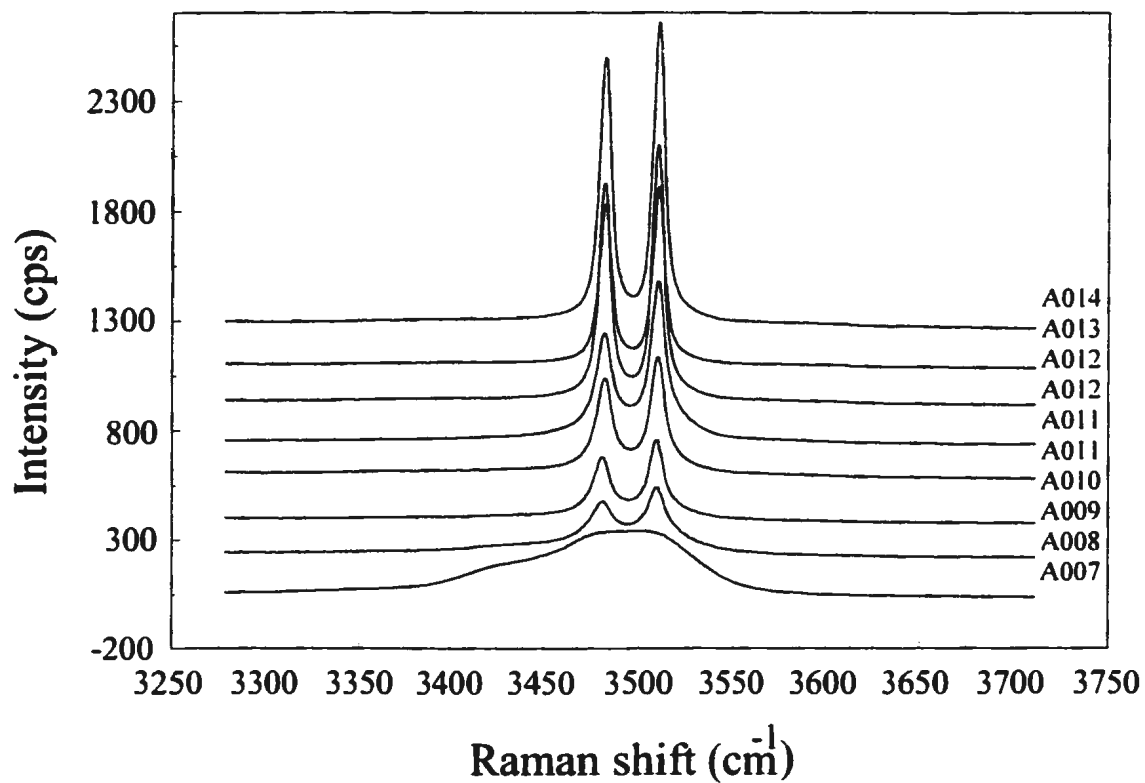
7.3. Raman spectra of alunite and alunite-d in the OH and OD stretching range, respectively.



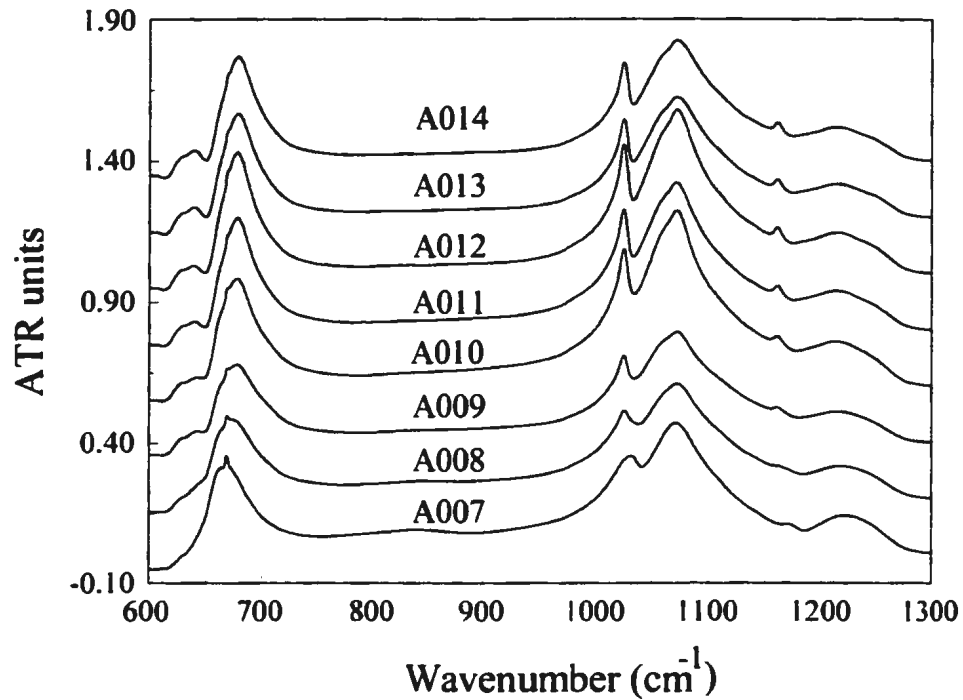
7.4. Raman and i.r. spectrum of hydronium alunite at 25 °C. Upper panel: infrared spectrum; lower panel: Raman spectrum.



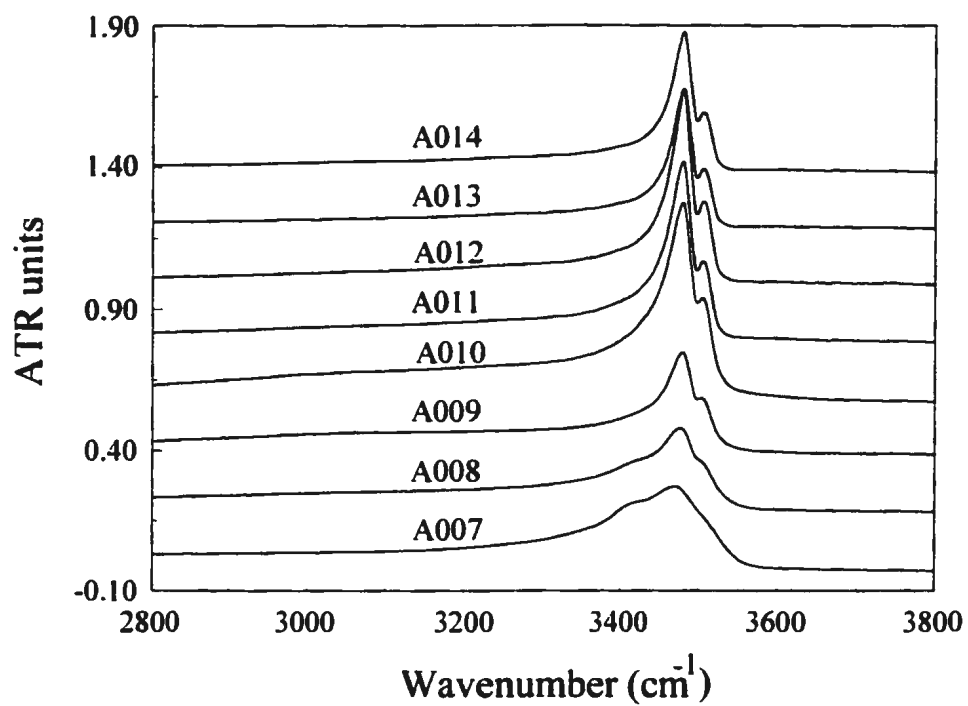
7.5 A. Raman concentration profile for solid solution series ( $[K_{1-x}(H_3O)_xAl_3(SO_4)_2(OH)_6]$ ; with  $x = 0$  to 1; samples A014 to A007) are presented in the wavenumber range from 100 to 1300  $cm^{-1}$ . For the composition of the solid solution samples compare Table 7.1.



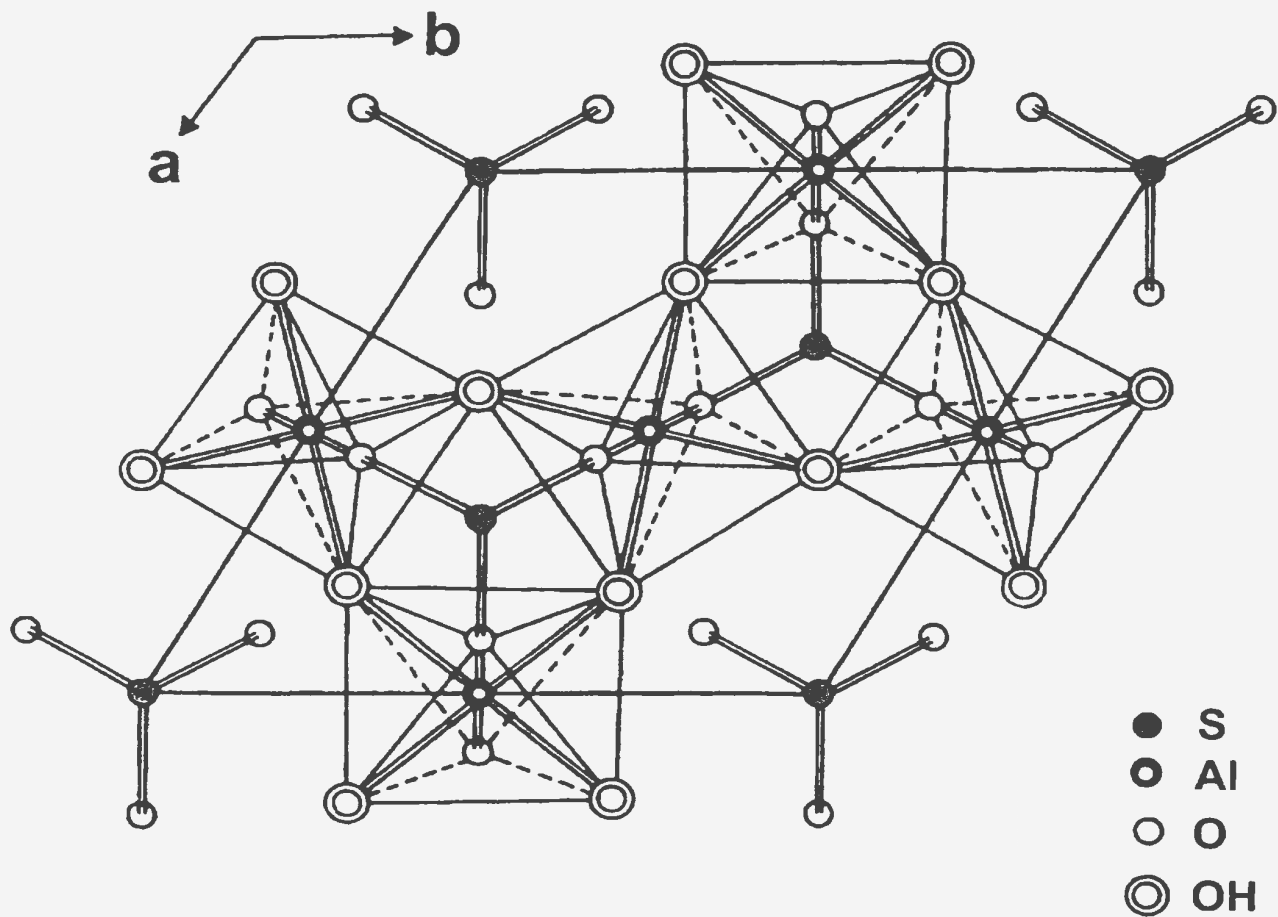
**7.5 B. Raman concentration profile for solid solution series**  
 ( $[\text{K}_{1-x}(\text{H}_3\text{O})_x\text{Al}_3(\text{SO}_4)_2(\text{OH})_6]$ ; with  $x = 0$  to 1; samples A014 to A007) are presented in the wavenumber range from 3250 to 3750  $\text{cm}^{-1}$ . For the composition of the solid solution samples compare Table 7.1.



7.6 A. Infrared (ATR spectra) concentration profile for solid solution series  $[\text{K}_{1-x}(\text{H}_3\text{O})_x\text{Al}_3(\text{SO}_4)_2(\text{OH})_6]$ ; with  $x = 0$  to 1; samples A014 to A007) are presented in the wavenumber range from 600 to 1800  $\text{cm}^{-1}$ . For the composition of the solid solution samples compare Table 7.1.



**7.6 B. Infrared (ATR spectra) concentration profile for solid solution series  $[(K_{1-x}(H_3O)_xAl_3(SO_4)_2(OH)_6)]$ ; with  $x = 0$  to 1; samples A014 to A007) are presented in the wavenumber range from 2000 to 3800  $cm^{-1}$ . For the composition of the solid solution samples compare Table 7.1.**



7.7. Drawing of the  $c$ -axis projection to illustrate the  $\text{AlO}_2(\text{OH})_4$  octahedra linked by corner-shared OH groups forming an octahedral sheet.

$\Gamma_{\text{molecule}}$	$\Gamma_{\text{site}}$	$\Gamma_{\text{unit cell}}$	activity	no. of modes
$T_d$	$C_{3v}$	$D_{3d}$		
$A_1$	$A_1$	$A_{1g}$	Ra	3
$E$		$A_{2u}$	i.r.	3
$F_2$	$E$	$E_g$	Ra	3
$F_2$		$E_u$	i.r.	3

7.8. Correlation diagram for the symmetry properties of the normal modes of  $SO_4$  in alunite space group R-3m ( $D_{3d}^5$ )

## 7. 7. References

- Brophy, G. P., Scott, E. S., Snellgrove, R. A., 1962. "Sulfate studies II Solid solution between alunite and jarosite". *Amer. Miner.*, **47**, 112- 126.
- Decius, J. C. and Hexter, R. M., 1977. "Molecular Vibrations in crystals". McGraw-Hill.
- Fateley, W. G., Dollish, F. R., McDevitt, N. T. and Bentley, F. F., 1972. "Infrared and Raman selection rules for molecular and lattice vibrations: The correlation method". *Wiley-Interscience*, New York, 1972.
- Härtig, C., Brand, P. and Bohmhammel, K., 1984. "Fe-Al- Isomorphie und Strukturwasser in Kristallen vom Jarosit-Alunit-Type". *Z. Anorg. Allg. Chemie.* **508**, 159-164.
- Hendricks, S. B., 1937. "The crystal structure of alunite and the jarosites"., *Amer. Miner.*, **22**, 773-784.
- Johansson, G., 1963. "On the crystal structure of a basic gallium sulfate related to alunite". *Arkiv Kemi*, **20**, 343-352.
- Jones, D. J. , Penfold, J., Tomkinson, J., Roziere, J., 1989. "Incoherent inelastic neutron scattering studies of proton-conducting materials:  $\text{Sn}(\text{HPO}_4)_2 \cdot \text{H}_2\text{O}$  and  $\text{HM}(\text{SO}_4)_2 \cdot \text{H}_2\text{O}$ , M = Fe, In, Part II. The vibrational spectrum of  $\text{H}_3\text{O}^+$ ". *J. Mol. Struct.* **197**, 113 - 121.
- Kiss, A. B., Keresztury, G., Farkas, L. 1980. "Raman and i.r. spectra and structure of boehmite ( $\gamma\text{AlOOH}$ ). Evidence for the recently discarded  $D_{2h}^{17}$  space group". *Spectrochim. Acta*, **36A**, 653-658.
- Kubisz, J., 1972. "Studies on synthetic alkaline-hydronium jarosites III. Infrared absorption

- study". *Mineralogia Polonica*, **3**, 23-36.
- Loiacono, G. M., Kostecky, G., and White, J. S. Jr. (1982). "Resolution of space group ambiguities in minerals". *Amer. Mineral.*, **67**, 846-847.
- Menchetti, S. and Sabelli, C., 1976. "Crystal chemistry of the alunite series: crystal structure refinement of alunite and synthetic jarosite". *N. Jb. Miner. Mh.* 406- 417.
- Moenke, H., 1962. "Mineralspektren, I". Akademie-Verlag, Berlin.
- Parker, R. L., 1962. "Isomorphous substitution in natural and synthetic alunite". *Amer. Miner.*, **47**, 127- 136.
- Pysiak, J. and Glinka, A., 1981. "Thermal decomposition of basic aluminium potassium sulphate. Part I. Stages of decomposition.", *Thermochim. Acta*, **44**, 21 - 28.
- Ripmeester, J. A., Ratcliffe, Ch. I., Dutrizac, J. E. and Jambor, J. L., 1986. "Hydronium in the alunite-jarosite group"., *Can. Miner.*, **24**, 435-447.
- Ross, S. D., 1972. "Inorganic Infrared and Raman Spectra". *McGraw-Hill*, London, 1972.
- Rudolph, W. W., 1996. "Structure and dissociation of the hydrogen sulfate ion in aqueous solution over a broad temperature range: a Raman study". *Z. Phys. Chem.* **194**, 73 - 95.
- Rudolph, W. W. , Mason, R. and Pye, C. C.. 2000. "Aluminium(III) hydration in aqueous solution. A Raman spectroscopic investigation and an *ab-initio* molecular orbital study of Aluminium(III) water clusters". *Phys. Chem. Chem. Phys.*, **2**, 5030 - 5040.
- Rudolph, W. W. and Mason, R., 2001. "Studies on synthetic alunites: synthesis and X-ray characterization". in preparation.
- Ryskin, Ya. I., 1975. "The vibrations of protons in minerals: hydroxyl, water and

- ammonium". 137-181. In V. C. Farmer, *The Infrared Spectra of Minerals*, Mineralogical Society, London, 1975.
- Scott, K. M., 1987. "Solid solution in, and classification of, gossan-derived members of the alunite-jarosite family, northwest Queensland, Australia". *Amer. Miner.*, **72**, 178 - 187.
- Siebert, H., 1966. "Anwendungen der Schwingungsspektroskopie in der anorganischen Chemie". Springer Verlag, Berlin.
- Slansky, E., 1973. "The thermal investigation of alunite and natroalunite." *N. Jb. Miner. Mh. H. 3*, 124 - 138.
- Stoffregen, R. E. and Alpers, Ch. N., 1992. "Observations on the unit-cell dimensions, H<sub>2</sub>O content, and  $\delta D$  values of natural and synthetic alunite". *Amer. Miner.*, **77**, 1092-1098.
- Wang, R., Bradley, W. F. and Steinfink, H., 1965. "The crystal structure of alunite". *Acta Cryst.* **18**, 249 - 252.
- Wilkins, R. W. T., Mateen, A. and West, G. W., 1974. "The spectroscopic study of oxonium ions in minerals". *Amer. Miner.* **59**, 811 - 819.
- Williams, J. M., 1976. "Spectroscopic studies of hydrated proton species, H<sup>+</sup>(H<sub>2</sub>O)<sub>n</sub>, in crystalline compounds". Chapter 14, 655- 682, In: *The Hydrogen Bond, II. Structure and Spectroscopy*, P. Schuster, G. Zundel, and C. Sandorfy, Eds., North-Holland Publishing Company, Amsterdam, New York, Oxford.

## 8. Summary

I. The weak, polarized Raman band assigned to  $\nu_1(a_{1g})$   $AlO_6$  mode of the hexaaqua  $Al(III)$  ( $T_h$  for the whole cluster and  $O_h$  symmetry for the  $AlO_6$  unit) has been studied over the temperature range from 25 to 125 °C. The isotropic scattering geometry in R format was employed in order to measure the true vibrational contribution of the band and account for the Boltzmann temperature factor  $B$  and the frequency factor,  $\nu$ . The band profile as a function of temperature has been examined analytically to extract the parameters: position of band maximum, fwhh, integral intensity of the band and relative molar scattering coefficient,  $S_h$ , over the temperature range measured. The dependence on concentration has also been measured. The position of the  $\nu_1(a_{1g})$   $AlO_6$  mode shifts only about 2  $cm^{-1}$  to lower frequencies and broadens about 19  $cm^{-1}$  for a 100 °C temperature increase. The Raman spectroscopic data suggest that the hexaaquaaluminium(III) ion is thermodynamically stable in chloride, perchlorate and nitrate solution over the temperature and concentration range measured.

Besides the polarized mode at 525  $cm^{-1}$ , two weak depolarized modes at 438  $cm^{-1}$  and 332  $cm^{-1}$  have been assigned to  $\nu_2(e_g)$  and  $\nu_3(f_{2g})$  of the aluminium hexaaqua ion. The infrared active mode at 598  $cm^{-1}$  has been assigned to  $\nu_3(f_{1u})$ .

*Ab initio* geometry optimizations of  $[Al(OH_2)_6]^{3-}$  were carried out at the Hartree-Fock and second order Møller- Plesset levels of theory, using various basis sets up to 6-31+G\*. The global minimum structure of the hexaaquaaluminium(III) species corresponds with symmetry  $T_h$ . The unscaled vibrational frequencies of the  $[Al(OH_2)_6]^{3-}$

were reported, and the unscaled vibrational frequencies of the  $\text{AlO}_6$  unit are lower than the experimental frequencies (ca. 15 %), but scaling the frequencies reproduces the measured frequencies. The theoretical binding enthalpy for  $[\text{Al}(\text{OH}_2)_6]^{3-}$  was calculated and accounts for ca. 64% of the experimental single ion hydration enthalpy for Al(III). *Ab initio* geometry optimizations and frequency calculations are also reported for a  $[\text{Al}(\text{OH}_2)_{18}]^{3-}$  (Al[6+12]) cluster with 6 water molecules in the first sphere and 12 water molecules in the second sphere. The global minimum corresponds with T symmetry. The calculated frequencies of the aluminium [6+12] cluster correspond well with the observed frequencies in solution. The  $\nu_1$   $\text{AlO}_6$  (unscaled) mode occurs at  $519\text{ cm}^{-1}$  in fair agreement to the experimental value. The internal water modes in the aquaaluminium(III) clusters are compared with water (gas phase) and discussed in terms of the polarizing effect of Al(III) and the subsequent formation of strong H-bonds of the water molecules of the first-sphere with the ones in the second sphere. The theoretical binding enthalpy for  $[\text{Al}(\text{OH}_2)_{18}]^{3-}$  was calculated and is very close to the experimental single ion hydration enthalpy for Al(III).

II. The results on the solution chemistry on aqueous aluminium(III) sulfate solutions can be summarized as follows:

i) At temperatures above  $100\text{ }^\circ\text{C}$  the hydrolysis reaction of the  $[\text{Al}(\text{OH}_2)_6]^{3-}$  is significant and  $\text{HSO}_4^-$  is formed in a corresponding reaction. The  $\text{p}Q_{11}$  values of the mono-hydroxo aluminum in solution could be estimated.

ii) The degree of sulfato complex formation is also increased and additionally complex species most likely a bidentate and tridentate bridging sulfato complexes are

formed.

iii) Hydronium alunite is formed in stoichiometric aluminum sulfate solutions in the temperature range from 135 to 184°C under hydrothermal conditions.

iv) The formation of hydronium alunite is discussed in terms of the aluminum(III) hydrolysis, the corresponding formation of hydrogen sulfate and the formation of sulfato complexes ions prior to hydronium alunite precipitation.

v) Hydronium alunite was characterized by chemical analysis and by ICP OES analysis, and X-ray diffraction measurements. The (hexagonal) unit cell parameters are reported.

vi) The i.r. and Raman spectra of hydronium alunite are reported and band assignments are given.

III. Hydrothermal synthesis studies of alunite's and their characterization using XRD can be summed up as follows:

i) Careful synthesis and chemical analysis are required in order to prepare and characterize stoichiometric end member alunites.

ii) There exists complete solid solution between alunite and hydronium alunite. Potassium is incorporated preferentially into the solid phase upon precipitation from aqueous solution at approximately 200 °C. Members of the solid solution can be prepared by suitable adjustment of solution composition. The ratio of the unit cell parameters  $c/a$  follows Vegard's rule.

iii) Excess water is commonly incorporated in synthetic alunite.

iv) With an increase in the effective ionic radius of the cation occupying the A site in the series from  $\text{Na}^+$ ,  $\text{K}^+$ ,  $\text{NH}_4^+$  to  $\text{Rb}^+$  there is a large increase in the  $c$  unit cell parameter accompanied by a subsequent slight increase in the  $a$  parameter.

v) Hydronium gallunite was hydrothermally synthesized and the unit cell parameters determined. Substitution of the B site in the alunite results in an increase in *the*  $a$  parameter and only a slight increase in the  $c$  parameter compared to the hydronium alunite end member.

IV: Hydrothermally synthesized alunites were characterized using infrared and Raman spectroscopy. The following conclusions could be drawn:

i) Alunite/hydronium alunite solid solution specimens were synthesized and characterized with wet chemical methods and ICP OES, and infrared and Raman spectroscopy.

ii) The infrared and Raman spectra of the alunite end members have been measured and assignments have been made. iii) The use of deuterated alunite samples allowed the unequivocal assignment of the OH/OD internal vibrations and the internal modes of the sulfate .

iv) The use of vibrational spectroscopy in order to refine the space group for alunite showed clearly that alunite belongs to the centrosymmetric space group R-3m ( $D_{3d}^5$ ).

## 9. Reference

- Altaner, St. P., Fitzpatrick, J. J., Krohn, M. D., Bethke, P. M. Hayba, D. O. Goss, J. A. and Brown, Z. A., 1988. "Ammonium in alunite". *Amer. Miner.* 73, 145- 152.
- Aoki, M., 1983. "Modes of occurrence and mineralogical properties of alunite solid solution in Osorezan geothermal area". Science Reports, Hirosake University, 30, 132 - 141.
- Botinelly, T., 1976. "A review of the minerals of the alunite-jarosite, beudantite, and plumbogummite groups". Journal of Research of the U.S. Geological Survey, 4, 213 - 216.
- Brimhall, G. H. Jr., 1980. "Deep hypogene oxidation of porphyry copper potassium-silicate protore at Butte, Montana: A theoretical evaluation of the copper remobilization hypothesis". *Econ. Geol.*, 75, 384 - 409.
- Chitale, D. V. and Guven, N., 1987. Natroalunite in a laterite profile over Deccan Trap basalts at matanumad, Kutch, India". *Clays and Clay Minerals*, 35, 196 - 202.
- Goldbery, R., 1978. "Early diagenetic, nonhydrothermal Na-alunite in Jurassic flint clays, Makhtesh Ramon, Israel". *Geological Society of America Bulletin*". 89, 687 - 698.
- Hemley, J. J., Hostetler, P. B., Gude, A. J., and Mountjoy, W. T., 1969. Some stability relations of alunite". *Econ. Geol.*, 64, 599 - 612.
- Hendricks, S. B.. 1937. "The crystal structure of alunite and the jarosites"., *Amer. Miner.*, 22, 773-784.
- Johansson, G., 1963. "On the crystal structure of a basic gallium sulfate related to

- alunite". *Arkiv Kemi*, 20 (28), 343 - 352.
- Kubisz, J., 1972. "Studies on synthetic alumin-hydronium jarosites III. Infrared absorption study". *Mineralogia Polonica*, 3, 23-36.
- Menchetti, S. and Sabelli, C., 1976. "Crystal chemistry of the alunite series: crystal structure refinement of alunite and synthetic jarosite". *N. Jb. Miner. Mh.*, 406- 417.
- Meyer, C. and Hemley, J. J., 1967. "Wall rock alteration". In Barnes, H. L. Editor, geochemistry of hydrothermal ore deposits, p. 166 - 235. Holt, Rhinehart, and Winston, New York.
- Ossaka, J., Hirabayashi, J., Okada, K., and Harada, J., 1982. "Crystal data for  $3\text{Al}_2\text{O}_3 \cdot 4\text{SO}_3 \cdot 8\text{H}_2\text{O}$ ". *Journ. Appl. Cryst.*, 15, 353 - 354.
- Ossaka, J., Otsuka, N., Hirabayashi, J., Okada, K. and Soga, H., 1987. Synthesis of minamiite,  $\text{Ca}_0.5\text{Al}_3(\text{SO}_4)_2(\text{OH})_6$ ". *N. Jb. Miner. Mh.*, (2), 49 - 63.
- Palache, C., Berman, H. and Frondel, C., 1951. Dana's system of mineralogy, 7<sup>th</sup> edition, vol. II. Wiley, New York.
- Radoslovich, E. W., 1982. "Refinement of gorceixite structure in Cm. *N. Jahrbuch für Mineralogie Monatshefte*, 446 - 464.
- Ramdohr, P. and Strunz, H., 1978. Klockmann's lehrbuch der Mineralogie, 16<sup>th</sup> edition. Ferdinand Enke Verlag, Stuttgart.
- Ripmeester, J. A., Ratcliffe, Ch. I., Dutrizac, J. E., and Jambor, J. L.. 1986. "Hydronium in the alunite-jarosite group"., *Can. Miner.*, 24, 435-447.
- Rudolph, W. W., Mason, R. and Pye, C. C., 2000. "Aluminium(III) hydration in aqueous

- solution. A Raman spectroscopic investigation and an *ab initio* molecular orbital study of aluminium(III) water clusters". *Phys. Chem. Chem. Phys.* , 2, 5030 - 5040.
- Rudolph, W. W., and Mason, R., 2001. "Study of aqueous  $\text{Al}_2(\text{SO}_4)_3$  solution under hydrothermal conditions: sulfate ion pairing, hydrolysis and formation of hydronium alunite". *J. Sol. Chem.*, 30, 1-22.
- Rudolph, W. W., and Mason, R., 2001. "Studies on synthetic alunites: synthesis and X-ray characterization". 2001. To be submitted.
- Rudolph, W. W., and Mason, R., 2001. "Raman and infrared absorption studies on synthetic alunites".. To be submitted.
- Schoch, A. E., Beukes, G. J. and Praekelt, H. E., 1985. " A natroalunite-zaherite-hotsonite paragenesis from Pofadder, Bushmanland, South Africa, *Can. Mineral.* 23, 29 - 34.
- Schoen, R., White, D. E., and Hemley, J. J., 1974. " Argillization by descending acid at Steamboat Springs, Nevada, *Clays and Clay Minerals*, 22, 1 - 22.
- Scott, K. M., 1987. "Solid solution in, and classification of, gossan-derived members of the alunite-jarosite family, northwest Queensland, Australia". *Amer. Miner.*, 72, 178 - 187.
- Shishkin, N. V., 1951. "The oxonium ions in the crystal lattice of inorganic compounds". *Zhur. Obshechi Khim.*, 21, 456 - 467.
- Stoffregen, R. E. and Alpers, Ch. N., 1992. "Observations on the unit-cell dimensions,  $\text{H}_2\text{O}$  content, and  $\delta\text{D}$  values of natural and synthetic alunite". *Amer. Miner.*, 77, 1092-1098.

Strunz, H., 1978. Mineralogische Tabellen, 7<sup>th</sup> edition. Akademische Verlagsgesellschaft

Geest und Portig K.- G., Leipzig.

Szymanski, J. T., 1985. "The crystal structure of Plumbojarosite

$\text{Pb}[\text{Fe}_3(\text{SO}_4)_2(\text{OH})_6]_2$ ". *Can. Min.*, 23, 659-668.

Wang, R., Bradley, W. F. and Steinfink, H., 1965. "The crystal structure of alunite". *Acta*

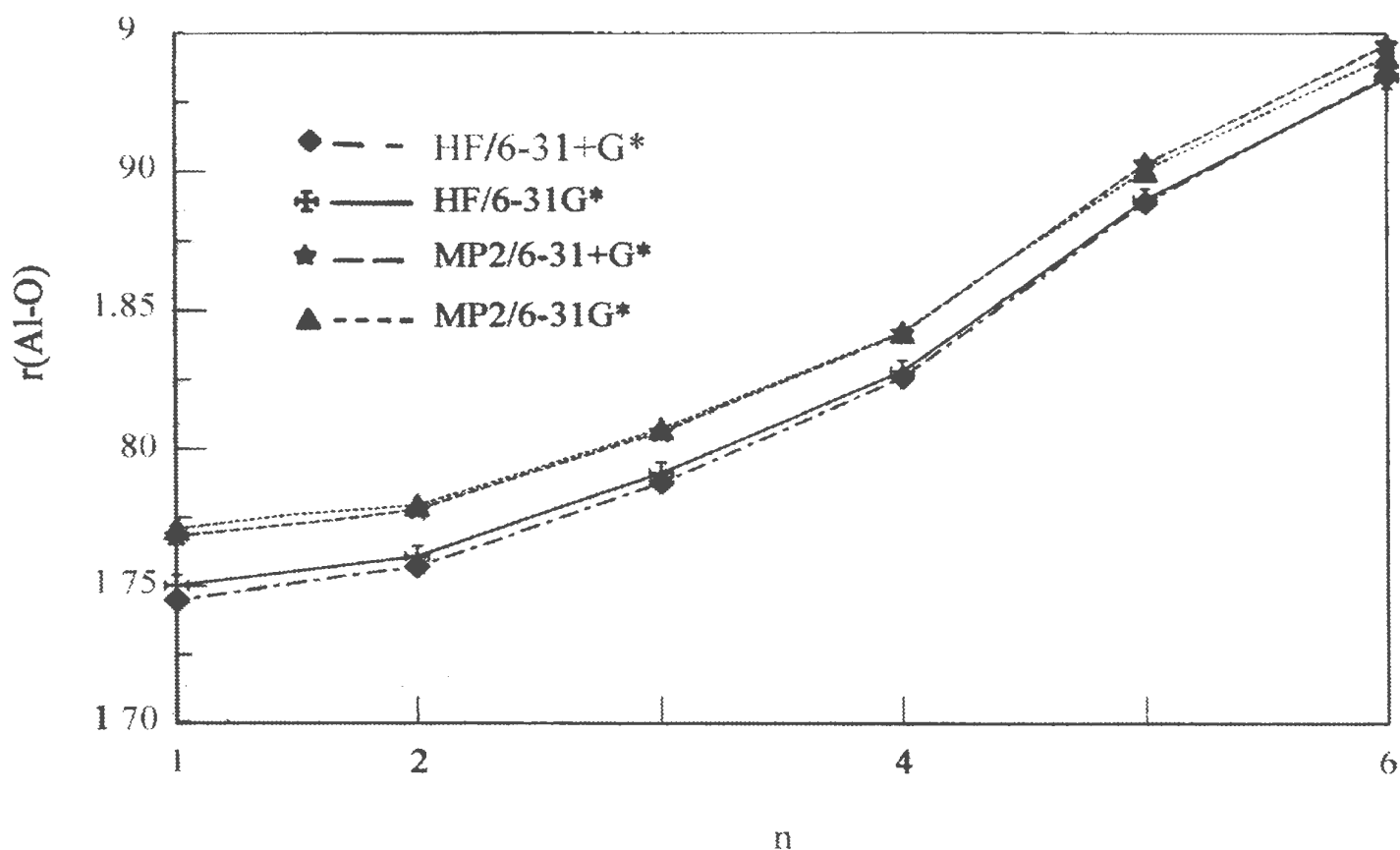
*Cryst.* 18, 249 - 252.

Wilkins, R. W. T., Mateen, A. and West, G. W., 1974. "The spectroscopic study of

oxonium ions in minerals". *Amer. Miner.* 59, 811 - 819.

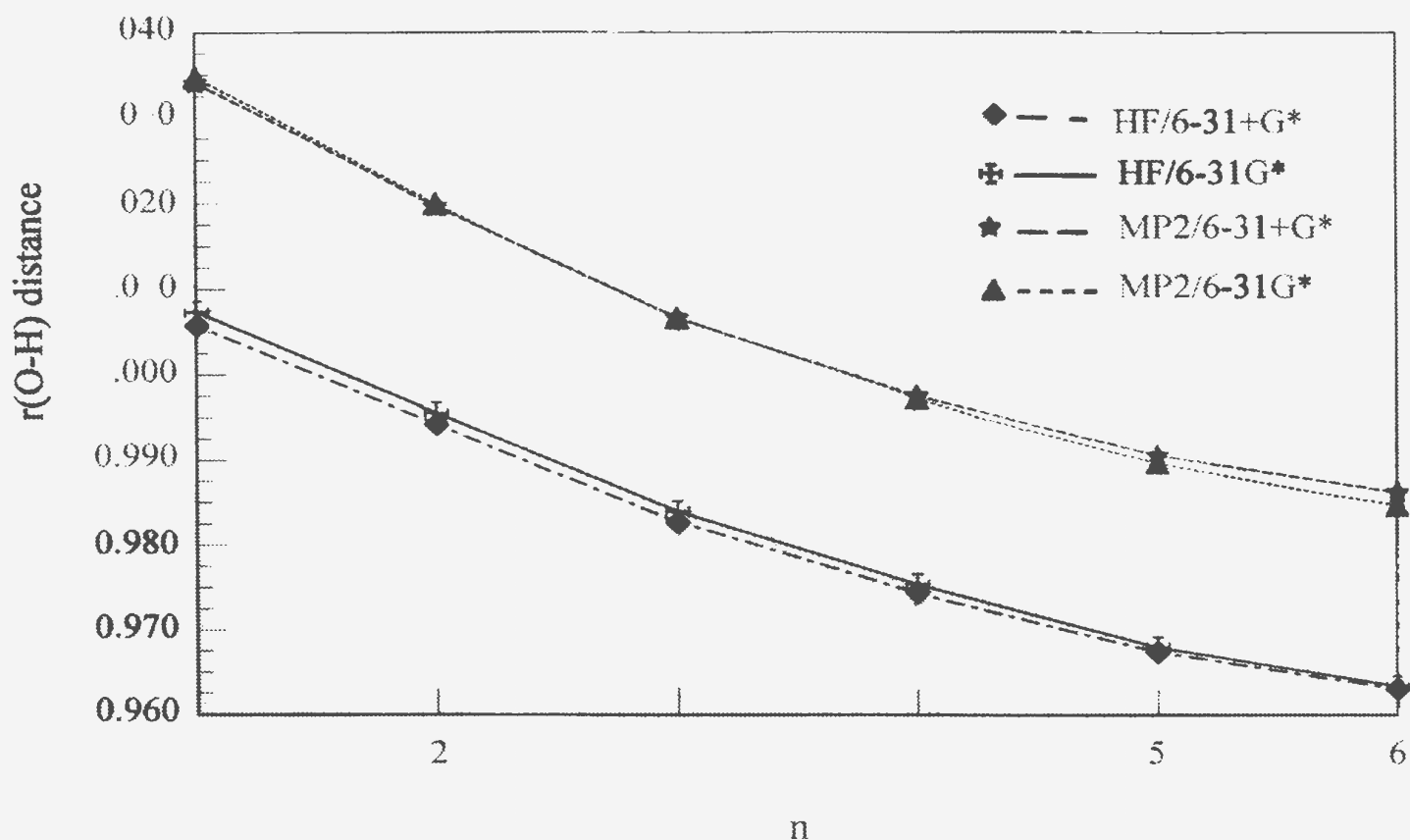
## 10. Appendices

$r(\text{Al-O})$  as fct. of  $n$



1S) The Al-O bond length,  $r(\text{Al-O})$  as a function of the coordination number  $n$  for the  $\text{Al}^{3+}(\text{OH}_2)_n$  cluster (at HF/6-31G\*, HF/6-31+G\*, MP2/6-31G\* and MP2/6-31+G\* levels of theory/basis set).

$r(\text{O-H})$



2S) The O-H bond length,  $r(\text{O-H})$  of the first-sphere waters as a function of the coordination number  $n$  for the  $\text{Al}^{3+}(\text{OH}_2)_n$  cluster (at HF/6-31G\*, HF/6-31+G\*, MP2/6-31G\* and MP2/6-31+G\* levels of theory/basis set).

